

CZECH TECHNICAL UNIVERSITY IN PRAGUE
FACULTY OF NUCLEAR SCIENCES AND PHYSICAL ENGINEERING

DOCTORAL THESIS

QUANTUM WALKS

2012

VÁCLAV POTOČEK

Acknowledgments

First and foremost, I would like to express my most sincere thanks to my supervisor, Professor Igor Jex, for his endless support and help during all the years I spent under his supervision, for the invaluable opportunities I was given in research, conference presentation and world-class international collaboration. His brilliant guidance was the perfect start as well as motivation for a scientific career.

Collaboration with partner scientific groups led by Christine Silberhorn (Max Planck Institute for the Science of Light, Erlangen, Germany), Erika Andersson (Heriott-Watt University of Edinburgh, UK), Tamás Kiss (Hungarian Academy of Sciences, Budapest, Hungary), and Eric Lutz (University of Augsburg, Germany) is most gratefully acknowledged and appreciated. I would particularly like to thank Dr. Andreas Schreiber and Dr. Katuscia N. Cassemiro for having always striving for the very best in the experiments they realized and for being excellent collaborators. I also feel deeply indebted to my colleagues at the Faculty of Nuclear Sciences and Physical Engineering, especially Aurél Gábris and Martin Štefaňák, for always being there to create a strong team.

Special thanks go to my family for providing a constant support, understanding my needs even in times when I was too busy to repay them by appropriate attention, and generally ensuring a harmonious environment for both my work as well as personal life.

Title:

Quantum Walks

Author: Ing. Václav Potoček

Study branch: Mathematical Engineering

Type of work: Doctoral thesis

Supervisor: Prof. Ing. Igor Jex, DrSc., Department of Physics, FNSPE, CTU in Prague

Abstract: The study of quantum walks—quantum mechanical systems defined similarly to random walks in classical physics—represent an active field of research on the boundary of the theories of quantum information, quantum communication, and quantum optics. This thesis gives a concise overview of the topic of quantum walking, with particular attention paid to the original results published in years 2009–2012. These works are attached as reprints from the respective journals and form the basis of the main part of the thesis. The aim of this thesis is to provide an unifying frame for these publications and to emphasize the importance of their respective results for the field of quantum walks. In the course of this thesis, quantum walks are studied from theoretical, experimental as well as numerical points of view.

Key words: Quantum algorithms, Quantum walks, Quantum simulation

Název práce:

Kvantové procházky

Autor: Ing. Václav Potoček

Obor: Matematické inženýrství

Druh práce: Dizertace

Vedoucí práce: Prof. Ing. Igor Jex, DrSc., Katedra fyziky FJFI ČVUT v Praze

Abstrakt: Studium kvantových procházek – kvantově mechanických systémů definovaných analogicky jako náhodné procházky v klasické fyzice – je aktivní oblastí výzkumu na rozhraní kvantové teorie informace, kvantové komunikace a kvantové optiky. Tato dizertace podává stručný přehled problematiky kvantových procházek s důrazem na originální výsledky publikované v letech 2009–2012, které jsou k práci přiloženy v původním znění a tvoří její základ. Cílem dizertace je poskytnout pro přiložené články jednotící podklad a obhájit význam jejich závěrů pro teorii kvantového procházení jako celek. V rámci práce je téma kvantových procházek zkoumáno z teoretického, experimentálního i numerického úhlu pohledu.

Klíčová slova: Kvantové algoritmy, kvantové procházky, kvantová simulace

Contents

Introduction	1
1. Basics of quantum algorithms and quantum walks	2
1.1 Quantum computing and quantum algorithms	2
1.2 The power of quantum computers	4
1.3 Quantum walking	5
1.4 Definition of quantum walks	5
1.5 Theoretical importance of quantum walks	6
1.6 Quantum walks as a computational resource	7
1.7 Quantum walks and database searching	8
1.8 Experimental realizations of quantum walks	9
1.9 Chapter summary	10
2. New results in quantum walk research	11
2.1 Discrete-time quantum walks on Cayley graphs	11
2.2 The homogeneous quantum walk on a line	13
2.3 Symmetries of quantum walks	15
2.3.1 Quantum walk on a line	17
2.3.2 Quantum walk on a two-dimensional lattice	17
2.4 Chapter summary	18
3. Novel experimental realization of quantum walks	19
3.1 The principle of the feedback loop realization	19
3.2 Quantum walk on a line	21
3.3 Upgrading the experiment	23
3.4 Quantum walk on a two-dimensional lattice	25
3.5 Quantum walk of two particles	28
3.6 Chapter summary and outlook	31
4. Exploring the effects of randomness in quantum walks	33
4.1 On-site randomness	33
4.2 Modelling randomness experimentally	35
4.2.1 Dynamic disorder	35
4.2.2 Static disorder	37
4.2.3 Slow fluctuations of the coin	37
4.3 Quantum walks with jumps	38
4.4 Chapter summary and outlook	40
Conclusion	41
References	42
Author's works	42
Cited works	43
Appendices	46

List of used symbols

The following list covers some of the mathematical symbols and conventions used in the work without prior definition.

Symbol	Meaning
\mathbb{N}	the set of positive integers, i.e., $\{1, 2, 3, \dots\}$
\mathbb{N}_0	the set of nonnegative integers, i.e., $\{0, 1, 2, 3, \dots\}$
\mathbb{Z}	the set of all integers, i.e., $\{0, 1, -1, 2, -2, \dots\}$
\mathbb{R}	the set of real numbers
\mathbb{C}	the set of complex numbers
(a, b)	an open interval from a to b
$\langle a, b \rangle$	a closed interval from a to b
\hat{n}	the set $\{1, 2, \dots, n\}$
$\text{Span}(S)$	the closed linear complex span of set S
$U(n)$	the group of unitary operators on \mathbb{C}^n
$ a\rangle, \langle a $	normalized ket- and bra-vectors in Dirac notation
\mathcal{H}_A	state space of a (sub-)system A
$U(t \mapsto t')$	unitary time-evolution operator taking states at time t to states at time t'
ρ	quantum state, density matrix
$\mathcal{U}(t \mapsto t')$	completely positive trace-preserving superoperator evolving mixed states
$\mathbb{1}$	identity operator, identity matrix
α^*	complex conjugate of a complex number α
A^\dagger	Hermitian adjoint of an operator A
$\text{Tr } A$	trace of an operator A
\otimes	tensor product of operators, vectors, or vector spaces
\oplus	bitwise addition modulo 2
$\sigma_X, \sigma_Y, \sigma_Z$	the Pauli matrices, taken as operators on \mathbb{C}^2
$\mathbb{P}(E)$	probability of an event E
$E[X]$	expectation value of a random variable X
$\mathbf{x} = x_1 x_2 \dots x_n$	a binary string
$\lfloor x \rfloor$	the integer part, the largest integer not greater than $x \in \mathbb{R}$
$\lceil x \rceil$	the smallest integer larger than or equal $x \in \mathbb{R}$

List of figures

Fig. 1. Comparison of classical and quantum random walks.	14
Fig. 2. Generic scheme of the optical feedback loop implementation of quantum walks. . .	20
Fig. 3. Projection of the (t, x) space onto a single real line.	21
Fig. 4. Scheme of the experiment realizing a quantum walk on a line.	22
Fig. 5. Scheme of the second experiment realizing a quantum walk on a line.	24
Fig. 6. Experimental observation of 27 steps of a quantum walk on a line.	25
Fig. 7. Experimental setup for realizing quantum walks on a two-dimensional lattice. . . .	26
Fig. 8. Projection of the (t, x, y) space onto a single real line.	27
Fig. 9. Experimental observation of a two-dimensional quantum walk.	28
Fig. 10. The equivalence of a two-dimensional walk with a walk of two particles.	29
Fig. 11. Results of a simulation of a quantum walk of two particles on a line.	31
Fig. 12. Observation of quantum walks on a line in three different disorder scenarios. . . .	37
Fig. 13. Numerical evidence of a new kind of behaviour in quantum walks with jumps. . .	39

Introduction

The field of quantum computing and information processing has been facing a true boom for the past few decades. The idea of reducing computational complexity of certain important algorithmic tasks is so tempting that even many scientific centres have been established for the sole purpose of theoretical and experimental studies of quantum computing and quantum information theory. With the number of scientific papers in prominent journals steadily growing every year, the whole community is bringing close the epoch of practical quantum computing.

The novelty of the branch allows the research to be broadly open-minded, unconstrained by established techniques, unlimited by commercially available equipment or backward compatibility. The ubiquity of quantum mechanics as a generic descriptive language for the whole of physics allows the theoretical framework to be implementation-independent. What is more, the very techniques of composing quantum logical operations from simple building blocks may vary significantly. Various approaches seen so far include quantum logic circuits, measurement-based (one-way) quantum computing, or adiabatic quantum computing.

The new quantum paradigm, replacing the computing model at its very pillars represented by Boolean logic, has significant implications across the whole field of computer science. New theories of quantum information, quantum complexity, quantum communication, quantum algorithms, or quantum games, needed to be established, to name a few. In most cases, these are rooted in their classical counterparts and much effort is put into studying the respective differences and generalizations. Quantum algorithms differ from this scheme rather significantly: despite the fact that a quantum algorithm might be designed as a direct translation of a classical algorithm, any real improvement only comes with algorithms which are completely unlike any classical pattern. There are also some cases of algorithmic tasks where a genuine polynomial-time quantum algorithm is known but no classical one has been found. In other words, not only new tools are made accessible but a whole new manner of thinking needs to be developed in order to harness the true power of quantum computers.

The aim of this doctoral thesis is to define and develop one of such concepts—quantum walks—not only as a very competitive means of designing, describing and realizing quantum algorithms, but more generally as a universal tool for studying quantum mechanics of simple systems and using these to reach far more involving goals. Starting with a brief review, various aspects of quantum walks are covered, from a theoretical as well as experimental point of view, focusing primarily on the areas where the original research presented in this thesis contributed to the global knowledge of the topic.

Chapter 1

Basics of quantum algorithms and quantum walks

In this chapter, I will define what quantum walks are and show the main points of motivation to study them as a main research topic. For this purpose, I will first need to make a brief introduction into quantum computing and quantum algorithms. I will use this framework to introduce the concept of quantum walks in Section 1.3 and specify it further in Section 1.4. The subsequent three sections show the importance of quantum walks in the theory of quantum algorithms, showing particular examples. Finally, the current state of art in experimental implementations of quantum walk system is summarized in Section 1.8.

1.1 Quantum computing and quantum algorithms

Quantum algorithms are any algorithms designed to be run on quantum computers, computational machines using quantum mechanical systems to store or transmit information and the laws of quantum mechanics to process it.

Quantum computation is usually performed on a quantum system composed of n two-state subsystems, called qubits. Larger partitions of the system, called quantum registers, may be used to store and process input/output variables or provide auxiliary space for computation.

For the i -th qubit, let $|0\rangle_i$ and $|1\rangle_i$ denote the basis vectors of a chosen orthonormal basis of its state space. The tensor product basis

$$|0\rangle_1 \otimes |0\rangle_2 \otimes \dots \otimes |0\rangle_n =: |00\dots 0\rangle \quad \text{through} \quad |1\rangle_1 \otimes |1\rangle_2 \otimes \dots \otimes |1\rangle_n =: |11\dots 1\rangle \quad (1.1)$$

is called the *computational basis* of the system. If the qubits are partitioned into quantum registers, one might also speak of their respective computational bases, built analogously.

A quantum algorithm consists of the specification of an initial state, a means of inserting input data into the system, a sequence of transformations applied to the state, and a measurement used for reading out the result of the algorithm. If no particular observable is stated in the measurement step, a complete measurement in the computational basis is automatically assumed and the result is interpreted as a binary string, or a binary representation of an integer between 0 and $2^n - 1$. Additional partial measurements may be applied during the run of the algorithm and used for conditioning of its further evolution; however, any such measurement can be deferred till the final step [1].

A classical input can be loaded into the quantum system in several ways: in the initial state, via conditioning of the operations applied to the state, or via tunable parameters of these operations.

Due to the unitary nature of quantum dynamics of closed systems, any computation performed in a quantum algorithm is inherently reversible. However this may seem limiting at first sight, even in classical computational models, reversible computation is capable of replacing any irreversible algorithm at the cost of a polynomial extension of the working space. Since any

reversible binary operation on n qubits can be expressed using a unitary matrix, and any unitary operation is reachable in quantum mechanics via a suitable Hamiltonian, quantum computation can also simulate any classical logical circuit effectively. For example, a commonly used way to reversibly store the result of a non-injective function $f: \{0,1\}^n \rightarrow \{0,1\}^m$ in a m -qubit register is using a unitary time-evolution operator (a *quantum gate*) of the form

$$U_f: |\mathbf{x}\rangle_{(n)} \otimes |\mathbf{y}\rangle_{(m)} \mapsto |\mathbf{x}\rangle_{(n)} \otimes |\mathbf{y} \oplus f(\mathbf{x})\rangle_{(m)}, \quad (1.2)$$

where \oplus denotes bitwise addition modulo 2. Note that upon a second application of the same operator, the function value $f(\mathbf{x})$ would get “un-computed”, which in turn proves reversibility of this gate.

The power of quantum computers stems primarily from the availability of creating and working with quantum superpositional states, which is the base of *quantum parallelism*. One must keep in mind that the superposition principle of quantum mechanics takes place on the state space of the whole system, as opposed to taking superpositions of $|0\rangle$ and $|1\rangle$ in its individual qubits only, so a generic state features a strong entanglement of all the qubits. For an example of quantum parallelism, consider a superposition of several computational basis states $(|\mathbf{x}_i\rangle)_{i=0}^k$ with amplitudes α_i in one quantum register augmented by $|\mathbf{y}\rangle = |\mathbf{0}\rangle := |00\dots 0\rangle$ in the second register as the input to the gate U_f defined in Eq. (1.2). As a result of the overall linearity of quantum mechanics, the result of its application on this superpositional state is

$$U_f \left(\left(\sum_{i=0}^k \alpha_i |\mathbf{x}_i\rangle_{(n)} \right) \otimes |\mathbf{0}\rangle_{(m)} \right) = \sum_{i=0}^k \left(\alpha_i U_f (|\mathbf{x}_i\rangle_{(n)} \otimes |\mathbf{0}\rangle_{(m)}) \right) = \sum_{i=0}^k \left(\alpha_i |\mathbf{x}_i\rangle_{(n)} \otimes |f(\mathbf{x}_i)\rangle_{(m)} \right). \quad (1.3)$$

We see that the function f is effectively computed for k different inputs simultaneously with only one use of the quantum gate implementing it.

Also, the set of quantum gates available for processing a register of quantum bits is a broad generalization of the set of classical reversible logic gates acting on the same number of bits. For example, the only operations applicable on a single bit in reversible classical computation are the identity and the NOT-gate. On the other hand, a single qubit is a system with two-dimensional complex linear state space and any unitary operator $U \in U(2)$ represents a possible single-qubit quantum gate, leaving the identity and the Pauli σ_X gate (the quantum version of the NOT gate) as only two special cases.

A set of quantum gates is called *universal* if any unitary operation on an arbitrary number of qubits can be decomposed into gates belonging to this set acting in succession on subsystems of corresponding number of qubits. An important universal set of quantum gates is the set of all single-qubit gates augmented by a two-qubit CNOT-gate, defined in the computational basis by the rule

$$U_{\text{CNOT}}: |a\rangle \otimes |b\rangle \mapsto |a\rangle \otimes |a \oplus b\rangle. \quad (1.4)$$

1.2 The power of quantum computers

The classical-to-classical data processing pattern allows us to compare quantum computing machines to the classical theoretical model of computation.

It can be easily proven that the class of problems decidable in a classical computer and a quantum one is the same. This follows from the possibility of simulating each kind of machine on the other, given unlimited resources. However, simulating quantum algorithms on classical computers is generally a hard problem, requiring a substantial amount of both memory and time due to an exponential dependence of the state space dimension on the number of qubits. The space complexity of the simulation may be reduced back to polynomial using techniques described in [1] but no such techniques are known for bounding the necessary running time. This justifies the question whether quantum algorithms can outperform classical ones in terms of time complexity. Indeed, several examples of quantum algorithms have been found that decide particular problems faster (even exponentially faster) than their best classical counterparts in various measures, most notably:

- Deutsch-Josza’s algorithm[2] (1992), showing an exponential speed-up of exact quantum algorithms against classical algorithms in determining the properties of a black-box function,
- Simon’s algorithm[3] (1994), displaying an exponential speed-up of bounded-error quantum algorithms against bounded-error classical algorithms in a similar setting,
- Shor’s algorithm[4] (1994), showing that integer factorization, *suspected* to be of exponential time complexity on a classical computer, can be solved in polynomial time on a quantum one,
- Grover’s algorithm[5] (1996), finding an element satisfying a binary function quadratically faster than both deterministic and probabilistic classical algorithms.

The first two examples present important separations of the power of quantum and classical computers, but for this purpose, they use a black box “oracle” function which itself might take an exponential time to evaluate, or allow for a simpler solution to be designed if its definition could be examined. Shor’s algorithm was an important milestone in quantum computing, marking the beginning of a broad interest in the field of the public. The importance of integer factorization is that its classical computational hardness, albeit never truly proven, is being exploited in many computer security schemes. This leaves Grover’s algorithm the only one of the four giving an example of a problem solved unconditionally faster in a quantum computing model, even though this speed-up is only quadratic.

This analysis leads us to defining new complexity classes valid for quantum computers. The most widely used class of problems considered feasible for a quantum computer is BQP, in which a decision problem belongs if and only if there is a polynomial-time quantum algorithm solving it with an upper bounded probability of error. This gives a quantum generalization of the classical complexity class BPP and indeed,

$$P \subseteq BPP \subseteq BQP. \tag{1.5}$$

The upper bound on the size of the class BQP is given by PP, the class of problems decidable on a probabilistic Turing machine with a probability of correct answer strictly larger than $\frac{1}{2}$,

but possibly arbitrarily close to it. This class is no longer considered feasible for a classical computer, because it might take an exponential number of tries to confirm a difference from an uniformly distributed (and thus useless) outcome. This leaves space for a possible exponential speed-up by quantum algorithms.

At present, it is not known whether there are any problems for which polynomial-time quantum algorithms exist but classical ones do not. Shor's algorithm would give a positive answer if integer factorization is proven to be of exponential time complexity in the future. Similarly, the relation of BQP to NP, the well-known classical class of nondeterministically polynomial problems, has not been established.

1.3 Quantum walking

The generic scheme of a quantum algorithm, defined above, allows for several generalizations. Primarily, the restriction to using two-level elementary subsystems and binary representations of all respective variables is often relaxed. Besides digital representations in other than binary number bases, the whole spectrum of any suitable physical quantity, discrete or continuous, may be employed.

An important example of this alternative is given by quantum walks. In the most direct model of quantum walking [6], the physical position of a quantum particle is used as a dynamical variable without the need for any numeric representation. The motion of the particle is driven by its wave equation, taken either in continuous time or discretized time steps. An indisputable benefit of directly using the naturally omnipresent kinematics and interactions with the confining environment is that this approach is certainly more straightforward and less error-prone than resorting to using abstract finite-dimensional systems and engineered Hamiltonians. The price to pay for this advantage is a limitation of synchronizing arrivals of the particle to the corresponding sites and a related time cost of the transitions. For this reason, the transitions are generally restricted to crossing exactly one edge of some underlying graph structure per one time step in the case of discretized time evolution, or to nearest-neighbour interaction Hamiltonians in continuous-time systems.

The quantum walk in [6] is not being presented as a quantum algorithm *per se*, rather a new formalism or language for describing simple quantum systems. However, it has provided ground for later works specifically oriented on quantum computing, e. g., [7] or [8], which can be interpreted in a similar straightforward real-world manner.

1.4 Definition of quantum walks

A generic pattern of quantum walk algorithms can be summarized as follows:

Primary assumptions. The walk is realized in a quantum system described by its position (in discretized Euclidean space or among the vertices of a prescribed graph) and a number of optional internal degrees of freedom. It is assumed that the internal state may be modified freely but the spatial motion can only happen at a speed of one unit per each time step.

Preparation. The quantum particle, or a walker, is prepared in a given initial state. This is typically, but not necessarily, a localized state in one of the possible positions with a fiducial internal state or, in the case of finite walking spaces, an equal weight superposition of all position and all internal states.

Time evolution. Time evolution takes place either in discrete steps or continuously in time. In the latter case, the system is governed by a Hamiltonian supported in the position space by the adjacency matrix of the walking graph. In the case of discrete-time quantum walks, the evolution operator applied in each time step can induce any change in the internal states, followed by a displacement connecting each position to its nearest neighbours. If the direction of this displacement is controlled by the internal state, one calls the system a quantum walk a walk with a coin, the quantum coin being the internal state register. The change in the internal state is then referred to as a quantum coin toss or an application of a quantum coin operator, similarly, the controlled displacement is governed by a step operator. N.B. that for both continuous- or discrete-time quantum walks, the evolution operator may also feature an explicit time dependence, and if the internal state is being altered, the transformation applied to it may be position-dependent.

Finish. After a prescribed time of evolution according to the previous rules, the quantum walk is stopped and the resulting quantum state is made available for arbitrary further processing. This usually, but not necessarily, involves a measurement of the position of the walker.

The need for any internal state dynamics can be dropped in continuous-time quantum walks. In many important discrete-time configurations, most notably all Euclidean lattices, however, the use of a quantum coin is inevitable in order to reach nontrivial time evolution [9]. The purpose of the coin is to introduce quantum superposition states in the low-dimensional internal state, which are translated via the controlled displacement to superpositions of different positions, causing a spread of the quantum walker's position.

1.5 Theoretical importance of quantum walks

Quantum walks were first proposed as a quantum analogue of random walks [6]. This also explains the original name "quantum random walks", which was later simplified by multiple authors to "quantum walks" conforming to the lack of randomness in an unitary evolution of a closed quantum system. The effort put into quantum walk research was motivated not only by the multitude of uses of classical random walks in computer science and algorithm design, but by the possibility of use of a similar description in a surprising number of branches of modern science, *e. g.*, mathematics, physics, biology, economy or genetics.

Already in the first studies, certain striking differences between quantum and classical walks were discovered. Most notably that the asymptotic behaviour of a quantum walk does not converge to a Gaussian probability distribution of the particle's position spreading over the allowed space. Instead, it forms one or more wavefronts travelling the space at asymptotically constant group velocities. This has a direct consequence of quickly covering large areas and reduced hitting times (for two given vertices in a graph, the hitting time is the time in which a walker starting in one vertex reaches the other with probability higher than a prescribed bound). The functional dependence of hitting time on the graph diameter depends on the

class of graphs of interest and might be as much as exponentially faster than the hitting time observed in classical diffusive systems [10].

Despite the major differences, a link between quantum and classical random walks can be observed when the ideal unitary time evolution is disturbed. Stochastic randomness and diffusive behaviour may emerge in a quantum walk system by introducing information decoherence, intermediate measurements of the system state, or random perturbations of the parameters of on-site interactions. Due to the simplicity of the unperturbed system and the perturbations sufficient to reach this behaviour, quantum walks provide a brilliant framework for studying the effects of quantum-to-classical transitions in theory, numerical simulations, and experiments.

Not unlike classical walks, quantum walks have also been used as a language to model or explain certain phenomena observed in other branches of science. Some important theoretical and numerical uses of quantum walks in connection with particular sources of randomness include a proposed explanation of rapid energy transport in photosynthesis [11,12] or a minimum assumptions example of a system featuring Anderson localization [13].

1.6 Quantum walks as a computational resource

Besides being a tool for understanding and modelling processes involving simple local or nearest-neighbour interactions, the time evolution of quantum walks can also be used indirectly in quantum algorithms.

In particular, one may ask whether a known quantum algorithm can be represented as a quantum walk. That is, whether one can use the definition of the algorithm to design a task-specific graph and a quantum walk on it, with the property that initial states encoding the input to the algorithm would evolve, in a given time, to states able to reveal the output upon measurement. This question has been settled by the work of Childs [14] for continuous-time quantum walks and later extended also to the discrete-time case by Lovett [15], showing that in either of these models, there is a simple mapping from the universal set of quantum gates to elements of a walking space that can be sequentiated to represent any composition of the former, and thus an arbitrary quantum algorithm. This means that quantum walks on their own present an universal language for expressing quantum algorithms and are capable of efficiently solving any BQP-class problem.

The result in both cases is a graph divisible into layers of vertices, connected by edges in a configuration resulting into an unidirectional flow of information from an input set of nodes towards the output. The only issue with the mappings presented in the two works is that the size of the resulting graphs depends exponentially on the size of the working register in the original algorithm. This is because, essentially, a separate path is kept for each computational basis state in [14] (two paths per a basis state in [15]). It is important to note that this only affects the “transverse” dimension of the graph—the time needed for the computation is linear in the running time of the original algorithm—but an exponential space complexity would still be a serious obstacle in any practical realization. To account for this, the authors claim that despite the size, the structure of the graph is extremely predictable, *e.g.*, the same motif on 4 concurrent paths appears in parallel on all 4-tuples of those. The high predictability of the

graph allows for its systematic *description* and a subsequent effective *simulation* of a quantum walk on its vertices on another quantum computing machine. One might be wondering why, if the authors aimed to present quantum walks as an alternative to a general quantum computer, they conclude by resorting to one to simulate the resulting walk. The answer is simple: if one finds any way of simulating arbitrary quantum walk dynamics effectively, or designs a quantum simulator limited to simulating quantum walks, the works of Childs and Lovett can be used to make it capable of running any quantum algorithm.

1.7 Quantum walks and database searching

In comparison with the last section, specific quantum walk-based algorithms can also be designed in more general geometric configurations, resulting in simpler and more directly realizable layouts. By dropping the assumption of an unidirectional flow of information across the graph, it is possible to reuse the same vertices many times. Similarly, it is not imperative to keep one edge per a computational basis state. Both these facts may be used to reduce the space requirements of a quantum realization of a particular algorithmic task.

More specifically, one might be interested in finding quantum algorithms which are intrinsically based on quantum walking, using the principal differences from classical random walks to reach an algorithmic speedup. A first example of such approach was a quantum database search algorithm presented by Shenvi, Kempe and Whaley, utilizing a quantum walk defined on a hypercube graph [16].

In general, the purpose of unordered database searching is to identify one or more elements which are identified by a binary function. This function, also called an *oracle*, may query and evaluate an element in an actual database, but for modelling purposes, one may take any prescribed mapping from the set of elements to $\{0, 1\}$. The well-known NP-complete saturation problem shows that even the knowledge of the full formula of the marking function may not give a clue of the preimage of $\{1\}$.

It can be easily seen that in an unstructured database, *i. e.*, a sole set of entries, no classical algorithm can possibly do better than querying one half of the database on average before hitting the marked element, provided it is unique. This is also the case for databases in which any implicit structure (*e. g.*, a metric) of the underlying space is independent on, and thus lacks any connection to, the particular search query the algorithm is performing.

However, it has been found that Grover's algorithm [5], mentioned in Section 1.2, solves the same task with a number of queries to the oracle proportional to the *square root* of the total size, using a technique later named *amplitude amplification* [17] and shown to be optimal for this purpose [18–20].

Comparing the results of Grover with those of Shenvi, Kempe and Whaley, one can easily note that the running time of the quantum-walk based search is twice as long on a database of the same size. More importantly, the former has an asymptotic unit probability of success in finding the marked element and can be theoretically made perfectly deterministic [21] whereas the latter suffers from the success probability being upper bounded by $\frac{1}{2}$ in any instance. At first sight, this might seem to be the cost of the restriction to using only nearest-neighbor

interaction on the walking space. However, a previously published result of mine [22] shows that both of these imperfections can be overcome.

The algorithm by Shenvi, Kempe and Whaley has attracted the interest of researchers to designing algorithms genuinely based on quantum walking. Many authors responded by giving examples of algorithmic speedup in quantum walk-based solutions. Quantum database search algorithms have been found on other kinds of graphs than hypercubes, used in [16], both in discrete-time [7,8] and continuous-time [23] settings. Algorithmic problems beyond database searching successfully approached by quantum walk-based algorithms include checking for element distinctness [24] or a conjectured quantum decision of the graph isomorphism problem [25].

1.8 Experimental realizations of quantum walks

Many experimental physics groups have succeeded at observing quantum walk behaviour in various physical systems. Most groups studied systems realizing a quantum walk on a line. Discrete-time settings include quantum walks of atoms trapped in optical lattices [26], ions held in a Paul trap [27,28], or Bose-Einstein condensate in phase space [29]. Implementations using photons in fully optical settings are of special interest because of their easy control, no need for ultra-low temperatures or pressures, and low decoherence. Among photonic quantum walk implementations, I would like to pinpoint a series of experiments partly developed by our group [A1,A2,A4], which will be discussed in detail in Chapters 3 and 4 of this thesis. Other important photonic implementations use birefringent beam displacers [30] and optical angular momentum manipulation [31]. Continuous-time quantum walks on a line were first observed in lattices of coupled waveguides [32].

At the time of writing of this thesis, not many works have gone beyond the model of walking on a line. Jiangfeng Du *et al.* [33] modeled a quantum walk on a circle graph with 4 vertices on a nuclear magnetic resonance based quantum computer able to carry operations on two qubits. A similar setup was later successfully used to demonstrate the Shenvi-Kempe-Whaley search algorithm on the same graph [34]. White's group used waveguides etched in crystals to observe a quantum walk on a circle graph of 6 vertices performed by two indistinguishable particles simultaneously [35]. Both of these generalized graph scenarios were studied in the continuous-time regime.

Quantum walks of two particles are the first step to study walks in higher-dimensional spaces. This is because any such a system is equivalent to a special case of a single-particle quantum walk on the Cartesian product of the walking graph with itself. For a discrete-time quantum walk, this equivalence is thoroughly studied in [36]. A quantum walk of two particles on a line was experimentally realized in waveguide lattices in the continuous-time variant [37,38] and using integrated photonics for a discrete-time walk [39].

The primacy in a genuine discrete-time quantum walk on a two-dimensional Euclidean lattice graph belongs to our group [A5]. Similarly as in the case of [A1], this setup represents a fully optical interferometric setup where the walking particles are single photons. This achievement is important not only because it opens up the field of experimental realizations of higher-dimensional quantum walks. The possibility of interpreting a coordinate pair in a

two-dimensional plane as a tuple of coordinates of two one-dimensional systems allows us to engineer and study various models of interaction of two particles moving on a discrete line. As the external control allows for simulations of even very unusual kinds of interactions, the presented approach has the potential to provide a direct access to experimental research in new unexplored areas of physics.

1.9 Chapter summary

In this introductory chapter, I presented the basic principles of quantum walks, arriving to the concept as to a natural extension of quantum computation model based on qubit systems. I presented the generic pattern of quantum walk algorithms, defining both discrete- and continuous-time variants. N. B. that the main results presented in the following chapters of this thesis were found in the discrete-time setting, so this differentiation is sometimes omitted for brevity.

Quantum walks were shown to provide a useful building block for quantum algorithm design. I argued that a quantum walk can be used as a resource in a quantum algorithm, *e. g.*, providing a way of scanning large data sets for the purpose of quantum searching. This is usually done in connection with a qubit circuit implementing the oracle function and thus making it possible to use quantum parallelism in its evaluation. However, quantum walks were also proved to be capable of providing equivalent formulations of universal quantum gates, making it theoretically possible to rewrite any quantum algorithm purely within the quantum walk formalism.

Finally, I presented an overview of the current state of implementing quantum walk systems experimentally. Many instances of quantum walks have been realized, in both discrete- and continuous-time variants, using various quantum systems including trapped ions or atoms, optical waveguides and more. Special attention was drawn to implementations of quantum walks using photons in optical interferometers for their numerous experimental benefits as well as good results.

This completes the general overview of the topic of quantum walks. Chapters 2, 3, and 4 form the main part of this thesis where new results will be summarized and embedded in the framework presented here.

Chapter 2

New results in quantum walk research

In this and the following chapters, I will present a selection of the original results on quantum walks published in [A1–A6]. A detailed description of all the methods used, full results and further bibliography can be found in the attached copies of these publications. The field of quantum walks is approached from various points of view: the current chapter opens the topic with a precise definition of the quantum systems to be studied and aims to provide a solid theoretical background for the subsequent parts. Chapter 3 describes the results of the long-term collaboration with the experimental group of Professor Christine Silberhorn with the goal to design a generic framework for realizing one- and two-dimensional quantum walks using photons in an interferometric setup. The last chapter focuses on quantum walks with specific sources of environmental errors and presents our numerical results in quantum walks with large sudden jumps along with a third experiment studying the effects of quantum phase decoherence in the optical framework. My contribution to the joint works is stated as a part of the summaries at the end of each chapter.

2.1 Discrete-time quantum walks on Cayley graphs

Since all the research topics covered in this thesis address discrete-time quantum walks on graphs which can be treated as Cayley graphs of certain discrete groups, I will start with a more precise definition of this concept.

Let G be a discrete group with a finite generating set S . The Cayley graph $\Gamma(G, S)$ is a directed graph (V, A) in which the set of vertices V is equal to the underlying set of G and the set of edges E is defined by

$$\forall g, h \in G: (g, h) \in E \Leftrightarrow \exists c \in S: h = gc. \quad (2.1)$$

If the set S is symmetric with respect to the group inverse operation then $\Gamma(G, S)$ is a symmetric graph and thus equivalent to a simple undirected graph.

For the purpose of quantum walking, we define a *position space* \mathcal{H}_S as a Hilbert space of dimension equal to the cardinality of G in which we assign each vertex $x \in \Gamma(G, S)$ to one element $|x\rangle$ of a fixed orthonormal basis. Alternatively, one may reach this space constructively by assuming the linear space of formal finite complex linear combinations of kets $|x\rangle, x \in G$, augmented by the unique scalar product making the set $\{|x\rangle\}_{x \in G}$ orthonormal, and closed with respect to the resulting norm. In either way, the *coin space* is a linear span reached by the same procedure applied on the set S . In the field of quantum information theory, one usually expresses this identification, or construction, by a short-hand notation

$$\mathcal{H}_S = \text{Span}(\{|x\rangle \mid x \in G\}), \quad \mathcal{H}_C = \text{Span}(\{|c\rangle \mid c \in S\}), \quad (2.2)$$

without explicitly emphasizing the facts that the linear span is taken in the field of complex numbers, that it also defines the scalar product (if the span is being constructed) or that it involves closure.

Any discrete-time coined quantum walk on the Cayley graph $\Gamma(G, S)$ takes place on the tensor product Hilbert space

$$\mathcal{H} = \mathcal{H}_S \otimes \mathcal{H}_C = \text{Span}(\{|x\rangle_S \otimes |c\rangle_C \mid x \in G, c \in S\}). \quad (2.3)$$

In the following, I will leave out the lower indices S and C where a misunderstanding is unlikely.

The class of possible quantum walks, conforming to the framework presented in Section 1.4, is very broad and leaves a substantial amount of freedom for variations on the basic principles. However, where needed, I will refer to the following setup as the referential quantum walk on the Cayley graph $\Gamma(G, S)$.

Let e be the identity element of the group G . Let us assume a fixed coin state (state of the coin register) $|c_0\rangle \in \mathcal{H}_C$. The initial state of the referential quantum walk is then $|e\rangle \otimes |c_0\rangle$. We say that the walker starts his walk in position e with coin state $|c_0\rangle$.

The evolution takes place in discrete steps, each of which has two phases. The first phase is the application of the unitary *quantum coin operator*, defined by the action

$$C: |x\rangle \otimes |\gamma\rangle \mapsto |x\rangle \otimes C_x |\gamma\rangle, \quad \forall x \in G, \forall |\gamma\rangle \in \mathcal{H}_C. \quad (2.4)$$

The operators $C_x \in U(\mathcal{H}_C)$ are called the *elements* of the coin operator. Their explicit form is left to be specified later in specific situations. Since there is a preferred basis in \mathcal{H}_C given by the elements of the set S , it is often illustrative to represent the operators C_x as matrices in this basis.

The coin operation may depend on the number of steps which have already taken place, $t \in \mathbb{N}_0$, also called the quantum walk time. In situations where this is the case, we denote this fact by adding the t index to the symbols C and C_x . If there is no dependence on t , we say that the coin is *homogeneous in time*.

Similarly, if the elements C_x are equal for all values of $x \in G$, we call the quantum coin operator *homogeneous in space*, or simply *homogeneous* if it is homogeneous in both space and time. In this case, the operator C can be expressed as tensor product

$$C = \mathbb{1} \otimes C_0, \quad (2.5)$$

where $C_0 \in U(\mathcal{H}_C)$ is the common value of all the elements C_x . The index 0 points out the difference from the operator C , which acts on the full state space $\mathcal{H} = \mathcal{H}_S \otimes \mathcal{H}_C$, as well as the indifference with respect to x .

After the coin operator is applied, the state is subject to conditional displacement described by the unitary *step operator*

$$S: |x\rangle \otimes |c\rangle \mapsto |xc\rangle \otimes |c\rangle. \quad (2.6)$$

The combined action of the coin and step operators gives a time evolution operator

$$U(t \rightarrow t + 1) = S \cdot C, \quad (2.7)$$

which takes states $|\psi_t\rangle \in \mathcal{H}$ at quantum walk time t to states at time $t + 1$.

In many cases, it is advantageous to replace the unitary evolution formalism by another means of describing how to obtain the state at a given quantum walk time t from the state valid for the system in the preceding step. One means of an exceptional importance for numerical simulations as well as theoretical study of quantum walks on Cayley graphs is the recurrence relation found for probability amplitudes

$$\alpha_c(t, x) = (\langle x | \otimes \langle c |) |\psi_t\rangle, \quad x \in G, c \in S, t \in \mathbb{N}_0. \quad (2.8)$$

N. B. that $\alpha_c(t, x)$ are also the coefficients in the decomposition of $|\psi_t\rangle$ in the orthonormal basis formed by the states $|x\rangle \otimes |c\rangle$. Using basic linear algebra in the Dirac notation, one arrives at the formula

$$\alpha_c(t, x) = \sum_{d \in S} \alpha_d(t-1, xc^{-1}) \langle c | C_0 | d \rangle, \quad \forall x \in G, \forall c \in S, \forall t \in \mathbb{N}. \quad (2.9)$$

This completes the description of time evolution of the referential quantum walk. We finally assume that these rules govern the state of the system for a finite time t , after which the position x of the particle is measured, irreversibly collapsing the state created by the unperturbed evolution. Unless stated otherwise, we will be studying the probability distribution of the possible outcomes of this final measurement.

2.2 The homogeneous quantum walk on a line

The class of graphs expressible as Cayley graphs of discrete groups is very broad, making the definition introduced in the last section an excellent alternative to a more general, but less instructive one allowing arbitrary regular directed graphs (see, e. g., [40]). However, to give a better idea of the concept, we start with one of the simplest instances, a quantum walk on a line with a homogeneous coin. Much of the work presented in the following chapters will relate to this section.

The definition of a discrete-time quantum walk on a line is obtained from the framework introduced in Section 2.1 when the additive group $(\mathbb{Z}, +)$ is supplied for G and the set of generators S is taken to be $\{-1, +1\}$. Therefore, we define

$$\mathcal{H}_S^{(\mathbb{Z})} = \text{Span}(\{|x\rangle \mid x \in \mathbb{Z}\}), \quad \mathcal{H}_C^{(2)} = \text{Span}(\{|-1\rangle, |+1\rangle\}) \simeq \mathbb{C}^2, \quad \mathcal{H}^{(\text{line})} = \mathcal{H}_S^{(\mathbb{Z})} \otimes \mathcal{H}_C^{(2)}. \quad (2.10)$$

Unless explicitly stated otherwise, the step operator transforms the basis states according to

$$S: |x\rangle \otimes |\pm 1\rangle \mapsto |x \pm 1\rangle \otimes |\pm 1\rangle. \quad \forall x \in \mathbb{Z} \quad (2.11)$$

For a homogeneous quantum walk on a line, the quantum coin operator is defined as

$$C = \mathbb{1} \otimes C_0: |x\rangle \otimes |\gamma\rangle \mapsto |x\rangle \otimes (C_0 |\gamma\rangle), \quad \forall x \in \mathbb{Z}, \forall |\gamma\rangle \in \mathcal{H}_C. \quad (2.12)$$

As noted above, the operator C_0 can be expressed as a unitary matrix in the $\{|-1\rangle, |+1\rangle\}$ basis. We can utilize the Pauli decomposition to parametrize all possible two-dimensional unitary matrices:

$$C_0 = e^{i\varphi} \begin{pmatrix} e^{i\alpha} & 0 \\ 0 & e^{-i\alpha} \end{pmatrix} \begin{pmatrix} \cos \beta & -\sin \beta \\ \sin \beta & \cos \beta \end{pmatrix} \begin{pmatrix} e^{i\gamma} & 0 \\ 0 & e^{-i\gamma} \end{pmatrix}. \quad (2.13)$$

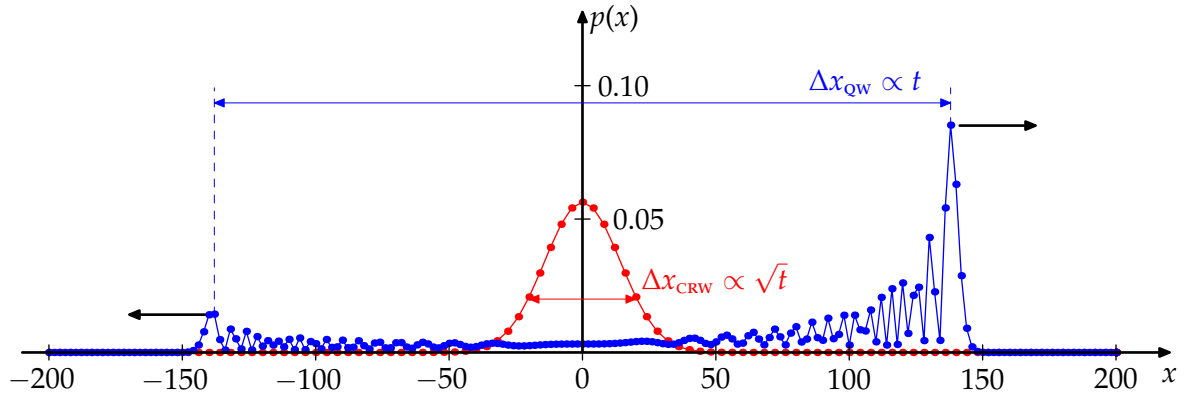


Fig. 1: Comparison of probability distributions and the standard deviation of the position of a walker in classical and quantum (Hadamard) walks on a line after $t = 200$ steps. The initial state of the quantum walk was chosen to be $|0\rangle \otimes |+1\rangle$. Only even-numbered positions are plotted as the probability is exactly zero in odd values of x . The probability distribution of a quantum walker's position (blue) forms two wavefront-like peaks which move away from the initial position at a constant speed (black arrows), causing the standard deviation of x , estimated by the distance Δx , to be linear in time, quadratically faster than in the case of classical random walks (red).

Among the variety of homogeneous discrete-time quantum walks on a line, the special choice of the Hadamard matrix

$$H = \frac{1}{\sqrt{2}} \begin{pmatrix} 1 & 1 \\ 1 & -1 \end{pmatrix} \quad (2.14)$$

for C_0 is often taken for an example as the closest to the classical model of balanced random walk [41–43]. We refer to the resulting system as to a *Hadamard quantum walk*.

Starting at a localized initial state and explicitly computing several iterations of the evolution rules (2.7) in this simple system, we can find that the wave function of the quantum walker spreads into the neighbourhood of the starting position. Using this wave function to find the probability distribution of a position measurement of the quantum walker, substantial differences from a classical random walk behaviour quickly appear. An example of this probability distribution after a larger number of time steps, in comparison with the distribution of a classical balanced random walk after the same number of steps, is shown in Fig. 1.

Studying the time evolution of the quantum walk on a line using techniques described in [44], it can be proven that the wave function assumes a shape dominated by two wavefronts (generally unequal in amplitude) moving away from the initial position as the quantum walk time t rises. This spread takes place at an asymptotically constant speed of $\pm \cos \beta$ units of the x axis per a time step. The two wavefronts also correspond to sharp maxima of the probability distribution observed in Fig. 1.

As a result of a high contribution of the positions near $x = \pm \lfloor t \cos \beta \rfloor$ to the total probability, the variance of the particle's position is asymptotically quadratic in t . This is in sharp contrast with classical random walks in which the variance is always linear in t as a consequence of the Law of large numbers from probability theory.

Another important feature distinguishing quantum walks from classical random walks is the impact of the choice of initial coin state on the whole run of the quantum walk. The strong bias towards positive positions in Fig. 1 is a practical example of this phenomenon. In contrast, in a classical random walk, the direction taken in each step is completely independent of the history.

In spite of the striking differences, there are many attributes common to classical and quantum walking. For example, it is possible to think of the set of trajectories a quantum walker could have taken to reach a given position from its initial position. This is a central idea in studying classical random walks, where one would assign a probability to each of these trajectories and sum these contributions to obtain the probability of reaching the above point. An analogous principle can be found in quantum walking but probability amplitudes need to be employed instead of probabilities. This approach, representing a discretized version of the Feynman path integral, is one of the core methods used in [44].

2.3 Symmetries of quantum walks

In comparison with a classical homogeneous random walk on a line, the time evolution of which is completely specified by the initial position of the walker and the probabilities to move to the right or to the left in any time step, we can note that an analogous quantum walk has significantly more parameters. Namely, one needs to specify, besides the initial position,

- the initial coin state (3 real parameters—the relative amplitude of the $| -1 \rangle$ and $| +1 \rangle$ components and their respective complex phases),
- the quantum coin matrix (4 real parameters according to Eq. (2.13)).

We know from essential quantum mechanics that global phase of the wave function does not influence the observable properties of a physical system in any way; indeed, two wave functions differing only by a constant multiple are considered to describe the same physical state of the system. This makes one of the three parameters of the initial state redundant.

Similarly, since the φ parameter in Eq. (2.13) can be factored out of Eq. (2.7) and also only influences the global phase of the quantum wave function evolved by the latter equation, one can require that $\varphi = 0$ without loss of generality.

The above two observations are both examples of continuous symmetries valid globally in quantum mechanics. There are further symmetries specific to quantum walks that prove the redundancy of even more out of the parameters listed above. This knowledge has very practical implications in experimental research of quantum walks as well as their numerical simulations when the parameter space needs to be covered as densely as possible. The advantage of knowing the symmetries is even more pronounced in quantum walks on more complex graphs where the number of parameters is higher than in a quantum walk on a line.

In the following, we will call symmetries any transformations that can be done on the initial state of the system and the definition of the coin operator but do not influence the observable properties of the resulting state of the quantum walk. We need to put a restriction on what kind of observations is allowed on the resulting state, otherwise this statement is meaningless, leaving for candidates only the two universal symmetries we found in the preceding paragraph. To this end, we will assume that the quantum walk is terminated by a measurement of the walking particle's position and a transformation of the parameters is a symmetry if and only if it leaves the probability distribution of position intact.

The continuous symmetries of this kind in discrete-time quantum walks on Cayley graphs, as defined in Section 2.1, are systematically studied in my recent manuscript [A6]. The methods

used in the analysis aim to give answers valid for all Cayley graphs without difference. The results are presented in the form of mathematical theorems.

Moreover, the paper gives separate results in the cases where the implementation of the quantum walk requires a time- or space-homogeneous coin, as introduced in Section 2.1. As this restriction itself reduces the number of parameters describing the quantum walk, the full set of symmetries must be filtered to contain only those which respect these restrictions.

I will be referring to the results of symmetry analysis in Sections 3.2 and 3.4. As both of these cases consider both time- and space-homogeneous quantum coin and a localized initial state, let me just cite the main result valid for this special case, reformulating it in the formalism used in the current work.

Let a discrete-time quantum walk on $\Gamma(G, S)$ have an initial state of the form

$$|\psi_i\rangle = \sum_{c \in S} \alpha_c |x\rangle \otimes |c\rangle, \quad (2.15 \text{ a})$$

where $x \in G$ is fixed, let the quantum coin is time- and space-homogeneous, $C = \mathbb{1} \otimes C_0$, where

$$C_0 = \sum_{c, d \in S} \langle c | C_0 | d \rangle \cdot |c\rangle \langle d|. \quad (2.15 \text{ b})$$

Let further $\beta(c)$ and $\gamma(c)$ be two arbitrary mappings from S to the unit circle in the complex plane. Then another quantum walk on the same Cayley graph, initiated in a state

$$|\tilde{\psi}_i\rangle = \sum_{c \in S} \beta(c) \alpha_c |x\rangle \otimes |c\rangle \quad (2.16 \text{ a})$$

and using a homogeneous quantum coin $\tilde{C} = \mathbb{1} \otimes \tilde{C}_0$, where

$$\tilde{C}_0 = \sum_{c, d \in S} \gamma(c) \beta^*(d) \langle c | C_0 | d \rangle \cdot |c\rangle \langle d|, \quad (2.16 \text{ b})$$

results in the same distribution of the quantum walker's position as the original quantum walk, after an arbitrary quantum walk time t . In other words, the transformation

$$|\psi_i\rangle \mapsto |\tilde{\psi}_i\rangle, \quad C \mapsto \tilde{C}, \quad (2.16 \text{ c})$$

is a quantum walk symmetry according to the definition above. Moreover, we learn that no other kind of continuous symmetries exists in the same system, the transformations obtained this way represent an exhaustive answer to the problem of finding symmetries.

If the elements of $S = \{c_i\}_{i=1}^n$ are identified with the elements of the standard basis in \mathbb{C}^n , where n is the cardinality of S , C_0 can be directly treated as a matrix. Similarly, we can write Eq. (2.15 a) in a vector form

$$|\psi_i\rangle = |x\rangle \otimes |\gamma\rangle, \quad |\gamma\rangle = \begin{pmatrix} \alpha_{c_1} \\ \alpha_{c_2} \\ \vdots \\ \alpha_{c_n} \end{pmatrix}. \quad (2.17)$$

N. B. that Eqs. (2.16) can then be written in a compact matrix form

$$\begin{aligned} |\psi_i\rangle \mapsto |\tilde{\psi}_i\rangle &= |x\rangle \otimes B|\gamma\rangle, \\ C \mapsto \tilde{C} &= \mathbb{1} \otimes \Gamma C_0 B^{-1} \end{aligned} \quad (2.18)$$

where B and Γ are diagonal matrices with the values of $\beta(c)$ and $\gamma(c)$ on their diagonal, respectively.

In the following two subsections, we apply these general formulas to two important quantum walk scenarios.

2.3.1 Quantum walk on a line

Applying Eq. (2.18) to a quantum walk on a line, we find that a walk initiated in the state $|0\rangle \otimes |\gamma\rangle$, where

$$|\gamma\rangle = \alpha_{-1}|-1\rangle + \alpha_{+1}|+1\rangle = \begin{pmatrix} \alpha_{-1} \\ \alpha_{+1} \end{pmatrix}, \quad (2.19)$$

and using a homogeneous coin $C = \mathbb{1} \otimes C_0$, where C_0 is of the form (2.13), is equivalent, in terms of distribution of position of the walker, to a walk with initial state $|0\rangle \otimes |\tilde{\gamma}\rangle$,

$$|\tilde{\gamma}\rangle = \begin{pmatrix} e^{ia} & 0 \\ 0 & e^{ib} \end{pmatrix} \begin{pmatrix} \alpha_{-1} \\ \alpha_{+1} \end{pmatrix} = \begin{pmatrix} e^{ia}\alpha_{-1} \\ e^{ib}\alpha_{+1} \end{pmatrix} \quad (2.20 \text{ a})$$

and quantum coin $\tilde{C} = \mathbb{1} \otimes \tilde{C}_0$,

$$\begin{aligned} \tilde{C}_0 &= e^{i\varphi} \begin{pmatrix} e^{ic} & 0 \\ 0 & e^{id} \end{pmatrix} \begin{pmatrix} e^{i\alpha} & 0 \\ 0 & e^{-i\alpha} \end{pmatrix} \begin{pmatrix} \cos \beta & -\sin \beta \\ \sin \beta & \cos \beta \end{pmatrix} \begin{pmatrix} e^{i\gamma} & 0 \\ 0 & e^{-i\gamma} \end{pmatrix} \begin{pmatrix} e^{-ia} & 0 \\ 0 & e^{-ib} \end{pmatrix} \\ &= \begin{pmatrix} e^{i(\alpha+c+\varphi)} & 0 \\ 0 & e^{i(-\alpha+d+\varphi)} \end{pmatrix} \begin{pmatrix} \cos \beta & -\sin \beta \\ \sin \beta & \cos \beta \end{pmatrix} \begin{pmatrix} e^{i(\gamma-a)} & 0 \\ 0 & e^{i(-\gamma-b)} \end{pmatrix}, \end{aligned} \quad (2.20 \text{ b})$$

for any $a, b, c, d \in \mathbb{R}$. From this form, we can immediately see that the freedom in choosing c and d allows us to reduce the leftmost diagonal matrix in the last line to the identity without affecting the quantum walk. The rightmost diagonal matrix can be brought to the identity, too, by choosing a and b to be equal to γ and $-\gamma$, respectively. These values will then appear in the transformed initial state (2.20 a). A simple trick of increasing all of a, b, c, d by the same amount can be used to transform out any desired global phase from $|\tilde{\gamma}\rangle$ while leaving \tilde{C}_0 intact.

As a result, any discrete-time quantum walk on a line with an initial state localized at $x = 0$ can be replaced by another quantum walk with the coin matrix reduced to

$$\tilde{C}_0 = \begin{pmatrix} \cos \beta & -\sin \beta \\ \sin \beta & \cos \beta \end{pmatrix} \quad (2.21)$$

at the cost of altering the initial coin state to the form (2.20 a). Together with a freedom in the global phase of the latter, also covered by the general result, this leaves 3 independent parameters out of the original 7. These 3 parameters are sufficient to provide a full control over the evolution of the probability distribution of the quantum walker's position the original set of parameters could.

2.3.2 Quantum walk on a two-dimensional lattice

A two-dimensional Euclidean lattice graph can be described in the Cayley graph formalism as $\Gamma(\mathbb{Z}^2, S^{(2)})$, where

$$S^{(2)} = \{(-1, 0), (1, 0), (0, -1), (0, 1)\}. \quad (2.22)$$

The coin space in this walk is thus 4-dimensional, isomorphic to \mathbb{C}^4 .

In order to find the total number of parameters and the number of independent parameters, one does not necessarily need to repeat the whole procedure demonstrated in the last subsection. It is also possible to obtain the answer non-constructively by simple counting.

Given an initial position of $(0, 0)$, a specification of an initial state needs 7 additional real parameters for the coin register, which is 8 real coordinates of \mathbb{C}^4 , reduced by 1 for the normalization constraint. The coin is determined by an element of $U(4)$ which is a 16-dimensional Lie group. This gives a total of 23 parameters of the generic system if no symmetries are used.

For any given two-dimensional quantum walk, the results of [A6] parametrize a manifold of quantum sharing the same evolution in terms of position probability distribution by two 4-tuples $\beta(c)$ and $\gamma(c)$. The freedom in the choice of these 8 variables allows one to reduce the number of parameters to a minimum of 15 independent ones. Using the same reasoning as in the case of a quantum walk on a line, one can take off 8 parameters off the coin matrix alone, leaving 8 substantial parameters of the coin and 7 of the initial state.

2.4 Chapter summary

In this chapter, I introduced a rigorous treatment of an important class of systems conforming to the quantum walk framework, as outlined in Section 1.4, for use throughout the following parts of this thesis. The theory of discrete-time quantum walks on Cayley graphs is particularly straightforward but also general enough to cover many important practical applications of quantum walks in quantum algorithm design, *e. g.*, [7,8,16].

In the second part, I presented my original results in the theoretical study of discrete-time quantum walks on Cayley graphs [A6]. I have shown the usefulness of the theory on two important cases of quantum walks. Some of the obtained results are used in full or in part in Sections 3.2 and 3.4.

Of course, the study of symmetries does not complete the research done on the theoretical aspects of quantum walks. Further work in this field was done as a part of the broader topics covered by the following chapters and its results are included therein.

Chapter 3

Novel experimental realization of quantum walks

Starting in 2008 and during all my Ph.D. studies, I have participated in an international collaboration aiming at presenting a novel way of implementing quantum walks experimentally, focusing on the minimization of resource requirements and scalability of the experiment. The principal idea was using photons as the quantum walkers and translate the quantum walk into time domain, *i. e.*, to allow the particles to take paths of different length and resolve the final position of the walker from its detection time.

3.1 The principle of the feedback loop realization

In the proposed framework, the photon is led into a feedback loop where it stays for some—not necessarily constant—number of rounds, t . Every round allows for n different routes, each taking a different time $\tau_i, i \in \hat{n}$. The total time for which the particle stays in the feedback loop is thus of the form

$$\tau = \sum_{i=1}^n k_i \tau_i, \quad \sum_{i=1}^n k_i = t, \quad (3.1)$$

where for each $i, k_i \in \mathbb{N}_0$ may be classically interpreted as the number of times the i -th route was taken.

If the set $\{t_i \mid i \in \hat{n}\}$ is algebraically independent, *i. e.*, no two elements have a rational ratio, it is theoretically possible to uniquely identify the constants k_i , given any τ from the range T of the mapping in Eq. (3.1). Practically, this inversion is limited by a finite time resolution of the detection as well as a nonzero temporal width of any quantum wave packet, which is further broadened by dispersion and other disruptive phenomena. Tools used to overcome these limitations will be discussed in specific cases in Section 3.2 through 3.4. In the following, we will idealize the particle to keep a purely singular wave function over the whole course of the thought experiment.

Since in quantum mechanics, a number of incoming modes can not be unitarily recombined into a smaller number of nodes, we can accept an abstraction that there indeed are exactly n parallel paths labelled by indices $1, 2, \dots, n$, which only meet in one point to mix according to an unitary transition matrix U , as shown in Fig. 2. Moreover, we can assume that the transition takes place in the beginning of the loop, before the paths separate. It is simple to prove that these assumptions are without loss of generality. This picture allows us to define—within closed system dynamics—the probability amplitude of finding a particle at the closing point of the feedback loop as a function of time τ and the index i of the path it arrived in. Let us denote this function $\alpha_i(\tau)$.

N. B. that the probabilities $|\alpha_i(\tau)|^2$ do not form a normalized probability mass function either on $\tau \in \langle 0, +\infty \rangle$ or on $i \in \hat{n}$. However, if only times τ according to the same number of t rounds are considered, the resulting sum

$$\sum_{(k_j) \in A} \sum_{i=1}^n \left| \alpha_i \left(\sum_{j=1}^n k_j \tau_j \right) \right|^2, \quad A = \left\{ (k_j)_{j=1}^n \mid \sum_{j=1}^n k_j = t \right\} \quad (3.2)$$

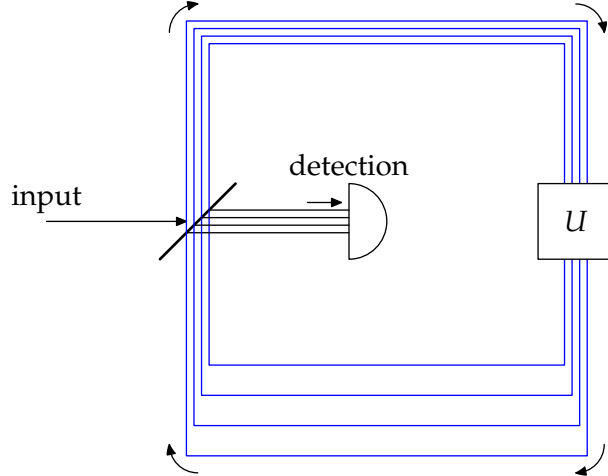


Fig. 2: Generic scheme of the optical feedback loop implementation of quantum walks. The main loop (blue) consists of n optical paths of different lengths. A photon can enter the through a beam splitter. The same component allows it to leave the loop, after which it is measured and its arrival time is recorded. Coherent transitions between the channels, capable of switching the path to be taken from one round to the next, are assumed to take place in an initial segment (counting from the input point) where no mutual time difference of the paths has been acquired yet. These transitions are described by a unitary matrix U .

becomes the total probability of the particle being present in the loop after t rounds, so the squared moduli of the amplitudes $\alpha_i(\tau)$ can be renormalized to a conditional probability distribution over the partitions (k_j) of t and path indices i .

By the construction of the system, it is obvious that the values $\alpha_i(\tau)$ are subject to a recurrence relation. Namely, if σ denotes the transmittivity of the input beam splitter, *i. e.*, the probability amplitude of the particle to re-enter the feedback loop at the end of a round, we can find that

$$\alpha_i(\tau) = \sigma \sum_{j=1}^n \alpha_j(\tau - \tau_j) \langle i|U|j \rangle, \quad \forall \tau \in T; \tau \neq 0, \quad (3.3)$$

where $\langle i|U|j \rangle$ is the probability amplitude of a particle that entered the loop in path j crossing over to the path i . Due to the invertibility of Eq. (3.1), the obtained recurrence relation is, up to the occurrence of σ , fully equivalent to Eq. (2.9) with the underlying group G being a free additive subgroup of \mathbb{R} generated by $S = \{\tau_j\}_{j=1}^n$.

From the equivalence of Eqs. (3.3) and (2.9), one can conclude that the amplitudes $\alpha_i(\tau)$ give the probability amplitudes of observing a hypothetical particle undergoing a quantum walk at point τ of this particular walking space with a coin state $|\tau_i\rangle$, only multiplied by $\sigma^{t(\tau)}$. The initial state of this quantum walk is a state localized at 0 with the initial coin state determined by the wave function of the actual particle immediately after its insertion into the loop.

The result of the above analysis is that the simple optical feedback loop system outlined in Fig. 2 is capable of realizing quantum walks on Cayley graphs of some finitely generated subgroups of the additive group of real numbers with a time- and position-homogeneous coin represented by the the matrix of transition coefficients between the paths forming the loop. One could object that the generators $\{\tau_i\}_{i=1}^n$ are all positive and thus do not allow for an undirected walking graph. However, the following sections prove the contrary.

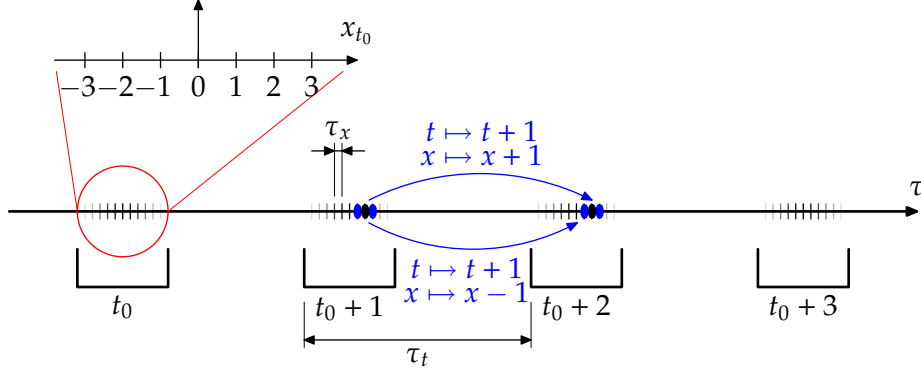


Fig. 3: Graphical meaning of Eq. (3.4) in the case $\tau_x \ll \tau_t$. The τ -axis can be divided into bins of size τ_t . The image of an arbitrary position x and its neighbours is marked in black and blue, respectively, in two consecutive times t . The blue arrows illustrate how a shift of $\tau_t \pm \tau_x$ in the τ coordinate can be interpreted as a transition in the (t, x) space according to one step of a quantum walk. The detail (red circled area) shows the locally valid x_{t_0} coordinate indexing the positions belonging to the same bin t_0 .

3.2 Quantum walk on a line

Applying the theory of the preceding section to a feedback loop with two different delay times, τ_1 and τ_2 , we can obtain a framework for an experimental realization of a quantum walk on a line. This is due to the fact that any combination τ of the form (3.1) can be assigned two nonnegative integers k_1 and k_2 , which we can use to define *position* $x = k_1 - k_2$ along the previously defined *time* $t = k_1 + k_2$. Eq. (3.1) can be rewritten in the new variables as

$$\tau = k_1\tau_1 + k_2\tau_2 = \frac{t+x}{2}\tau_1 + \frac{t-x}{2}\tau_2 = \frac{\tau_1 + \tau_2}{2}t + \frac{\tau_1 - \tau_2}{2}x =: t\tau_t + x\tau_x. \quad (3.4)$$

Taking into consideration a particle entering the feedback loop at time τ given by Eq. (3.4), closing the loop with a delay of $\tau_1 = \tau_t + \tau_x$ or $\tau_2 = \tau_t - \tau_x$ causes a shift of 1 or -1 in x , respectively, and an advance of 1 in t in either case. We can interpret this as a virtual walker taking an unit time to make one step along its x axis to the left or right.

The single detection time axis τ will cover all the possible combinations of t and x . By grouping of the detection events corresponding to a common t , we can reconstruct the probability distribution of a quantum walk along the x coordinate in time t . The grouping is particularly straightforward if τ_x is chosen much smaller than τ_t , *i. e.*, if the difference between τ_1 and τ_2 is much smaller than their mean, as shown in Fig. 3. If we define $n_{\max} = \lfloor \tau_t/2\tau_x \rfloor$, one can observe up to n_{\max} steps of the quantum walk without the overlap of the t -bins, provided the initial state is localized. It is easy to make the upper bound n_{\max} much higher than the number of rounds sufficient for the single photon visibility to drop below the detection noise.

We report on a successful observation of quantum walk behaviour in this kind of interferometer in [A1]. In this experiment, the shorter or longer route is chosen by the photon according to its polarization. It is used with benefit that two orthogonal polarizations can travel along a single interferometric arm and still be easily separated using a polarizing beam splitter (PBS).

The use of polarization as the internal degree of freedom determining the path taken by the photons, and thus the coin of the quantum walker, makes it particularly easy to establish and control the cross communication between the two modes. In the case of [A1], the unitary

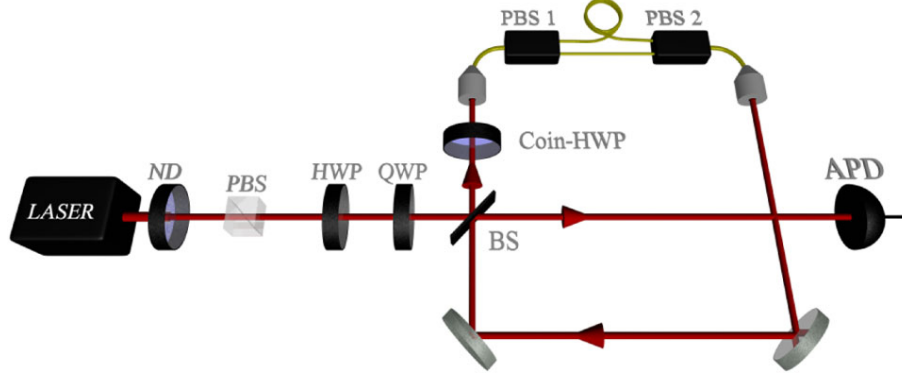


Fig. 4: Scheme of the experiment realizing a homogeneous discrete-time quantum walk on a line [A1]. The parts of the path drawn in red are realized in free space, the parts drawn in yellow in a polarization-maintaining optical fibre. *Explanation of abbreviations:* ND—neutral density attenuation filters, PBS—polarizing beam splitter, HWP—half-wave plate, QWP—quarter-wave plate, BS—nonpolarizing beam splitter, APD—avalanche photodiode single-photon detector.

mixing was accomplished by a single half-wave plate (HWP). In the basis of horizontal and vertical polarization eigenstates, the operation applied on a polarization state by a HWP with its optical axis rotated at an angle θ to the horizontal is

$$C_{\text{HWP}} = \begin{pmatrix} \cos 2\theta & \sin 2\theta \\ \sin 2\theta & -\cos 2\theta \end{pmatrix}. \quad (3.5)$$

N. B. that the special choice of $\theta = \frac{\pi}{8}$ corresponds to the Hadamard matrix (2.14).

According to Section 2.3.1, any discrete-time homogeneous quantum walk on a line can be realized using a coin of the form (3.5) and a full control over the initial polarization state. The latter is realized in our experiment by two more wave plates, which guarantees the universality of the setup.

A schematic of the actual experiment is depicted in Fig. 4. A pulsed laser light source is first attenuated near the single-photon level using neutral density filters (ND). The following polarizing beam splitter (PBS) leaves only one pure polarization state, which is further manipulated by a half- and a quarter-wave plate (HWP and QWP, respectively) to reach an arbitrary desired polarization. The photons then enter the main optical feedback loop through a 50 : 50 beam splitter (BS). As a result, one half of the incoming light intensity is transmitted and absorbed in the avalanche photodiode detector (APD) having not entered the loop at all. This further reduces the mean photon number per pulse entering the loop, and gives a temporal reference $\tau = 0$.

In the feedback loop, the two polarization states are unitarily mixed on the “Coin HWP” as determined by Eq. (3.5), and coupled into an optical fibre. The two corresponding modes are then spatially separated using an in-fibre manufactured polarizing beam splitter. Horizontally polarized incoming photons are led to an arm of length 7 m while vertically polarized photons take another arm 8 m long. The polarization state is strictly controlled in the fibre so that the two paths merge coherently into two polarization modes of the same running wave on a second PBS. After this moment, they exit the fibre at an out-coupling element and take a common route back to the beginning of the feedback loop.

The detection of photons passing the feedback loop is done passively using the beam splitter originally inserting photons into the loop. With a probability of 0.5 at every round, the

photons can be reflected out of the loop and detected in the APD, in which the avalanche effect is exploited for single photon detection. The time of arrival is compared to the initial pulse, provided that both events have been detected, and recorded in a histogram. If desired, it is possible to split the two basis polarization states using a PBS before reaching the detector in order to measure the joint probability distribution of the arrival time and the internal state of the photons.

In the formalism of Section 3.1, we can identify, up to the mixing done at the Coin HWP, two closed paths in the feedback loop, taking times 40 ns and 45 ns, respectively. These values follow from the dimensions of the respective parts and the index of refraction of the used fibre. According to Eq. (3.4), this gives the mean time of one step $\tau_t = 42.5$ ns and a separation of $2\tau_x = 5$ ns between two adjacent positions of the same parity. This allows for observing $n_{\max} = 8$ steps of the quantum walk in non-overlapping time bins, as shown in Fig. 3. In reality, the losses on imperfect optical elements and limited detection efficiency of the APD, in connection with the inherent 50 % loss of intensity per each round due to passive out-coupling, lead to a practical maximum of 5 steps observed with sufficient level of confidence.

The most noticeable result of [A1] is not the observed probability distribution following the predicted probability distribution of position in a quantum walk on a line but the use of these data for the estimation of the amount of decoherence taking place in the setup. The methods used for this purpose resulted in a striking finding: that no effects of decoherence disruptive to the quantum walk simulation were observed at all. More precisely, any dephasing or depolarization effects could be safely neglected in the setup. The main source of error is the loss of photons. However, due to the coherent nature of the setup, linear losses only damp the detection probabilities but keep the renormalized probability distributions intact. This gives the implementation of quantum walks using optical feedback loops a great potential.

The work [A1] does not aim at presenting a flawless observation of a high number of steps of the quantum walk. Rather, it is to be perceived as a pioneering work showing that a fully optical implementation of a quantum walk with a number of optical elements constant in the intended number of steps is possible. It gives an important proof of principle, identifying the sources of the limited performance and proposing means of fighting them.

3.3 Upgrading the experiment

The follow-up experiment to [A1] made by the same experimental group addresses several points where the performance of the original experiment could be enhanced, which lead to increasing the number of observed steps up to 27. We report on this upgraded version of the experiment in [A4].

One of the weak points in the experimental realization described in Section 3.2 is obviously the 50 : 50 in-/out-coupling done on a balanced nonpolarizing beam splitter. This causes a 50 % loss of probability of a photon staying in the experiment in each round in the feedback loop, and thus each step of the simulated quantum walk. Replacing the coupling by an unbalanced beam splitter can increase the probability of the particle staying in the loop.

As a side effect, the same change further reduces the mean photon number inserted into the loop from the laser pulse and increases the amount of light evading the feedback loop

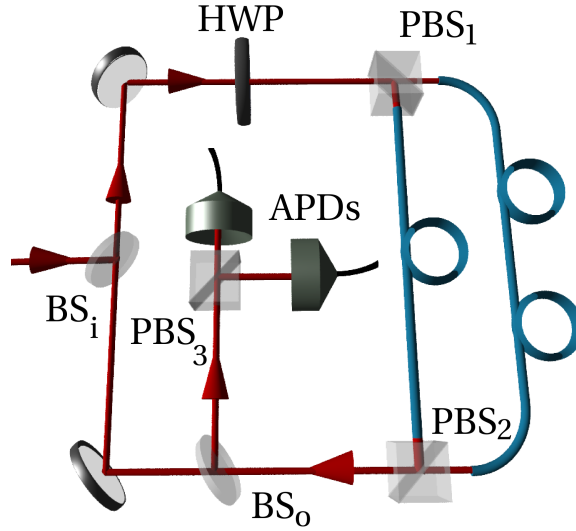


Fig. 5: Scheme of the second experiment for realizing discrete-time homogeneous quantum walks on a line [A4]. The pulse preparation chain is left out for simplicity. The new features are separate beam splitters for input and output and moving the PBS's out of the fibre, which allowed for a more precise control over the splitting.

completely. In order not to damage the APD, the directly transmitted laser light was blocked. A second out-coupling unit, using a 88 : 12 beam splitter, was inserted into the feedback loop for the purpose of detection, as depicted in Fig. 5. This allowed a further increase in the laser power.

Some of the optical elements were replaced by higher quality equivalents. More importantly, the polarizing beam splitters separating the two polarization states were realized in free space and the single-polarization modes were coupled into two distinct single-mode optical fibres. The new configuration gives $\tau_t = 59.7$ ns and $\tau_x = 2.9$ ns, so that one time bin in Fig. 3 can accommodate $n_{\max} = 10$ different positions of the quantum walker. As up to 27 steps of the quantum walk were successfully observed, the observed arrival times were decoded via a direct application of Eq. (3.4). Taking the laser pulse duration of $\Delta\tau = 88$ ps as the ultimate minimum of resolution of the arrival time, the delay between the images of (t_0, x_0) and $(t_0, x_0 + 2)$ in Eq. (3.4) could theoretically accommodate up to

$$n_x = \left\lfloor \frac{2\tau_x}{2\Delta\tau} \right\rfloor = 32 \quad (3.6)$$

extra pulses from overlapping time bins. In the currently presented case, no more than $\lceil 27/10 \rceil = 3$ time bins overlap at any τ .

The main result of [A4] is the observation of the probability distribution of the walker's position in 27 steps of a symmetric Hadamard quantum walk on a line featuring an excellent agreement with the theoretical prediction (see Fig. 6 for details), proving the easy scalability of the layout designed in Section 3.2. As a final note, we argue that the milestone of one hundred steps could be achieved if one replaced the coupling into and out of the feedback loop, currently achieved by beam splitters, by an active optical component switching between zero and full transmittivity.

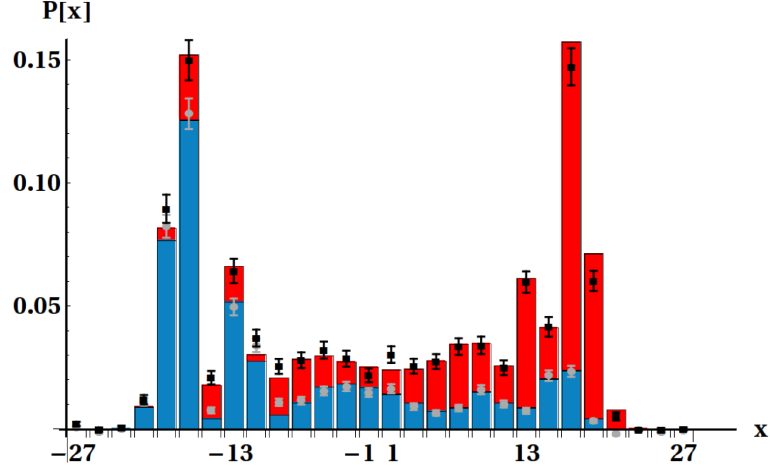


Fig. 6: Theoretical prediction (coloured bars) and experimental observation (dots with error bars) of the joint probability distribution of the position and coin state of a particle undergoing a quantum walk on a line with the Hadamard coin, starting from $x = 0$ in $t = 0$, after 27 steps [A4]. The red and blue bars (red drawn atop of blue) represent the probability of measuring the walker in position x and with coin state $|+1\rangle$ and $|-1\rangle$, respectively.

3.4 Quantum walk on a two-dimensional lattice

Employing more complex changes, it is possible to design an experimental setup similar to the one described in the previous two sections realizing a quantum walk on a 2-dimensional Euclidean lattice \mathbb{Z}^2 , *i. e.*, the Cayley graph $\Gamma(\mathbb{Z}^2, S^{(2)})$ where

$$S^{(2)} = \{(-1, 0), (1, 0), (0, -1), (0, 1)\}, \quad (3.7)$$

as already mentioned in Section 2.3.2.

For this purpose, we need a total of 4 routes of different times closing the feedback loop. It is no more possible to use a single optical fibre or free space path with different polarizations, since only two orthogonal polarization states can be separated deterministically.

One possible solution is using a different internal state of the photons. There are several possibilities, for example, frequency or optical angular momentum. The latter option is theoretically studied in [45], where a combined approach using photon two polarization states along with two optical angular momentum states is proposed.

In our approach, we used two different spatial paths, each allowing two orthogonal polarizations, to implement the 4 combinations needed for the implementation of a four-dimensional quantum coin, in the scheme outlined in Fig. 7. The separate in-/out-coupling from Fig. 5 is reused: photons can enter the feedback loop in one of the two spatial paths in either polarization (despite the fact that in the experiment, a fixed initial polarization state was actually used) but can leave for the detectors in either arm.

According to Fig. 7, the four delay times a photon can take to complete one round in the feedback loop is determined by whether it took the inner or outer free space arm (taking times τ_A or τ_B , respectively), and whether it was later coupled to a shorter or longer segment of optical fibre (taking times τ_C or τ_D , respectively). This gives

$$\begin{aligned} \tau_1 &= \tau_A + \tau_C, \\ \tau_2 &= \tau_B + \tau_C, \\ \tau_3 &= \tau_A + \tau_D, \\ \tau_4 &= \tau_B + \tau_D. \end{aligned} \quad (3.8 a)$$

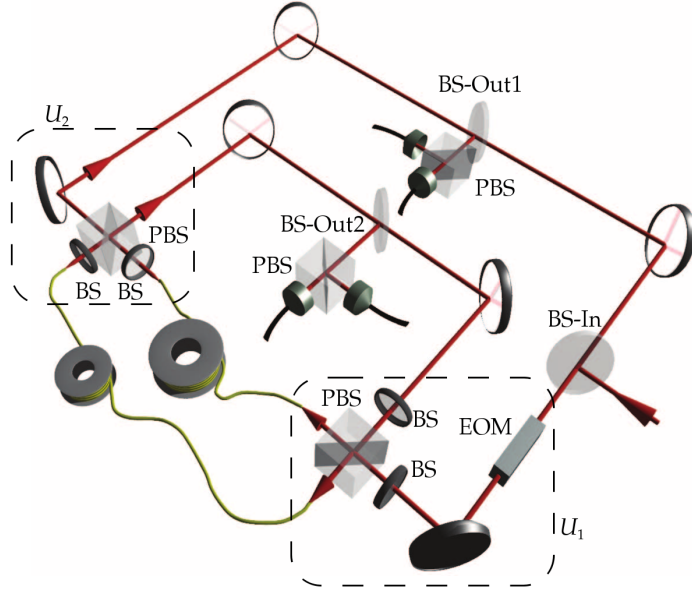


Fig. 7: Experimental setup for realizing discrete-time quantum walks on the two-dimensional Euclidean lattice [A5]. The feedback loop is formed by two parts: a pair of free space arms of different length (in red) and a pair of arms realized in polarization-maintaining optical fibres (in yellow). The transitions between the paths are controlled by a total of four half-wave plates, two polarizing beam splitters, and an optional electro-optical modulator (EOM). The unitary mixing of the paths is spatially separated into regions labelled U_1 and U_2 but can be made fully consistent with Fig. 2 by moving the two BS from U_2 to the other side of the fibres they are connected to.

If we denote

$$\begin{aligned}\tau_t &= \frac{\tau_A + \tau_B + \tau_C + \tau_D}{2}, \\ \tau_x &= \frac{\tau_B - \tau_A + \tau_D - \tau_C}{2}, \\ \tau_y &= \frac{\tau_A - \tau_B + \tau_D - \tau_C}{2},\end{aligned}\tag{3.8 b}$$

then the times $(\tau_i)_{i=1}^4$ can be written in the form

$$\begin{aligned}\tau_1 &= \tau_t - \tau_x, \\ \tau_2 &= \tau_t - \tau_y, \\ \tau_3 &= \tau_t + \tau_y, \\ \tau_4 &= \tau_t + \tau_x.\end{aligned}\tag{3.8 c}$$

N. B. that the equation $\tau_1 + \tau_4 = \tau_2 + \tau_3$, necessary for this equivalence, is automatically satisfied by Eq. (3.8 a). An independent choice of $(\tau_i)_{i=1}^4$ would not, in general, allow for the introduction of the values τ_t, τ_x, τ_y in the same manner.

A translation in the τ axis by one of the four delays can be interpreted as one step of a simulated quantum walk in the x or the y direction, in a complete analogy to Eq. (3.4) and the subsequent discussion. The transition between the walking space parametrized by coordinates x and y with the quantum walk time t and a single time axis τ is described by the mapping

$$\tau = \sum_{i=1}^4 k_i \tau_i = t\tau_t + x\tau_x + y\tau_y.\tag{3.9}$$

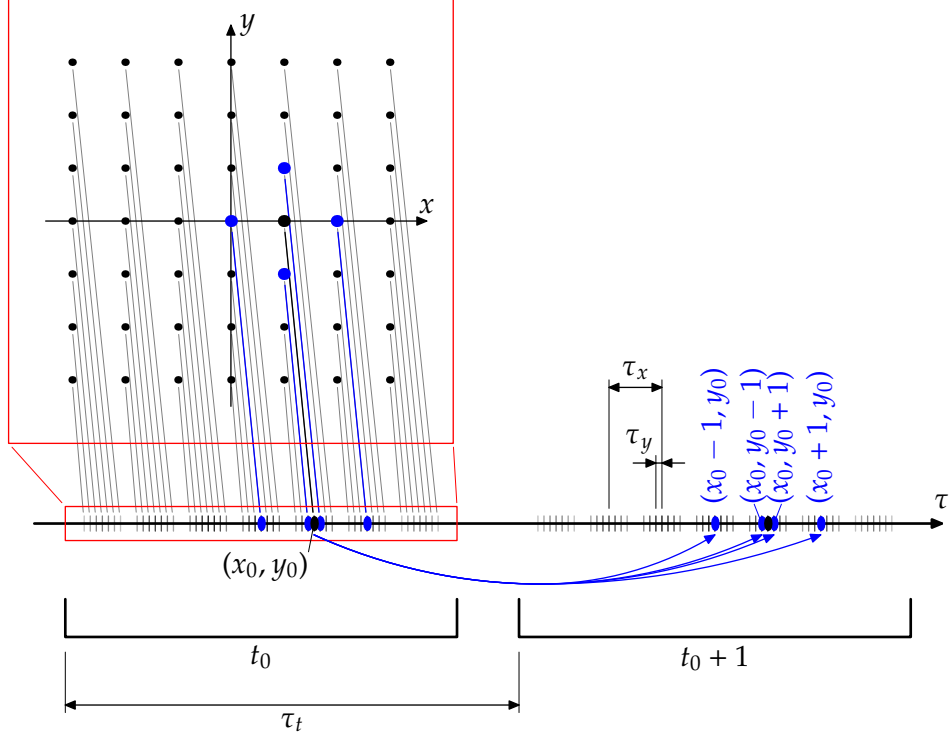


Fig. 8: Projection of the (t, x, y) space onto a single real line (detail in red). Blue arrows show the four possible round times of a pulse in the delay loop, transferring the image of an arbitrary position (x_0, y_0) at time t_0 (black) along the τ axis to that of either of its neighbours at time $t_0 + 1$ (blue).

Fig. 8 illustrates this reduction graphically in the conditions $\tau_y \ll \tau_x \ll \tau_t$. Similarly to the discussion in Section 3.3, however, these conditions are not crucial in the framework.

The main results of [A5] are the measurements of the probability distributions of the position of a particle undergoing 10 steps of a 2-dimensional quantum walk with a fixed initial state $|0, 0\rangle \otimes |-1, 0\rangle$. The coin matrices corresponding to the settings used in the experiment are

$$C_1 = H \otimes H = \frac{1}{2} \begin{pmatrix} 1 & 1 & 1 & 1 \\ 1 & -1 & 1 & -1 \\ 1 & 1 & -1 & -1 \\ 1 & -1 & -1 & 1 \end{pmatrix} \quad (3.10 \text{ a})$$

and

$$C_2 = C_1 \begin{pmatrix} 1 & 0 & 0 & 0 \\ 0 & 1 & 0 & 0 \\ 0 & 0 & 0 & -1 \\ 0 & 0 & 1 & 0 \end{pmatrix} = \frac{1}{2} \begin{pmatrix} 1 & 1 & 1 & -1 \\ 1 & -1 & -1 & -1 \\ 1 & 1 & -1 & 1 \\ 1 & -1 & 1 & 1 \end{pmatrix}. \quad (3.10 \text{ b})$$

The reason for choosing (3.10 a) was that a tensor product of Hadamard matrix with itself is the most straightforward generalization of Hadamard walk to the higher-dimensional walking space. Indeed, a striking resemblance of the measured profile in Fig. 9 a) to the Hadamard walk in Fig. 6 is readily seen. The second coin was chosen as a minimum variation of C_1 resulting in a far more involving dynamics (Fig. 9 b)).

In this work, the primary measure of the match between the probability distribution predicted by the theoretical description and the empirical probability distribution, obtained by observing a large number of repetitions of the experiment, is the *similarity*

$$S = \left(\sum_{x \in \mathbb{Z}} \sqrt{p_{\text{theory}}(x)p_{\text{exp}}(x)} \right)^2, \quad (3.11)$$

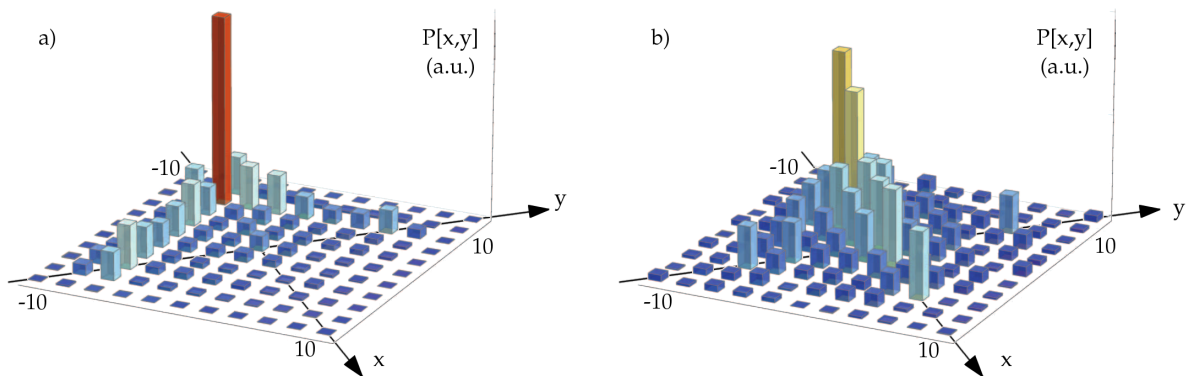


Fig. 9: Experimental observation of a two-dimensional quantum walk [A5]. The probability distribution of the position of the quantum walker after 10 time steps has been measured using the experiment in Fig. 7. The initial coin state of the walker was $| -1, 0 \rangle$. The direction of motion in the negative x -axis is strongly prevalent in the two-dimensional Hadamard walk (*Inset a*). The effect is less pronounced in the case of a different coin, given by Eq. (3.10b) (*Inset b*), where the probability distribution is spread over the walking spaces, but remains noticeable. Only the positions actually reached by the walker are plotted, which results in the diamond shape of the graph.

a quantity related to the Hellinger distance of the two probability distributions. As stated in the publication, the similarity ranged from 0.903 ± 0.018 for the C_2 coin to 0.957 ± 0.003 for the Hadamard C_1 coin after 10 steps of the quantum walk.

As a final note, we emphasize that unlike the one-dimensional experiment described in Section 3.2, the experimental setup used in [A5] is not directly able to realize an arbitrary $U(4)$ operation on the coin state of the simulated quantum walk. In order to cover all distinct cases, according to Section 2.3.2 one would need a minimum of 8 tunable parameters to match the number of free parameters of $U(4)$ reduced by the number of removable outer phases. However, only 4 parameters are controllable using the half-wave plates in the experiment. This discrepancy can be fixed by adding more polarization-sensitive elements into the setup, but such a solution would also involve topological modifications of the experiment, at which no attempt was purposely taken in [A5] in favour of the comprehensibility of the report.

3.5 Quantum walk of two particles

A new element introduced in the experimental setup in Fig. 7 is the electro-optical modulator (EOM), an active element allowing to induce a dynamically controlled phase shift on the two polarization components of the photons passing it. The EOM acts as a wave plate of a variable width, controlled by the voltage applied on the element by a computer interface. The EOM is capable of switching between different configurations within the nanosecond time scale, allowing one to control individual pulses passing through the element independently in the current setup.

In the experiment described in the last section, we can use the EOM to apply an additional position-dependent change in the coin of the simulated quantum walk. This is achieved by sending a periodic input signal with period τ_t to the element such that the phase setting of the EOM is the same in the projection of points differing only in their t coordinate.

We use this framework to simulate a quantum walk of two interacting quantum particles on a line.

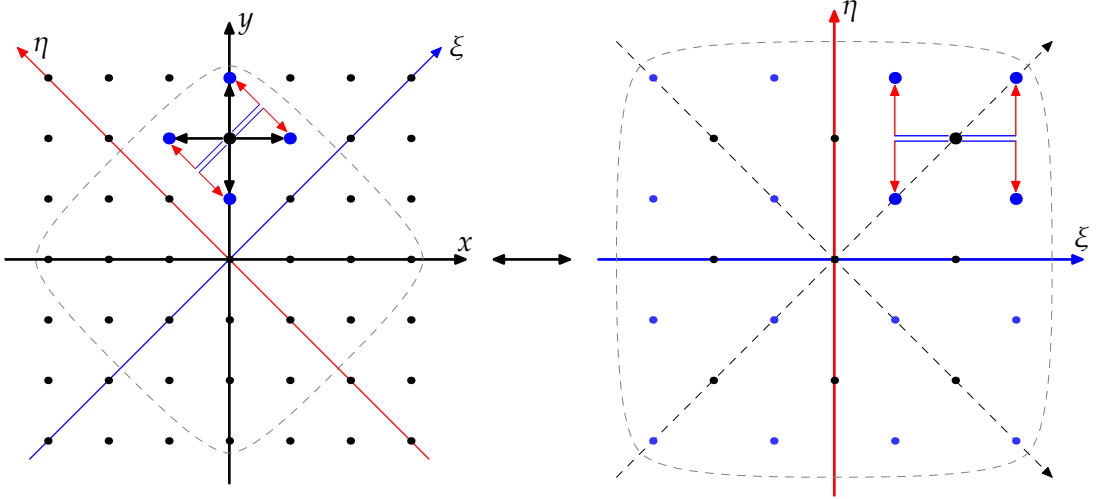


Fig. 10: The equivalence of a two-dimensional walk with a walk of two particles. *Left inset:* One step over an edge of a Cartesian lattice in coordinates x and y can be interpreted as a composition of one step in the coordinate ξ followed by one step in the coordinate η . *Right inset:* Redrawing the same picture rotated by 45° , one can see that a walker starting in a localized state is confined at each instant to one out of two Cartesian lattices (blue and black points) in the latter coordinates, too.

Firstly, we note that the relation between a walk on a two-dimensional lattice and a walk of two particles in a classical setting is straightforward—by defining a transformation of the coordinates (x, y) to a new coordinate system (ξ, η) , where

$$\xi = x + y, \quad \eta = y - x, \quad (3.12)$$

any step along either of the original coordinates changes both the new coordinates by $+1$ or -1 , as depicted in Fig. 10. Interpreting ξ and η as single coordinates of two imaginary particles constrained to the one-dimensional lattice of integer numbers \mathbb{Z} , one can say that both of these particles make one random walk step as t goes to $t + 1$.

In a discrete-time quantum walk, the motion of the particle, or particles, is controlled by the respective coin state. In the picture of the two walkers, it must be accepted as a fact that the original coin transformation applied on the 4-dimensional coin register generally creates entanglement between the 2-dimensional coins of the two imaginary walkers.

More precisely, the state space of a system of two distinguishable quantum walks on a line is

$$(\mathcal{H}_S^{(\mathbb{Z})} \otimes H_C^{(2)}) \otimes (\mathcal{H}_S^{(\mathbb{Z})} \otimes H_C^{(2)}) \quad (3.13 \text{ a})$$

with $\mathcal{H}_S^{(\mathbb{Z})}$ and $\mathcal{H}_C^{(2)}$ defined in Eq. (2.10). This space is isomorphic to

$$(\mathcal{H}_S^{(\mathbb{Z})} \otimes \mathcal{H}_S^{(\mathbb{Z})}) \otimes (H_C^{(2)} \otimes H_C^{(2)}), \quad (3.13 \text{ b})$$

which in turn can be identified with the state space of a two-dimensional quantum walk, analogously denoted as

$$\mathcal{H}_S^{(\mathbb{Z}^2)} \otimes \mathcal{H}_C^{(4)}. \quad (3.13 \text{ c})$$

Here, any operator $U \in U(4)$ acting on the $\mathcal{H}_C^{(4)}$ space that lacks the structure of a tensor product of two 2-dimensional unitary operators inevitably brings separable states in $\mathcal{H}_C^{(2)} \otimes \mathcal{H}_C^{(2)}$ to entangled states.

N. B. that we can identify a similar effect in the classical scenario, too. If a two-dimensional classical random walk is not balanced, the random displacements in the coordinates ξ and η in its two-particle equivalent generally become mutually dependent random variables.

Coming back to the experimental setup described in the last section, we can simulate specific walks of two particles choosing various parameters of the coin and/or initial state of the simulated two-dimensional walk. One of the operational modes is a simulation of two noninteracting distinguishable particles, for which a homogeneous separable quantum coin operation is sufficient.

One can, however, also simulate the quantum dynamics of pairs of indistinguishable particles. In many-body quantum mechanics, indistinguishability manifests itself as a restriction of the state space to states symmetric or antisymmetric with respect to a formal (passive) particle exchange, as well as a restriction of operations applicable on the state by any physical means to those which conserve this property. By imposing the same set of restrictions to the simulated pair of quantum walkers, *i. e.*, a symmetry or antisymmetry of the initial state and quantum coin operator with respect to a swap of the roles of ξ and η , one could receive results consistent with bosonic or fermionic behaviour of the walkers, respectively.

Systems with interactions between the two walkers can also be simulated; however, for this purpose, the need for a fast-switching EOM is inevitable. For example, a point-like interaction between the two walkers influences the wave function of the composite system only in points satisfying $\xi = \eta$, or $x = 0$ in the original coordinates. This is modelled by activating the EOM only in the appropriate times τ , as given by Eq. (3.9).

In [A5], we report on observing the probability distribution of 10 steps of a quantum walk of two identical noninteracting distinguishable walkers performing a Hadamard walk, which is identical to the result in Fig. 9 a). As a more involving example, we present the simulation of 7 steps of a two-particle quantum walk of distinguishable particles featuring an engineered point-like interaction.

The interaction is implemented as an additional unitary transform acting in the coin state in points where $\xi = \eta$. Namely, for all points in the plane where ξ and η have different values, a coin matrix of the form (3.10 a) is applied. For points on the diagonal, where the particles interact, the coin matrix

$$C_{\text{int}} = C_1 \begin{pmatrix} 1 & 0 & 0 & 0 \\ 0 & 1 & 0 & 0 \\ 0 & 0 & 1 & 0 \\ 0 & 0 & 0 & -1 \end{pmatrix} = \begin{pmatrix} 1 & 1 & 1 & -1 \\ 1 & -1 & 1 & 1 \\ 1 & 1 & -1 & 1 \\ 1 & -1 & -1 & -1 \end{pmatrix} \quad (3.14)$$

is used instead. This is inspired by nonlinear systems, where a site exhibits a higher or lower potential energy if more than one particle occupies it; however, the particular interaction defined by Eq. (3.14) has no known real-world equivalent. Generally, nonlinearity in systems of multiple particles can result in a formation of bound “molecule” states. As seen in Fig. 11, a similar behaviour can indeed be observed in the simulated two-particle dynamics. The data needed to decide whether we are really observing a stable state of the two-particle system in question is currently unavailable due to the limited number of steps, which suffers significantly from the low transmittivity of the included EOM. We believe, however, that a future version of the experiment using a light source of different wavelength, better suiting the commercially available optical components, could provide an outstanding experimental tool for this new intriguing area of physics of small systems.

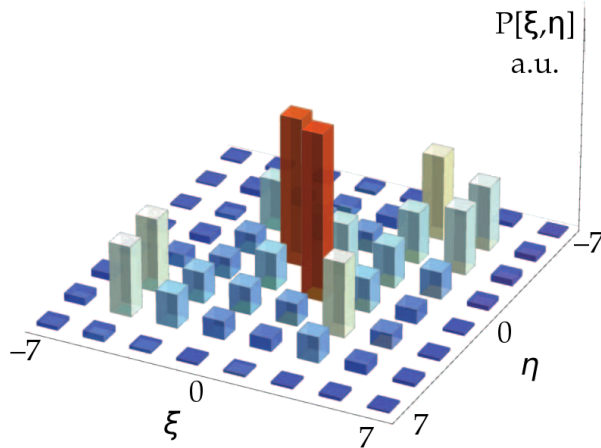


Fig. 11: Results of a simulation of a quantum walk of two particles on a line with a point-like interaction [A5]. The high probability concentrated on the diagonal of the graph where $\xi = \eta$ is a noticeable signature of bound states. 7 steps were observed with a similarity of 0.957 ± 0.013 with a numerical prediction. Only positions with both coordinates odd are plotted as all other positions have a vanishing probability of occupation.

3.6 Chapter summary and outlook

The topic of this chapter were optical implementations of discrete-time quantum walks, presented from a theoretical introduction to a report on a series of successful experimental realizations published in leading scientific journals [A1,A4,A5]. The method of optical feedback loop simulation proves to be a very promising experimental scheme, featuring negligible decoherence and high control of the experiment, both while keeping the build and maintenance costs at very affordable rates. 27 observed steps of a one-dimensional walk and 10 steps in the two-dimensional case make it one of the world's top tools for the purpose of quantum walk realization.

A very important aspect of being able to control and measure quantum walks in two-dimensional lattices is the possibility of simulation of two-particle dynamics. The direct access to the two-dimensional configuration spaces allows us to imprint even very elaborate models of interactions onto the two-particle system, unavailable by other means, and gives hope to study or even discover new physical phenomena happening under such conditions.

By using a feeble yet classical light source and benefiting from the stability of coherent light pulses in the presence of losses, the experimental setup also opens new intriguing questions about physics at the boundary between classical and quantum theories of coherence [A5].

My contribution in this joint work dates back to the very design of the experimental layout. Some primal attempts at optical feedback schemes can be found in my Master's thesis [46]. Later I participated in data analysis and processing in the first experiment [A1] and in the identification of sources of errors using this input. In more recent experiments, I actively participated in the design of the upgrades of the experiment and the optimization of its setup.

I conclude this chapter by a brief overview of the possible directions of future development of the optical feedback loop implementation of quantum walks.

Firstly, new schemes need to be explored to generalize the setup to simulate quantum walks in higher-dimensional lattices. One option is to further enlarge the number of interferometric

arms forming the feedback loop. Alternatively, some of the properties of photons pointed out in the beginning of Section 3.4 could be utilized. The employment of optical angular momentum state of light for this purpose is being actively studied [45].

New possible applications of the current version of the experiment include the study of quantum walks on graphs with percolations, simulation of bosonic or fermionic modifications of the two-particle quantum walk, or an implementation of a search algorithm based on quantum walks on an Euclidean lattice in the model of [7] or [8].

Chapter 4

Exploring the effects of randomness in quantum walks

Despite the fact that quantum walks are usually defined and often studied in closed quantum systems using unitary quantum dynamics, in realistic scenarios, the consideration of effects of various kinds of errors is inevitable. The possible sources of errors may be sorted into several categories:

1. decoherence in internal state of the walker [47,48], including dephasing [49–51] and thermal effects [11,12];
2. topological errors, *e. g.*, broken links or percolations [52–54], sudden jumps across several edges [A3], imperfect wave packet localization [55];
3. information leakage, random measurements, full or partial [56,57], and particle loss [A1].

In spite of the conceptual differences between the errors considered in the first two items, numerous reports indicate a common observation. Namely that if a random position-dependent error of almost arbitrary kind chosen independently from identical distributions is applied in each time step of the walk, the quantum nature of the walk recedes in favour of a classical random walk. The same holds for projective measurements of the position and/or coin (in coined quantum walks) at random points. It follows directly from the corresponding definitions that the limit case of performing a full projective measurement of the position and a full mixing of the internal state of the walker at every step (a continuous measurement in the case of continuous-time quantum walks) recovers a fully classical random walk. As shown in the following sections, some dephasing models can be shown to be equivalent to projective quantum measurements or mixing in their strongest case, therefore sharing the same limit.

It is worth noting that random fluctuations may not necessarily make quantum walking less useful. The authors of [11] and [12] argue that the environmental noise in photosynthetic energy transfer caused by room temperature actually helps to focus and target the excitation. The authors of [47] explicitly show the benefits of a small amount of decoherence for mixing and hitting times of discrete-time quantum walks.

A different kind of randomization in quantum walks is static disorder [58,59,A2,A3]. In this model, fluctuations in the on-site parameters of the walking space are chosen randomly but stay constant during the quantum walk. The measurable quantities are studied in terms of their expectation values under the prior random selection; alternatively, one may inquire on the averaged final quantum state of many samples of the same procedure. It has been shown in the cited works that these systems are capable of displaying Anderson localization effects [13].

4.1 On-site randomness

We studied the effects of random environment or random fluctuations in a quantum walk modeled by introducing randomness in the quantum coin operator. That is, the time evolution operator of one step of a quantum walk, Eq. (2.7), is replaced by a random operator, allowing an explicit time dependence, too:

$$U(t \mapsto t + 1; \omega) = S \cdot C_t(\omega), \quad (4.1 \text{ a})$$

where

$$C_t(\omega): |x\rangle \otimes |\gamma\rangle \mapsto |x\rangle \otimes C_{t,x}(\omega)|\gamma\rangle, \quad \forall x \in G, \forall |\gamma\rangle \in \mathcal{H}_C, \quad (4.1 \text{ b})$$

and ω is chosen from an appropriate sample space Ω .

The object in question is the mean probability distribution of the particle's position after a fixed number of steps t ,

$$p_t(x) = \mathbb{E}[\mathbb{P}_t(X = x)]. \quad (4.2)$$

In the model of *dynamic disorder*, where the random operators C_t applied at different times t are mutually independent, the evolution of the system becomes Markovian and the averaging over Ω can be performed at every step at the level of quantum state. In this case, the dynamics is fully described by the evolution of a quantum state ϱ_t which follows the recurrence relation

$$\varrho_{t+1} = \mathbb{E} \left[U(t \mapsto t+1; \omega) \varrho_t U^\dagger(t \mapsto t+1; \omega) \right] = \int_{\Omega} U(t \mapsto t+1; \omega) \varrho_t U^\dagger(t \mapsto t+1; \omega) \mathbb{P}(d\omega). \quad (4.3)$$

Given a specification of $C_t(\omega)$, the final integral may be evaluated to give a completely positive trace-preserving (CPTP) superoperator acting on the state ϱ_t :

$$\varrho_{t+1} = \mathcal{U}(t \mapsto t+1)[\varrho_t]. \quad (4.4)$$

Due to the form of Eq. (4.1), the step operator can be factored out of the superoperator \mathcal{U} and the action of the coin remains local. Moreover, if the coin operator components $C_{t,x}$ are homogeneous in x for each realization ω , Eq. (4.4) can be rewritten as

$$\varrho_{t+1} = \mathcal{S}[\mathcal{C}_t[\varrho_t]], \quad \mathcal{S}[\varrho] = S\varrho S^\dagger, \quad \mathcal{C}_t[\varrho] = \sum_{x,y \in G} |x\rangle \tilde{\mathcal{C}}_t[\langle x|\varrho_t|y\rangle] \langle y|, \quad (4.5 \text{ a})$$

where

$$\tilde{\mathcal{C}}_t[X] = \int_{\Omega} C_{t,x_0}(\omega) X C_{t,x_0}^\dagger(\omega) \mathbb{P}(d\omega) \quad (4.5 \text{ b})$$

is a superoperator acting on bounded operators on the coin register alone. Alternatively, if for various x , $C_{t,x}$ are independent and identically distributed with $\mathbb{E}[C_{t,x}] = \Gamma_t$, \mathcal{C}_t takes a more complicated form

$$\mathcal{C}_t[\varrho] = \sum_{x \in G} |x\rangle \tilde{\mathcal{C}}_t[\langle x|\varrho_t|x\rangle] \langle x| + \sum_{\substack{x,y \in G \\ x \neq y}} |x\rangle \Gamma_t \langle x|\varrho_t|y\rangle \Gamma_t^\dagger \langle y|. \quad (4.5 \text{ c})$$

However, if Γ_t is zero, Eq. (4.5 c) shows that any superposition of different positions is lost in the action of \mathcal{C}_t , which is equivalent to a full projective measurement in the position basis (ignoring the measurement result), followed by a CPTP operation $\tilde{\mathcal{C}}_t$ on the coin register. Note in particular that a sufficient condition for $\Gamma_t = 0$ is that the coin elements $C_{t,x}$ are of the form

$$C_{t,x} = e^{i\varphi_{t,x}(\omega)} C_0, \quad \forall x \in G, \quad (4.6)$$

where the phase $\varphi_{t,x}(\omega)$ is uniformly distributed for each $x \in G$, *i. e.*, if different sites $x \in G$ only apply a uniformly distributed random additional phase atop of a constant coin operator element.

Various schemes of coin randomization may be studied. An illustrative example is a “fuzzy” coin centered at C_0 , defined by

$$C_{t,x}(\omega) = F(\omega)C_0, \quad (4.7)$$

where $F(\omega)$ is a random unitary matrix on \mathcal{H}_C following any distribution invariant to all basis rotations. In this case, Eq. (4.5 a) applies with

$$\tilde{C}_t[X] = (1 - p)C_0XC_0^\dagger + p\frac{\text{Tr } X}{\dim \mathcal{H}_C}\mathbb{1}_C, \quad p \in \langle 0, 1 \rangle \quad (4.8)$$

This is a standard model of decoherence in the coin register. For a full decoherence, $p = 1$, the coin becomes separated from the position register and completely mixed in each step of the quantum walk, resulting in a step in any direction with equal probability, recovering a fully classical random walk.

Specific systems or experimental realizations can motivate the consideration of more specialized models of randomization of the coin operator. We will address one such decoherence model, particular to quantum walks on a line, in Section 4.2.

Complementary to the concept of dynamic disorder is *static disorder*. In this model, the random operators $C_{t,x}(\omega)$ in Eq. (4.1 b) are independent of t . Therefore, every instance $\omega \in \Omega$ corresponds to a quantum walk with a possibly position-inhomogeneous, but always time-homogeneous coin. This assumption can be used to model quantum walks on random but stable environments. The expected distribution of the particle’s final position must be computed by averaging different such quantum walks, which corresponds to finding the *typical* behaviour of the quantum walk in a randomly selected environment. Systems with static disorder are usually studied using Monte Carlo methods.

4.2 Modelling randomness experimentally

A simulation of random effects described in the last section can be easily realized using the optical feedback loop implementation of a quantum walk on a line. For a coin operator transforming the internal coin state of the walker differently at different positions x and quantum walk times t , we use an electro-optical modulator inserted into the main feedback loop, as outlined earlier in Section 3.5 within the two-dimensional quantum walk setting.

In [A2], we present results of the experiment built for this purpose. Its design is identical to Fig. 5 with the difference that a fast-switching EOM is inserted between the Coin-HWP and PBS₁. This seemingly small modification opens up a multitude of new possible applications.

4.2.1 Dynamic disorder

Dynamic disorder can be reached by connecting the EOM to a pseudorandom signal generator. The mathematical model of the quantum walk simulated in the experiment is then described by Eqs. (4.5 a) and (4.5 c). The operator applied to the coin state of the walker in time t and at

position x by the combined effect of the HWP and the EOM can be expressed by a matrix in the preferred polarization state basis of the form

$$C_{t,x}(\omega) = \begin{pmatrix} e^{i\varphi_H(\omega)} & 0 \\ 0 & e^{i\varphi_V(\omega)} \end{pmatrix} C_{\text{HWP}}, \quad (4.9)$$

where C_{HWP} is of the form (3.5). The random values φ_H and φ_V are correlated, it has been found that for the EOM used in the experiment at the wavelength of the laser,

$$\varphi_V(\omega)/\varphi_H(\omega) = r = \text{const.}, \quad r \approx 3.5 \quad (4.10)$$

for all ω . Hence, we can write

$$C_{t,x}(\omega) = \exp(i\varphi_H(\omega)R) C_0, \quad R = \begin{pmatrix} 1 & 0 \\ 0 & r \end{pmatrix}. \quad (4.11)$$

We can see that the operation applied on the polarization state by the EOM is a random element of a fixed one-parametric subgroup of $U(2)$ generated by the matrix R .

For the following derivation, let us assume a more general form of the generator R ,

$$R = \lambda_1 \Pi_1 + \lambda_2 \Pi_2, \quad (4.12)$$

where Π_1 and Π_2 are two orthogonal projectors forming a decomposition of unity. For convenience, let the parameter $\varphi_H(\omega)$ is distributed symmetrically around zero. Then the components of Eq. (4.5 c) can be found in the form

$$\begin{aligned} \Gamma_t &= (E[\cos \varphi_H \lambda_1] \Pi_1 + E[\cos \varphi_H \lambda_2] \Pi_2) C_0, \\ \check{C}_t[X] &= p C_0 X C_0^\dagger + (1-p)(\Pi_1 C_0 X C_0^\dagger \Pi_1 + \Pi_2 C_0 X C_0^\dagger \Pi_2), \end{aligned} \quad (4.13 \text{ a})$$

where

$$p = E[\cos \varphi_H (\lambda_2 - \lambda_1)]. \quad (4.13 \text{ b})$$

The explicit properties of the distribution of $\cos(\varphi_H \lambda_{1,2})$ and $\cos(\varphi_H (\lambda_1 - \lambda_2))$ depend on the details of the implementation of the random source and the response characteristic of the EOM. However, it is simple to find the limit case of Eq. (4.13) when the expected values of all these functions reach zero. Here,

$$\Gamma_t = 0, \quad \check{C}_t[X] = \Pi_1 (C_0 X C_0^\dagger) \Pi_1 + \Pi_2 (C_0 X C_0^\dagger) \Pi_2. \quad (4.14)$$

According to Eq. (4.5 c), this result is equivalent to the application of C_0 on the coin register followed by a full projective measurement of the walker's position and a projective measurement of the coin state. The measurement operators of the coin are the projectors Π_1 and Π_2 , *i. e.*, the generator R is measured as an observable (the result of the measurement is irrelevant).

It can be easily seen that a quantum walk with this kind of decoherence becomes a classical random walk where the direction, given by the coin state after its equivalent measurement, depends probabilistically on the coin state in the previous time step. The transition probabilities of this Markovian process are the squared moduli of the C_0 matrix.

In the experiment, the random source was fine-tuned so that this limit case could be observed. Given R in the form (4.11), the equivalent measurement applied on the coin is a measurement in the basis of horizontal and vertical polarizations, *i. e.*, $| -1 \rangle$ and $| +1 \rangle$. Moreover, the coin HWP was rotated by $\frac{\pi}{8}$ so that it applied the Hadamard transform on the polarization states. The resulting transition probabilities between each pair of classical coin states are then $|\langle \pm 1 | H | \pm 1 \rangle|^2 = \frac{1}{2}$, *i. e.*, any information of the previous coin state is deleted. Indeed, the experiment confirmed a fully classical unbiased binomial random walk. The observed probability distribution is plotted in Fig. 12 a).

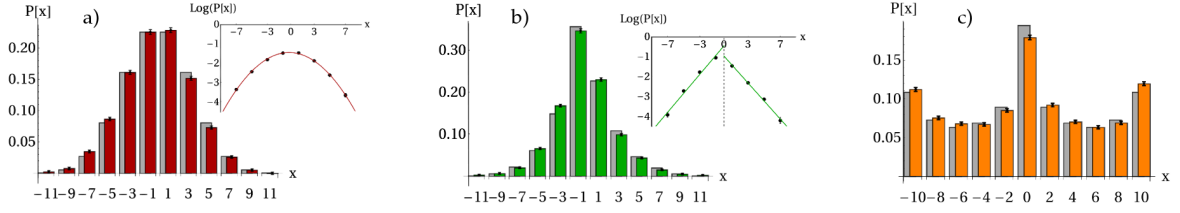


Fig. 12: Results of the observation of quantum walks on a line in three different disorder scenarios [A2]. *Inset a:* Dynamic disorder, $t = 11$ steps, showing purely classical random walk behaviour. *Inset b:* Static disorder, $t = 11$ steps, resulting in exponential localization near the initial position (*cf.* the logarithmic plot). *Inset c:* Slow variation of a homogeneous coin, also displaying localization effect. The averaged probability distribution in position after 10 steps is shown. *All insets:* Coloured bars with error marks—experimental data, colourless bars (behind)—theoretical prediction.

4.2.2 Static disorder

The effects of static disorder in quantum walks on a line can be observed if the pseudorandom source controlling the EOM is configured to produce periodic output, with the period equal to τ_t of Eq. (3.4), but changing between the runs of the experiment, *i. e.*, on the time scale given by the repetition rate of the pulsed laser source. This creates a random coin operator expressed by a matrix formally equivalent to Eq. (4.9), but with $C_{t,x}(\omega)$ constant in t .

The result of the experiment is the observation of exponential localization after 11 steps of the quantum walk. The experimental data, shown in Fig. 12 b), display a clear manifestation of the phenomenon.

4.2.3 Slow fluctuations of the coin

As a special case complementing the static and dynamic disorder models, we studied a model of coin randomization where the coin operator is homogeneous both in time in space in each run of the experiment but its parameters vary randomly between individual runs. This is called the assumption of slow fluctuations, as opposed to fast fluctuations which define the dynamic disorder. The intention of the measurement is to find a set of *typical* features characterizing the probability distributions of homogeneous quantum walks with different coin settings.

As expected, we observe two peaks at the end points of the interval $\{-t, \dots, t-1, t\}$ reachable in t steps as a remnant of the two-peak character of pure discrete-time quantum walks on a line. The peaks are most pronounced at the very boundary of the interval. There is an additional peak in the center of the distribution, which may seem unexpected at first sight (see Fig. 12 c)).

As shown in many works, *e. g.*, by Konno [44], the probability distribution of position of a quantum walker after t steps of a homogeneous discrete-time quantum walk on a line, if the initial position is, for simplicity, $|0\rangle \otimes | +1\rangle$, can be approximated by the function

$$p_t(x) = \frac{s}{\pi t (1 - \xi^2) \sqrt{c^2 - \xi^2}} (1 - (c^2 - s^2)\xi), \quad (4.15 a)$$

where

$$\begin{aligned} \xi &= \frac{x}{t}, \\ c &= |\langle +1|C_0|+1\rangle| = |\langle -1|C_0|-1\rangle|, \\ s &= |\langle +1|C_0|-1\rangle| = |\langle -1|C_0|+1\rangle|, \end{aligned} \quad (4.15 b)$$

as $t \rightarrow +\infty$. Integrating this function for fixed t over various angles θ in Eq. (3.5), which is the parametrization of the C_0 used in [A2], we indeed obtain a theoretical prediction of a peak of probability at $x = 0$. Surprisingly, we obtain as a side result that the two peaks at the boundary of the interval are artifacts of the low value of t and are asymptotically suppressed.

4.3 Quantum walks with jumps

In [A3], we study randomness manifested in the form of topological errors in the walking graph, represented by random jumps of a fixed length. More specifically, the step operator in the one-step evolution operator of a quantum walk on a line, (2.11), is augmented by a random jump operator,

$$S(\omega) = (J_t(\omega) \otimes \mathbb{1}_C)S, \quad (4.16)$$

where $J_t(\omega)$ is chosen from a subset of permutation operators on the position space satisfying

- the permutations contain only cycles of lengths 1 and 2,
- 2-cycles transpose only couples of basis elements corresponding to positions in a fixed distance j .

In the numerical treatment of the model, the system is constrained to a finite subinterval of the line of size N . The size of the walking space is large enough for the boundary conditions not to influence the evolution of a walker initiated in a state localized in the middle of the interval during n steps. The probability assigned to a jump composed of k transpositions is proportional to $p^k(1-p)^{N-2k}$, where $p \leq \frac{1}{2}$. This model does not have any limit probability distribution as $N \rightarrow +\infty$ —without the restriction on the size of the walking space, the source of errors would have to be redefined to cover the area the walker can actually reach in each step. The meaning of the distribution is, however, that a walker at any position and time has a probability of $2p$ of encountering a jump. The coin operator is left unperturbed.

It is assumed that a jump does not cause any disruption to the synchronization of the steps of the quantum walk. Rather than the walker missing some vertices, an occurrence of a jump should be perceived as a random fluctuation in the media in which the quantum walk takes place that cause it to become transparent to the walker and thus allow it to cover a bigger distance during a single time step. This could be related to a similar effect known in plasma physics or semiconductor science as ballistic flights (see, e. g., [60]). For further compliance with the introductory chapters, the presence of jump should be understood as an extra edge in the walking graph, redefining the “nearest neighbors” of the affected vertices when present.

We define dynamic disorder and static disorder in a complete analogy to Section 4.1. In the former case, one can observe a convergence to a Gaussian-like distribution when the probability of elementary error p is large, similarly to on-site randomization models. However, one can identify traces of the choice of the constant j in the form of an additional oscillatory structure superimposed over the overall probability distribution. This is because the randomized step operator (4.16) acts like a classical random walk step of size j as p approaches $\frac{1}{2}$.

The study of static disorder reveals another observation. The global evolution of the averaged probability distribution $p_t(x)$ in time t displays significantly different behaviour in the cases of even and odd parity of the jump size j , respectively. In the former case, the probability

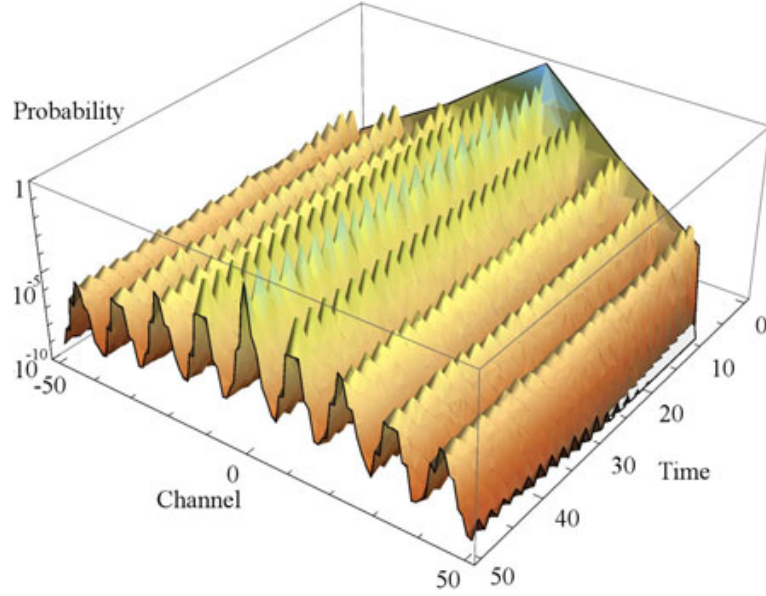


Fig. 13: Numerical evidence of a new kind of behaviour in quantum walks with jumps [A3]. When the probability of making a random jump approaches unity within the static model of disorder, with an odd jump size j , the mean probability distribution p_t assumes the shape of an exponential distribution modulated by sharper exponential peaks separated by the constant j (in this figure, $j = 11$). The static disorder was simulated using Monte Carlo method, averaging over 20,000 runs in randomly varied configurations. Minor oscillations of period 2 in time T can be observed, attributed to parity considerations. N. B. that the term “channel” is used for the quantum walk position in accordance with the terminology used in the source.

distribution displays strong artifacts of a classical random walk performed by the incoherent jumps. Surprisingly, though, this is not the case when even-sized jumps are replaced by odd-sized ones. Here, for jump probabilities $p \lesssim \frac{1}{2}$, a new behaviour unlike any case described so far becomes dominant (see Fig. 13). An exponential localization takes place at two different length scales, in the form of an overall Laplace-like distribution modulated by periodic exponential peaks located at distances of integer multiples of j from the initial position of the walker. There is a numerical evidence that the variance of this distribution becomes sub-linear in time t , which replaces both linear dependence of classical random walks and a quadratic one typical for quantum walks. However, an analytic proof of this conjecture has not yet been given.

The final area studied in [A3] is the analysis of the spread of the quantum walker’s position in the static disorder scenario with jumps of odd size j and searching for fitting functions of various measures of delocalization. We primarily focus on the variance of the walker’s position as a function of time t , probability p and jump size j . Interpolating simulation data, we provide a numerical fit of the variance at $t = 200$ parametrized by the values of p and j . According to our findings, a simple fitting function can be found which the two parameters do not enter independently but always forming a term of the form pj^α , where $\alpha = \text{const}$. This hints at a possible relationship between instances of the system at different length scales given by j .

Besides the variance of position, we also study several entropy measures of the corresponding distribution. The most interesting result is the numerical evidence that unlike other quantities taken into account, the Tsallis q -entropy of the distribution $p_t(x)$ for $q = 2$, defined by

$$S_2(p_t) = 1 - \sum_{x \in \mathbb{Z}} p_t^2(x), \quad (4.17)$$

taken as a function of the parameters p and j and time t , is very robust with respect to j even for values of t in hundreds of steps.

4.4 Chapter summary and outlook

Studying the effects of randomization in quantum walks is an important prerequisite in understanding quantum walk systems in the presence of environmental noise, as well as designing possible uses of controlled noise sources. The connection between static disorder in quantum walks and the model of disorder in semiconductors leading to Anderson localization is especially intriguing and opens up a lot of unexplored theoretical questions.

In this chapter, I introduced a model for studying systems featuring dynamic or static disorder, and described an experiment bringing the theory to reality [A2], directly based on the realizations of quantum walks studied in Chapter 2. In this joint project, I was responsible for exploring the effects of randomization on a quantum walk on a line and subsequently developing the theoretical background for the work.

In Section 4.3, I report on a paper exploring a particular scheme of incoherent topological errors using numerical methods, [A3]. In this work, we explored the behaviour of a quantum walk on a line, allowed to make random jumps of a fixed size, in several distinct modes of its operation. The simulations were generally set up to run for a fixed number of quantum walk steps and the behaviour observed at $t = 200$ (the maximum made possible by the available resources) was conjectured to be stable even for higher quantum walk times. Finding a theoretical confirmation of the findings is an open problem.

The latter paper, despite reporting mostly on empirical results, provides many interesting insights into the behaviour of quantum walks augmented by a special source of topological errors. The most striking findings are the similarities to scenarios where only the coin register of the walker is affected by the randomization. It is worth particular attention that artificial jumps are also capable of decreasing the variance of the quantum walker's position to a sub-linear function of time.

The main open questions in this topic certainly comprise the effects of the described randomization modes on quantum walks on higher-dimensional lattices, or on a simulated multi-particle dynamics. The two-dimensional experimental framework could also be used for simulating walks on dynamically changing graph structures.

Conclusion

In this work, I presented an introduction to the general theory of quantum walks and some recent developments in this field. The primary reasons for studying quantum walks are their importance in the implementation, or even design, of particular quantum algorithms. Almost equally important is their significance in describing, modelling, simulating and finally understanding the dynamics of a rich variety of microscopic quantum systems. Behaviour compatible with an underlying quantum walk model has been reported even in mesoscopic molecular systems where thermal quantum decoherence was previously thought to keep any quantum effects well beyond the detection threshold.

I started the thesis with a brief introductory part, placing quantum walks into the much broader context of quantum computing. In the main part, results in theoretical, experimental as well as numerical studies of quantum walks were presented, aiming at covering the topic from a number of important points of view as well as showing the close relations between all these fundamental areas of quantum walk research. I presented and explained selected original results of my work in all the three parts.

The theoretical Chapter 2 opened the topic with definitions of the structure, evolution rules, and properties of discrete-time quantum walks on a special class of regular graphs with an underlying group structure. This not only provided a common formalism for the following parts of the thesis but also gave an anchor point for the subsequent work on optical implementations of quantum walks by introducing the equivalent reformulation of quantum walk dynamics using recurrence relations.

The experiments described in Chapter 3 are all examples of the optical feedback loop implementation of quantum walks. The results obtained in these experiments clearly manifest the flexibility and the versatility of the optical implementations of quantum walks as a whole. The optical feedback loop framework was also presented as a means of simulating quantum walk behaviour under engineered conditions. This opens an important follow-up question whether the same set of key ideas could be exploited to build a more general (universal, if possible) quantum simulator.

Chapter 4 completes the triad by introducing results obtained by numerical simulation methods in studying quantum walks interrupted by random occasional jumps across several positions at once. In the broader context of quantum walks affected by external errors, one additional experimental setup is also described, designed to simulate quantum walks in a particular random environment. Comparing the results of the two examples of randomization—one enforcing random jumps and the other affecting local properties of the walker only—unexpected similarities can be observed. A bridge seems to be open between topological and environmental sources of error. Numerical and experimental methods were also shown to be practical in simulating open quantum dynamics of quantum walks caused by dissipation or the loss of full informational control of the system.

Clearly, quantum walks represent an active field of research on the boundary of many sub-disciplines of quantum theory. It was the aim of this thesis to justify this claim and expand as well as unite the knowledge of the topic. Still, many questions remain open and many new interesting problems constantly come into view as possible topics for a future research. It seems that experiments are quickly catching up with the theory and many experimental surprises can be expected in the near future. It remains our conviction that the studied optical feedback loop will be among the frontrunners.

References

Author's works

- [A1] Schreiber, A., Cassemiro, K.N., Potoček, V., Gábris, A., Mosley, P., Andersson, E., Jex, I., Silberhorn, Ch. *Photons Walking the Line: A Quantum Walk with Adjustable Coin Operations*. Phys. Rev. Lett. **104**, 050502 (2010)
- [A2] Schreiber, A., Cassemiro, K.N., Potoček, V., Gábris, A., Jex, I., Silberhorn, Ch. *Decoherence and disorder in quantum walks: From ballistic spread to localization*. Phys. Rev. Lett. **106**, 180403 (2011)
- [A3] Lavička, H., Potoček, V., Kiss, T., Lutz, E., Jex, I. *Quantum walks with jumps*. Eur. Phys. J. D **64**, p. 119 (2011)
- [A4] Schreiber, A., Cassemiro, K.N., Potoček, V., Gábris, A., Jex, I., Silberhorn, Ch. *Photonic quantum walks in a fiber based recursion loop*. AIP Conf. Proc. **1363**, p. 155 (2011)
- [A5] Schreiber, A., Gábris, A., Rohde, P.P., Laiho, K., Štefaňák, M., Potoček, V., Hamilton, C., Jex, I., Silberhorn, Ch. *A 2D Quantum Walk Simulation of Two-Particle Dynamics*. Science **336**, p. 55, (2012)
- [A6] Potoček, V. *Symmetries in discrete time quantum walks on Cayley graphs*. (pre-print version) arXiv:1211.0172 [quant-ph] (2012)

Futher works authored during the Ph.D. studies (not part of this thesis)

- [A7] Potoček, V., Štefaňák, M., Gábris, A., Jex, I. *Náhodné a kvantové procházky* (in Czech). Čs. čas. fyz. **62**, p. 91 (2012)
- [A8] Oi, D.K.L., Potoček, V., Jeffers, J. *Measuring Nothing*. submitted to Nature Photonics, arXiv: :1207.3011 [quant-ph] (2012)

Cited works

- [1] Nielsen, M. A., Chuang, I. L. *Quantum Computation and Quantum Information*. Cambridge University Press, Cambridge, UK (2000)
- [2] Deutsch, D., Josza, R. *Rapid solutions of problems by quantum computation*. Proc. Roy. Soc. London A **439**, p. 553 (1992)
- [3] Simon, D. R. *On the power of quantum computation*. SIAM J. Comput. **26**, p. 116 (1997)
- [4] Shor, P. W. *Polynomial-Time Algorithms for Prime Factorization and Discrete Logarithms on a Quantum Computer*. SIAM J. Comput. **26**, p. 1510 (1997)
- [5] Grover, L. K. *A fast quantum mechanical algorithm for database search*. Proc. STOC'96, p. 212 (1996)
- [6] Aharonov, Y., Davidovich, L., Zagury, N. *Quantum random walks*. Phys. Rev. A **48**, p. 1687 (1993)
- [7] Ambainis, A., Kempe, J., Rivosh, A. *Coins Make Quantum Walks Faster*. Proc. 16th ACM-SIAM SODA, p. 1099 (2005)
- [8] Tulsi, A. *Faster quantum-walk algorithm for the two-dimensional spatial search*. Phys. Rev. A **78**, 012310 (2008)
- [9] Meyer, D. A. *On the absence of homogenous scalar unitary cellular automata*. Phys. Lett. A **223**, p. 337 (1996)
- [10] Kempe, J. *Quantum Random Walks Hit Exponentially Faster*. Proc. 7th RANDOM, p. 354 (2003)
- [11] Mohseni, M., Rebentrost, P., Lloyd, S., Aspuru-Guzik, A. *Environment-Assisted Quantum Walks in Photosynthetic Energy Transfer*. J. Chem. Phys. **129**, 174106 (2008)
- [12] Rebentrost, P., Mohseni, M., Kassal, I., Lloyd, S., Aspuru-Guzik, A. *Environment-assisted quantum transport*. New J. Phys. **11**, 033003 (2009)
- [13] Anderson, P. W. *Absence of diffusion in certain random lattices*. Phys. Rev. **109**, p. 1492 (1958)
- [14] Childs, A. M. *Universal Computation by Quantum Walk*. Phys. Rev. Lett. **102**, 180501 (2009)
- [15] Lovett, N. B., Cooper, S., Everitt, M., Trevers, M., Kendon, V. *Universal quantum computation using the discrete time quantum walk*. Phys. Rev. A **81**, 042330 (2010)
- [16] Shenvi, N., Kempe, J., Whaley, K. *Quantum Random Walk Search Algorithm*. Phys. Rev. A **67**, 052307 (2003)
- [17] Brassard, G., Høyer, P., Mosca, M., Tapp, A. *Quantum Amplitude Amplification and Estimation*. arXiv:quant-ph/0005055v1
- [18] Bennett, C. H., Bernstein, E., Brassard, G., Vazirani, U. *The strengths and weaknesses of quantum computation*. SIAM J. Comput. **26**, p. 1510 (1997)
- [19] Boyer, M., Brassard, G., Høyer, P., Tapp, A. *Tight bounds on quantum searching*. Fortsch. Phys. **46**, p. 493 (1998)
- [20] Zalka, C. *Grover's quantum searching algorithm is optimal*. Phys. Rev. A **60**, p. 2746 (1999)
- [21] Chi, D. P., Kim, J. *Quantum Database Searching by a Single Query*. Chaos, Solitons, and Fractals **10**, p. 1689 (1999)

- [22] Potoček, V., Gábris, A., Kiss, T., Jex, I. *Optimized quantum random-walk search algorithms on the hypercube*. Phys. Rev. A **79**, 012325 (2009)
- [23] Childs, A. M., Goldstone, J. *Spatial search by quantum walk*. Phys. Rev. A **70**, 022314 (2004)
- [24] Ambainis, A. *Quantum walk algorithm for element distinctness*. SIAM J. Comput. **37**, p. 210 (2007)
- [25] Gamble, J. K., Friesen, M., Dong Zhou, Joynt, R., Coppersmith, S. N. *Two-particle quantum walks applied to the graph isomorphism problem*. Phys. Rev. A **81**, 052313 (2010)
- [26] Karski, M., Förster, L., Choi, J.-M., Steffen, A., Alt, W., Meschede, D., Widera, A. *Quantum Walk in Position Space with Single Optically Trapped Atoms*. Science **325**, p. 174 (2009)
- [27] Zähringer, F., Kirchmair, G., Gerritsma, R., Solano, E., Blatt, R., Roos, C. F. *Realization of a Quantum Walk with One and Two Trapped Ions*. Phys. Rev. Lett. **104**, 100503 (2010)
- [28] Schmitz, H., Matjeschk, R., Schneider, Ch., Glueckert, J. Enderlein, M., Huber, T., Schaetz, T. *Quantum Walk of a Trapped Ion in Phase Space*. Phys. Rev. Lett. **103**, 090504 (2009)
- [29] Ciampini, D., d'Arcy, M. B., Grossman, J. M., Helmerson, K., Lett, P. D., Phillips, W. D., Rolston S. L. *Realization of a quantum random walk with ultracold atoms*. Proc. IQEC'04, p. ITuA6 (2004)
- [30] Broome, M. A., Fedrizzi, A., Lanyon, B. P., Kassal, I., Aspuru-Guzik, A., White, A. G. *Discrete single-photon quantum walks with tunable decoherence*. Phys. Rev. Lett. **104**, 153602 (2010)
- [31] Pei Zhang, Xi-Feng Ren, Xu-Bo Zou, Bi-Heng Liu, Yun-Feng Huang, Guang-Can Guo *Demonstration of one-dimensional quantum random walks using orbital angular momentum of photons*. Phys. Rev. A **75**, 052310 (2007)
- [32] Perets, H. B., Lahini, Y., Pozzi, F., Sorel, M., Morandotti, R., Silberberg, Y. *Realization of Quantum Walks with Negligible Decoherence in Waveguide Lattices*. Phys. Rev. Lett. **100**, 170506 (2008)
- [33] Jiangfeng Du, Hui Li, Xiaodong Xu, Mingjun Shi, Jihui Wu, Xianyi Zhou, Rongdian Han *Experimental Implementation of Quantum Random Walk Algorithm*. Phys. Rev. A **67**, 042316 (2003)
- [34] Dawei Lu, Jing Zhu, Ping Zou, Xinhua Peng, Yihua Yu, Shanmin Zhang, Qun Chen, Jiangfeng Du *Experimental implementation of a quantum random-walk search algorithm using strongly dipolar coupled spins*. Phys. Rev. A **81**, 022308 (2010)
- [35] Owens, J. O., Broome, M. A., Biggerstaff, D. N., Goggin, M. E., Fedrizzi, A., Linjordet, T., Ams, M., Marshall, G. D., Twamley, J., Withford, M. J., White, A. G. *Two-photon quantum walks in an elliptical direct-write waveguide array*. New J. Phys. **13**, 075003 (2011)
- [36] Rohde, P. P., Schreiber, A., Štefaňák, M., Jex, I., Silberhorn, Ch. *Multi-walker discrete time quantum walks on arbitrary graphs, their properties and their photonic implementation*. New J. Phys. **13**, 013001 (2011)
- [37] Peruzzo, A., Lobino, M., Matthews, J. C. F., Matsuda, N., Politi, A., Poulios, K., Xiao-Qi Zhou, Lahini, Y., Ismail, N., Wörhoff, K., Bromberg, Y., Silberberg, Y., Thompson, M. G., O'Brien J. L. *Quantum Walks of Correlated Photons*. Science **329**, p. 1500 (2010)
- [38] Matthews, J. C. F., Poulios, K., Meinecke, J. D. A., Politi, A., Peruzzo, A., Ismail, N., Wörhoff, K., Thompson, M. G., O'Brien, J. L. *Simulating quantum statistics with entangled photons: a continuous transition from bosons to fermions*. arXiv:1106.1166 [quant-ph] (2011)

- [39] Sansoni, L., Sciarrino, F., Vallone, G., Mataloni, P., Crespi, A., Ramponi, R., Osellame, R. *Two-Particle Bosonic-Fermionic Quantum Walk via Integrated Photonics*. Phys. Rev. Lett. **108**, 010502 (2012)
- [40] Aharonov, D., Ambainis, A., Kempe, J., Vazirani, U. *Quantum walks on graphs*. Proc. STOC'01, p. 50 (2001)
- [41] Feldman, E., Hillery, M. *Quantum walks on graphs and quantum scattering theory*. Cont. Math. **381**, p. 71 (2005)
- [42] Hillery, M., Bergou, J., Feldman, E. *Quantum walks based on an interferometric analogy*. Phys. Rev. A **68**, 032314 (2003)
- [43] Kempe, J. *Quantum random walks – an introductory overview*. Cont. Phys., **44** (4), p. 307 (2003)
- [44] Konno, N. *Quantum Random Walks in One Dimension*. Quantum Information Processing **1**, p. 345 (2002)
- [45] Hamilton, C. S., Gábris, A., Jex, I., Barnett, S. M. *Quantum walk with a four-dimensional coin*. New J. Phys. **13**, 013015 (2011)
- [46] Potoček, V. *Optical Interferometers and Quantum Walks*. Master's thesis, FNSPE, Czech Technical University in Prague (2009)
- [47] Kendon, V., Tregenna, B. *Decoherence can be useful in quantum walks*. Phys. Rev. A **67**, 042315 (2003)
- [48] Brun, T. A., Carteret, H. A., Ambainis, A. *Quantum random walks with decoherent coins*. Phys. Rev. A **67**, 032304 (2003)
- [49] Mackay, T. D., Bartlett, S. D., Stephenson, L. T., Sanders, B. C. *Quantum walks in higher dimensions*. J. Phys. A: Math. Gen. **35**, p. 2745 (2002)
- [50] Košík, J., Bužek, V., Hillery, M. *Quantum walks with random phase shifts*. Phys. Rev. A **74**, 022310 (2006)
- [51] Shapira, D., Biham, O., Bracken, A. J., Hackett, M. *One-dimensional quantum walk with unitary noise*. Phys. Rev. A **68**, 062315 (2003)
- [52] Romanelli, A., Siri, R., Abal, G., Auyuanet, A., Donangelo, R. *Decoherence in the quantum walk on the line*. Physica A **347**, p. 137 (2003)
- [53] Leung, G., Knott, P., Bailey, J., Kendon, V. *Coined quantum walks on percolation graphs*. New J. Phys. **12**, 123018 (2010)
- [54] Kollár, B., Kiss, T., Novotný, J., Jex, I. *Asymptotic dynamics of coined quantum walks on percolation graphs*. Phys. Rev. Lett. **108**, 230505 (2012)
- [55] Dür, W., Raussendorf, R., Kendon, V., Briegel, H.-J. *Quantum random walks in optical lattices*. Phys. Rev. A **66**, 052319 (2002)
- [56] Kendon, V., Sanders, B. C. *Complementarity and quantum walks*. Phys. Rev. A **71**, 022307 (2005)
- [57] Romanelli, A. *Measurements in the Lévy quantum walk*. Phys. Rev. A **76**, 054306 (2007)
- [58] Törmä, P., Jex, I., Schleich, W. *Localization and diffusion in Ising-type quantum networks*. Phys. Rev. A **65**, 052110 (2002)
- [59] Yue Yin, Katsanos, D. E., Evangelou, S. N. *Quantum walks on a random environment*. Phys. Rev. A **77**, 022302 (2008)
- [60] Levi, A. F. J., Hayes, J. R., Platzman, P. M., Wiegmann, W. *Injected-Hot-Electron Transport in GaAs*. Phys. Rev. Lett. **55**, p. 2071 (1985)

Appendix 1

A. Schreiber, K.N. Cassemiro, V. Potoček, A. Gábris, P. Mosley,
E. Andersson, I. Jex, Ch. Silberhorn

Photons Walking the Line: A Quantum Walk with Adjustable Coin Operations

Physical Review Letters **104**, 050502 (2010)

Photons Walking the Line: A Quantum Walk with Adjustable Coin Operations

A. Schreiber,¹ K. N. Cassemiro,^{1,*} V. Potoček,² A. Gábris,^{2,†} P. J. Mosley,^{1,‡} E. Andersson,³ I. Jex,² and Ch. Silberhorn¹

¹Max Planck Institute for the Science of Light, Günther-Scharowsky-Strasse 1/Bau 24, 91058 Erlangen, Germany

²Department of Physics, FNSPE, Czech Technical University in Prague, Břehová 7, 115 19 Praha, Czech Republic

³SUPA, School of EPS, Heriot-Watt University, Edinburgh EH14 4AS, United Kingdom

(Received 12 October 2009; published 4 February 2010)

We present the first robust implementation of a coined quantum walk over five steps using only passive optical elements. By employing a fiber network loop we keep the amount of required resources constant as the walker's position Hilbert space is increased. We observed a non-Gaussian distribution of the walker's final position, thus characterizing a faster spread of the photon wave packet in comparison to the classical random walk. The walk is realized for many different coin settings and initial states, opening the way for the implementation of a quantum-walk-based search algorithm.

DOI: 10.1103/PhysRevLett.104.050502

PACS numbers: 03.67.Ac, 03.65.-w, 05.40.Fb, 42.50.Dv

Random walks are one of the fundamental models of natural sciences. The concept is common to many branches of research, for example, describing material transport in media and the evolution of stock market shares [1]. By endowing the walker with quantum properties, many new interesting effects appear. As first noted by Aharonov *et al.* [2], quantum interference leads to a new type of walk that spreads much faster than its corresponding classical counterpart. Since classical walks constitute a computational primitive, it can be expected that their quantum extensions provide an alternative platform for the implementation of quantum information protocols. It has been theoretically proven that quantum walks allow the speed-up of search algorithms [3,4] and the realization of universal quantum computation [5]. Moreover, they can be employed for testing the transition from the quantum to the classical world by applying a controlled degree of decoherence [6]. In the context of time-dependent phenomena, recent theoretical studies of quantum walks with a sufficiently large number of sites have shown highly nontrivial dynamics, including localization and recurrence [7]. Applying such ideas, for example, to a biophysical system, can give important insights into effects like photosynthesis [8].

While theoretical analysis of quantum walks is advanced, only few experiments have been reported. The system chosen for implementation has to allow for quantum interference and maintain coherence for a sufficiently long time. To date, different experimental approaches have been taken. Several steps of a quantum walk were realized with trapped ions or atoms [9]. Taking advantage of the simple preparation and manipulation of light states [10], the realization of quantum walks with photons has also attracted attention [11]. In this Letter, we report on the implementation of a one-dimensional coined quantum walk based on optical networks, which corresponds to a quantum analogue of a Galton board. While our primary aim is a demonstration of the experimental feasibility with a low degree of decoherence, the employed configuration

is scalable in terms of reachable number of steps and accessible position Hilbert space. In contrast to previous implementations, we designed a setup for an optical implementation of the coined quantum walk, which presents the distinct advantage of high flexibility in the manipulation of the walker's internal degree of freedom.

In our implementation, we exploit the polarization of the photon as the internal degree of freedom, which can be described with the basis states $|H\rangle = (1, 0)^T$ and $|V\rangle = (0, 1)^T$. In the elementary version, the quantum walker performs a spatial shift (step) conditioned on its internal state. If the motion is restricted to a line, the shift occurs either to the left or to the right, and the resulting position is represented by integer values x . In mathematical terms, one step of the quantum walk is determined by the product of two unitary operators. After n steps, the evolution operator \hat{U} is given by $\hat{U} = (\hat{S}\hat{C})^n$, with

$$\hat{S} = \sum_x |x-1\rangle\langle x| \otimes |V\rangle\langle V| + |x+1\rangle\langle x| \otimes |H\rangle\langle H|, \quad (1)$$

describing the spatial shift (step operator), and \hat{C} the tossing of the quantum coin, which operates on the polarization of the photon (see below). The coherent action of the step and coin operators leads to entanglement between the position and the internal degree of freedom. After several steps, the counterintuitive profile of the quantum walk probability distribution emerges as a result of quantum interference among multiple paths.

Despite the appeal of performing a quantum walk using only linear optical components, a straightforward implementation of the Galton board requires the use of multiple beam splitters and phase shifters [12]. This increases the experimental complexity in terms of optical stability, alignment, and cost. In our implementation, we circumvent this obstacle by translating the position of the walker (photon) into arrival times at the detector. Since the coin operator acts on the polarization subspace, it is simply implemented using a half-wave plate (HWP). Its matrix

representation on the $\{|H\rangle, |V\rangle\}$ basis is

$$C = \begin{pmatrix} \cos(2\theta) & \sin(2\theta) \\ \sin(2\theta) & -\cos(2\theta) \end{pmatrix}, \quad (2)$$

where θ is the rotation angle of the HWP relative to one of its optical axes. The evolution of the walk is perpetuated using an optical feedback loop [13], which allows us to completely avoid the use of additional optical elements to realize several steps of the walk. Similar ideas employing optical networks have been applied with considerable success in other experiments for obtaining a time-multiplexed detector [14]. Here, we advance this concept significantly by realizing a network that includes interferences among multiple paths.

Our experimental setup is sketched in Fig. 1. The photon's wave packet is provided by a pulsed laser source with central wavelength of 805 nm, pulse width of 88 ps, and repetition rate of 1 MHz. The pulses are attenuated to the single-photon level by using neutral density filters. The initial polarization is prepared using standard half- and quarter-wave plates, the coin is realized by another HWP, and the step operation by an optical feedback loop. The "stepper" is composed of a polarization-maintaining fiber network, such that the horizontal and vertical components are first separated spatially and then temporally in a deterministic way. Horizontally polarized photons traverse the fiber loop network in 40 ns, while vertical ones take 5 ns longer. At the output of the "stepper," the two paths are coherently recombined, and the photon is sent back to the input beam splitter for the next step. An illustration of the evolution of the photon's wave packet through the optical network is shown in Fig. 2. At first inspection, it seems that no interference can occur due to the orthogonal nature of the states that are recombined at the end of the fiber. Nevertheless, in the next iteration, the coin operation creates a superposition of the states, thus displaying interference when analyzing in the $|H\rangle$ and $|V\rangle$ basis (PBS 1 on Fig. 1). Finally, at each step of the walk (corresponding to one loop), there is a 50% probability of coupling the

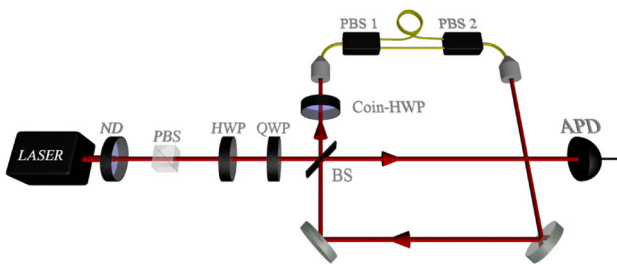


FIG. 1 (color online). Sketch of the setup. A laser field is attenuated to the single-photon level via neutral density filters (ND) and coupled into the network loop through a 50/50 beam splitter (BS). HWP: half-wave plate; QWP: quarter-wave plate; PBS: polarizing BS; APD: avalanche photodiode. Setup dimensions: 1.5 m in free space and 7 m (8 m) in fiber when horizontal (vertical) polarization is used.

photon out of the loop, in which case an avalanche photodiode (APD with time jitter < 1 ns) will register a click. The detection efficiency is $\eta_{\text{det}} = 0.24(1)$, and the losses in the setup are characterized by an efficiency of $\eta_{\text{setup}} = 0.18(1)$ per step, neglecting the input coupling. Measurements of the transmitted (and/or reflected) count rates after each optical component enable us to characterize the losses for $|H\rangle$ and $|V\rangle$ polarizations. A glass plate was introduced in the setup to equalize the losses; nevertheless, $|H\rangle$ polarized photons experienced 3% less loss per step than $|V\rangle$ ones.

The characterization of the walk consisted of a series of consecutive runs of the experiment, each generating at most a single click at a specific time, which is recorded by a computer via a time-to-digital converter interface. From the technical point of view, we stress that phase stability is required only during the short time scale of a single experiment (e.g., 225 ns for five steps), in contrast to the longer time required for an ensemble measurement. This fact brings the advantage that no active phase stabilization was required in our experiment.

To demonstrate the crucial properties of our implementation, we conducted two different types of measurements. In the first experiments, we show a high degree of coherence and the scalability of the system by studying the evolution of the walk over five steps. The second set of experiments show the flexibility achieved for the manipulation of the coin. We begin with the study of coherence properties over an increasing number of steps. The probability distribution of the quantum walk is highly sensitive to the initial state. The best way to emphasize the differences between the quantum and the classical walk—or in other words, to test for coherence—is to use a particular balanced input state, i.e., a circularly polarized photon. In addition, by using the Hadamard coin ($\theta = 22.5^\circ$), which creates an equal superposition of horizontal $|H\rangle$ and vertical $|V\rangle$ polarizations, the wave packet of the photon evolves into a highly delocalized state.

We prepared the initial circular polarization state $|p\rangle_i = a_H|H\rangle + e^{i\Phi}a_V|V\rangle$ with an accuracy characterized by the factor $|a_H|^2/|a_V|^2 = 0.94(4)$, yielding a fidelity of $F = 99.9\%$. The initial mean photon number was $\langle n \rangle_{\text{initial}} = 8(2)$ and, after the fifth step, $\langle n \rangle_{5\text{step}} \approx 7 \times 10^{-4}$. The measured evolution of the probability distribution for the

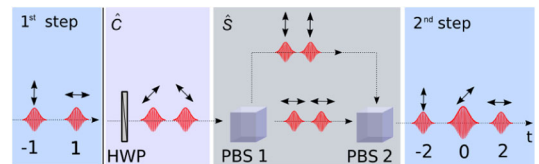


FIG. 2 (color online). Illustration of the working principle of the setup. From left to right, the walk evolves from the end of the first step to the end of the second. The arrows represent the polarization of the photon, which was assumed to be initially vertical ("zero" step).

photon's arrival time from the first to the fifth step is shown in Fig. 3(a). Here, one can see the gradual decrease of the probabilities of a photon arriving in the central time bins alongside the growth of arrivals in the outer wings—a distinctive feature of the quantum walk. This is a clear signature of a high degree of coherence throughout the complete evolution of the walk.

The delocalization effect can be better appreciated in Fig. 3(b), in which we show the measured distribution after five steps. In addition to our experimental data, we present a comparison with both the theoretical model applied to our setup [Figs. 3(b) and 3(c)] and the classical Gaussian distribution [Fig. 3(d)]. While in the classical case the standard deviation is given by $\sigma_C = \sqrt{5} \approx 2.24$, a higher deviation occurs in the quantum case ($\sigma_Q = 2.83$). Our measured value $\sigma = 3.03(10)$ agrees well with the expected ballistic spread. The presented error bars include only statistical errors, calculated as the standard deviation of the finite number of experiments ($N = 3016$ in the fifth step). By analyzing the evolution of the walk over several steps, we find that the current limitation in implementing more than 5 steps arises from spurious optical reflections. Those can be largely suppressed by appropriate time gating, but they still lead to a systematic error in the probability distribution. In addition, the use of the 50/50 beam-splitter (BS) coupler introduces high losses, which in turn causes a low signal-to-noise ratio at the detection of further steps. We stress that these problems are not intrinsic to this implementation, since the setup can be optimized to give better performance (discussed below).

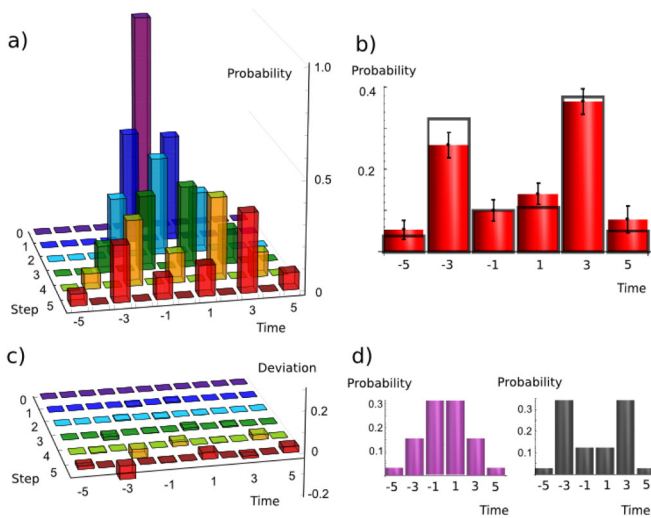


FIG. 3 (color online). Measured probability distribution of the photon's arrival time. (a) Evolution of the distribution from the initial circularly polarized state (rear part) to the state after the fifth step (front part). (b) Detail of the measured distribution after five steps. Filled bars: measured results. Frames: predictions from our theoretical model. (c) Difference between experimental and theoretical values. (d) Detail of ideal distributions after five steps. Left: classical walk; right: quantum walk.

Our second experimental result highlights the flexibility of our implementation with respect to the easy adjustability of different coin settings. In Fig. 4, we show how the probability distribution after three steps changes as a function of the angle of the half-wave plate. In this case, the photon is initially prepared with horizontal polarization, leading to an asymmetric distribution when the Hadamard coin is applied. Setting the HWP at zero degrees is essentially equivalent to applying the identity operation, thus resulting in the photon being found at the first time bin, labeled $t = 3$. From zero to 45° , interference among multiple paths takes place, giving rise to a probability of finding the photon at $t = 1$ ($t = -1$) that is increased (decreased) in comparison to the classical result. At exactly 45° , the NOT operation is realized; i.e., incoming $|H\rangle$ polarized photons are converted into $|V\rangle$ and vice-versa. For these measurements, the initial polarization state $|p\rangle_i = a'_H|H\rangle + a'_V|V\rangle$ was characterized by $|a'_V|^2/|a'_H|^2 = 0.003(4)$ ($F = 99.7\%$), and the initial mean photon number was given by $\langle n \rangle = 0.58(5)$. The experimental results agree well with the theoretical prediction and are clearly distinct from the classical values.

We performed a detailed theoretical analysis of the system by taking into account possible sources of coherent and incoherent errors. The imperfections are modeled as additional linear optical elements and represent the effect of depolarization, relative phase shifts, and efficiency ratio ϵ between the two polarizations, undesired polarization rotations by an angle φ , and imperfect preparation of the initial state $|\psi'\rangle$. By analyzing the output signal, the strength of decoherence has been found to be equal to

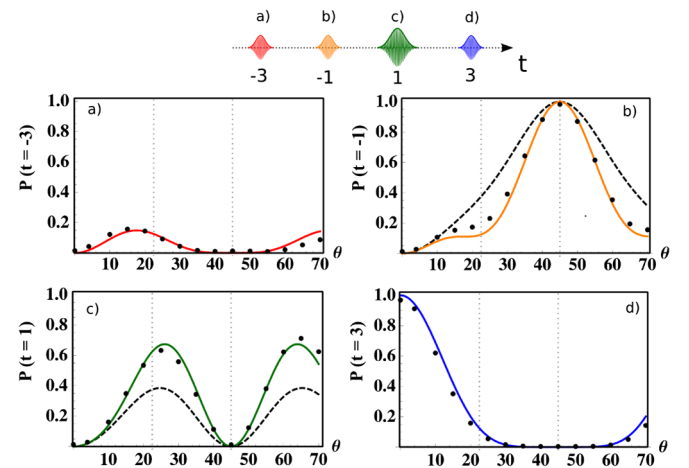


FIG. 4 (color online). Effect of different coin operations on the probability distribution after the third step for an initially horizontally polarized photon. In each inset, from (a) to (d), we show the probability for the photon to arrive at a particular time bin, as depicted in the top illustration. At time bins $t = \pm 3$, the classical and quantum descriptions coincide. Dots: Measured quantum walk (error bars are smaller than used symbols). Solid line: Theoretical model for the quantum walk. Dashed line: Classical random walk.

zero within the statistical error, indicating that effects such as depolarization and rapid phase fluctuations can be neglected. The system can be described by an effective coin operation \hat{C}' , with matrix representation given by

$$C' = L(\epsilon_L)R(\varphi)R(\theta)L(-\epsilon_{\text{HWP}})R(-\theta)L(\epsilon_{\text{BS}}), \quad (3)$$

where $L(\epsilon)$ is a matrix characterizing differential losses and $R(\alpha)$ a rotation:

$$L(\epsilon) = \begin{pmatrix} 1 & 0 \\ 0 & \epsilon \end{pmatrix}, \quad R(\alpha) = \begin{pmatrix} \cos(\alpha) & \sin(\alpha) \\ -\sin(\alpha) & \cos(\alpha) \end{pmatrix}. \quad (4)$$

Values $\epsilon < 1$ for the efficiency ratio indicate loss imbalance between the $|H\rangle$ and $|V\rangle$ polarizations. This parameter was characterized at the different components of the setup: at the coupling beam splitter $\epsilon_{\text{BS}} = 0.99$, at the delay loop $\epsilon_L = 0.96$, and between the slow and the fast axis of the HWP $\epsilon_{\text{HWP}} = 0.98$. The results indicate that $|V\rangle$ polarization undergoes higher loss than $|H\rangle$. The rotation introduced by the mirrors has been determined to be $\varphi = 1.4^\circ$. The final state of the walk is calculated as $|\psi_{\text{final}}\rangle = (\hat{S}\hat{C}')^n|\psi'\rangle$.

Discrepancies between the experiment and the theoretical model are due to reflections of the optical signal and imperfections of the detector, e.g., dead time and dark counts. Considering only intrinsic problems of the actual proposal, i.e., supposing the use of the best available components, thereby suppressing the reflections, we can estimate the maximum number of steps that are in principle possible to achieve. In the optimized scenario, it is reasonable to suppose $\eta_{\text{setup}} = 71\%$, considering that the 50/50 coupler is replaced by a 99/1 coupler. Since the properties of the quantum walk can be simulated by using an intense coherent field, we could employ a laser with 1 W power (250 kHz). By adding an active switch to couple the photon out of the loop, the signal-to-noise ratio is improved, thus allowing us to reach 100 steps. The measurements can still be done in a time scale shorter than typical unavoidable low frequency mechanical vibrations (lower than 500 Hz), thus preserving phase coherences.

In conclusion, we have implemented a compact and efficient way of realizing coined quantum walks. In contrast to many other experiments, we benefit from employing quantum states of light, which are simple to manipulate. For instance, one could achieve a higher dimensional coin by using the optical angular momentum of photons [15] instead of their polarization, therefore increasing the dynamical richness of the walk. Moreover, the ability to operate with different coins and the ease of addressing individual position states opens exciting new possibilities for the realization of quantum information protocols. The present experimental setup constitutes a starting point for implementing a one- or two-dimensional quantum-walk-based search algorithm.

We acknowledge financial support from the German Israel Foundation (Project 970/2007). K.N.C. and I.J. acknowledge financial support from the Alexander von Humboldt Foundation; V.P., A.G., and I.J. from MŠMT LC06002, MSM 6840770039, and CZ-10/2007; V.P. from GA CR 202/08/H078; A.G. from the Hungarian Scientific Research Fund (T049234 and NF068736); E.A., I.J., V.P., and A.G. from the Royal Society International Joint Project Grant No. 2006/R2-IJP.

*Katuscia.Casemiro@mpl.mpg.de

†Secondary address: Research Institute for Solid State Physics and Optics, Hungarian Academy of Sciences, H-1525 Budapest, P. O. Box 49, Hungary.

‡Present address: Centre for Photonics and Photonic Materials, Department of Physics, University of Bath, Claverton Down, Bath, BA2 7AY, United Kingdom.

- [1] S. Chandrasekhar, *Rev. Mod. Phys.* **15**, 1 (1943); L. Bachelier, *Ann. Sci. Ecole Norm. Super.* **17**, 21 (1900).
- [2] Y. Aharonov, L. Davidovich, and N. Zagury, *Phys. Rev. A* **48**, 1687 (1993).
- [3] N. Shenvi, J. Kempe, and K. Birgitta Whaley, *Phys. Rev. A* **67**, 052307 (2003); A. Ambainis, J. Kempe, and A. Rivosh, in *Proc. 16th ACM-SIAM SODA, Vancouver* (SIAM, Philadelphia, USA, 2005), p. 1099.
- [4] V. Potoček, A. Gábris, T. Kiss, and I. Jex, *Phys. Rev. A* **79**, 012325 (2009).
- [5] A. M. Childs, *Phys. Rev. Lett.* **102**, 180501 (2009); N. B. Lovett *et al.*, arXiv:0910.1024v2.
- [6] T. A. Brun, H. A. Carteret, and A. Ambainis, *Phys. Rev. Lett.* **91**, 130602 (2003).
- [7] P. Törmä, I. Jex, and W. P. Schleich, *Phys. Rev. A* **65**, 052110 (2002); P. W. Anderson, *Phys. Rev.* **109**, 1492 (1958); M. Štefaňák, I. Jex, and T. Kiss, *Phys. Rev. Lett.* **100**, 020501 (2008).
- [8] M. Mohseni *et al.*, *J. Chem. Phys.* **129**, 174106 (2008).
- [9] H. Schmitz *et al.*, *Phys. Rev. Lett.* **103**, 090504 (2009); M. Karski *et al.*, *Science* **325**, 174 (2009); F. Zähringer *et al.*, arXiv:0911.1876v1.
- [10] M. Reck, A. Zeilinger, H. J. Bernstein, and P. Bertani, *Phys. Rev. Lett.* **73**, 58 (1994); M. Hillery, J. Bergou, and E. Feldman, *Phys. Rev. A* **68**, 032314 (2003); P. L. Knight, E. Roldán, and J. E. Sipe, *ibid.* **68**, 020301(R) (2003).
- [11] D. Bouwmeester *et al.*, *Phys. Rev. A* **61**, 013410 (1999); P. Zhang *et al.*, *ibid.* **75**, 052310 (2007); P. H. Souto Ribeiro *et al.*, *ibid.* **78**, 012326 (2008); H. B. Perets *et al.*, *Phys. Rev. Lett.* **100**, 170506 (2008).
- [12] B. Do *et al.*, *J. Opt. Soc. Am. B* **22**, 499 (2005).
- [13] T. B. Pittman and J. D. Franson, *Phys. Rev. A* **66**, 062302 (2002); K. Banaszek and I. A. Walmsley, *Opt. Lett.* **28**, 52 (2003).
- [14] M. J. Fitch, B. C. Jacobs, T. B. Pittman, and J. D. Franson, *Phys. Rev. A* **68**, 043814 (2003); D. Achilles *et al.*, *Opt. Lett.* **28**, 2387 (2003).
- [15] J. Leach *et al.*, *Phys. Rev. Lett.* **88**, 257901 (2002).

Appendix 2

A. Schreiber, K. N. Cassemiro, V. Potoček, A. Gábris, I. Jex, Ch. Silberhorn

Decoherence and disorder in quantum walks: From ballistic spread to localization

Physical Review Letters **106**, 180403 (2011)

Decoherence and Disorder in Quantum Walks: From Ballistic Spread to Localization

A. Schreiber,^{1,*} K. N. Cassemiro,¹ V. Potočjek,² A. Gábris,^{2,†} I. Jex,² and Ch. Silberhorn^{1,3}

¹Max Planck Institute for the Science of Light, Günther-Scharowsky-Straße 1/Bau 24, 91058 Erlangen, Germany

²Department of Physics, FNSPE, Czech Technical University in Prague, Břehová 7, 115 19 Praha, Czech Republic

³University of Paderborn, Applied Physics, Warburger Straße 100, 33098 Paderborn, Germany

(Received 13 January 2011; published 6 May 2011)

We investigate the impact of decoherence and static disorder on the dynamics of quantum particles moving in a periodic lattice. Our experiment relies on the photonic implementation of a one-dimensional quantum walk. The pure quantum evolution is characterized by a ballistic spread of a photon's wave packet along 28 steps. By applying controlled time-dependent operations we simulate three different environmental influences on the system, resulting in a fast ballistic spread, a diffusive classical walk, and the first Anderson localization in a discrete quantum walk architecture.

DOI: 10.1103/PhysRevLett.106.180403

PACS numbers: 03.65.Yz, 05.40.Fb, 71.23.-k, 71.55.Jv

Random walks describe the probabilistic evolution of a classical particle in a structured space resulting in a diffusive transport. In contrast, endowing the walker with quantum mechanical properties typically leads to a ballistic spread of the particle's wave function [1]. The coherent nature of quantum walks has been theoretically explored, providing interesting results for a wide range of applications. They state not only a universal platform for quantum computing [2] but also constitute a powerful tool for modeling biological systems [3–5], thus hinting towards the mechanism of energy transfer in photosynthesis. Quantum walks of single particles on a line have been experimentally realized in several systems, e.g., with trapped atoms [6] and ions [7,8], energy levels in NMR schemes [9,10], photons in waveguide structures [11], a beam splitter array [12], and in a fiber loop configuration [13]. Although these experiments opened up a new route to higher dimensional quantum systems, more sophisticated quantum walks need to be implemented to pursue the realm of real applications. A first step in the direction of photonic quantum computation has been recently reported [14], in which two particles execute a simultaneous walk and display intrinsic quantum correlations. However, their static system misses the ability to access and manipulate the walker's state in a position dependent way, which is an important requirement for implementing quantum-walk-based protocols [15].

In this Letter we present the first experimental realization of quantum walks with controlled dynamics. We use the flexibility to investigate the evolution of quantum particles moving in a discrete environment presenting static and dynamic disorders.

As predicted by Anderson in 1958 [16], static disorder leads to an absence of diffusion and the wave function of the particle becomes localized, which, e.g., would render a conductor to behave as an insulator. Anderson localization has been experimentally investigated in different physical scenarios, e.g., employing photons moving in semiconduc-

tor powders [17] and photonic lattices [18,19], or even via Bose-Einstein condensates [20,21]. However, although theoretically predicted in the context of quantum walks [22–24], the effect has never been observed in a discrete quantum walk scenario.

Furthermore, it is interesting to note that the energy transport in photosynthetic light-harvesting systems is influenced by both static and dynamic disorders, and it is precisely the interplay between the two effects that leads to the highly efficient transfer in those molecular complexes [4,5]. Thus, in order to simulate a realistic influence of the environment, we go further in our studies by investigating the effect of dynamical noise, which typically induces decoherence [25–27]. Utilizing the ability to easily tune the conditions for the quantum walk, we demonstrate here the diverse dynamics of quantum particles propagating in these different systems.

In our experiment we realize the quantum walk of photons by employing a linear optical network. The evolution of the particle's wave function $|\psi(x)\rangle$ is given by

$$|\psi(x)\rangle \rightarrow \gamma_x |\psi(x)\rangle + \sum_{k \neq x} \beta_{x,k} |\psi(k)\rangle, \quad (1)$$

with the position dependent amplitudes γ_x and $\beta_{x,k}$ determining the probability of the particle to stay at the discrete position x or evolve to the adjacent sites k , respectively.

We study the expansion of the particle's wave packet in four different scenarios. (i) First of all we implement the quantum walk in a homogeneous lattice, showing that it presents an evolution that is free from decoherence. (ii) Next, we introduce static disorder by manipulating the lattice parameters γ_x and $\beta_{x,k}$, thus observing Anderson localization. We then examine two scenarios leading to decoherence, which essentially differ in the time scales of the occurring dynamic perturbations. (iii) In this case a dynamic randomization of the lattice parameters γ_x and $\beta_{x,k}$ simulates the evolution of a particle interacting with a fast fluctuating environment.

The resulting dephasing suppresses the underlying interference effects and hence causes the particle to evolve just like in a classical random walk [6,8]. (iv) In the last scenario we simulate a slowly changing homogeneous environment. While γ_x and $\beta_{x,k}$ are stable during a single realization, a slow drift leads to different conditions for subsequent particles, thus affecting results obtained in an ensemble measurement.

In a discrete quantum walk the position of a particle evolves according to its internal coin state $|c\rangle$. For our photonic implementation we use the linear horizontal $|H\rangle = (1, 0)^T$ and vertical $|V\rangle = (0, 1)^T$ polarization of light. The state of the photon after N steps of the walk is found by applying the unitary transformation $U = \prod_{n=1}^N \hat{S} \hat{C}_n$ to the initial state $|\psi(x)_0\rangle = |x_0\rangle \otimes |c_0\rangle$. The coin operation $\hat{C}_n(x)$ manipulates the polarization of the photon in dependence on the position x and the step number n . In the basis $\{|H\rangle, |V\rangle\}$ the coin operator is given in matrix form by

$$C(x) = \begin{pmatrix} e^{i\phi_H(x)} & 0 \\ 0 & e^{i\phi_V(x)} \end{pmatrix} \begin{pmatrix} \cos(2\theta) & \sin(2\theta) \\ \sin(2\theta) & -\cos(2\theta) \end{pmatrix}, \quad (2)$$

with the diagonal matrix representing a phase shift $\phi_H(x)$ for horizontal and $\phi_V(x)$ for vertical polarizations, while the second matrix corresponds to a polarization rotation of 2θ . The step operation \hat{S} shifts the position x of the photon by $+1$ if the polarization is horizontal and by -1 if it is vertical.

Following Eq. (1), the evolution of the wave function with the step number n is given by

$$|\psi(x)_{n+2}\rangle = \gamma_x |\psi(x)_n\rangle + \beta_{x,x\pm 2} (|\psi(x+2)_n\rangle + |\psi(x-2)_n\rangle). \quad (3)$$

Note that the transition coefficients γ_x and $\beta_{x,x\pm 2}$ are fully set by the coin operations $C_{n+1}(x)$ and $C_{n+2}(x)$. By changing the parameters $\phi(x)_{H/V}$ and θ in a controlled way we can alter the coefficients and hence create diverse types of physical conditions for a quantum walk scenario.

A simple measure to quantify the spread of the wave function in the different systems is provided by the variance σ^2 of the final spatial distribution. While the decoherence-free quantum walk presents a ballistic spread, with $\sigma^2 \propto n^2$, the classical random walk is diffusive, characterized by $\sigma^2 = n$. In contrast to both, in a one-dimensional system with static disorder the wave packet shows exponential localization after a short initial expansion. The stagnation of the wave packet spread is thus evidenced by a constant variance.

The functional principle of our experimental setup is sketched in Fig. 1(a) and is discussed in detail in [13]. We generate the input photons with a pulsed diode laser with a central wavelength of 805 nm, a pulse width of 88 ps, and a repetition rate of 110 kHz. The initial polarization state of the photons is prepared with retardation plates. Each coin operation consists of a polarization rotation, which is

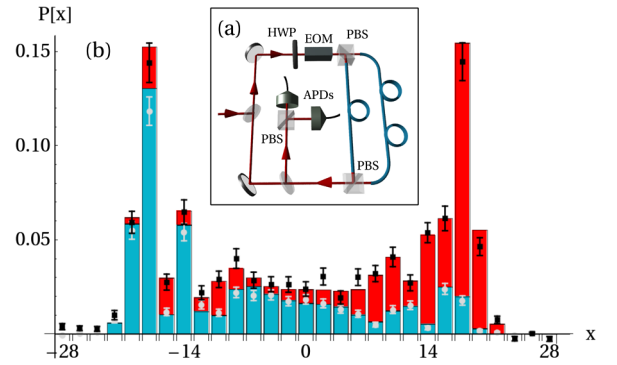


FIG. 1 (color online). (a) Schematic setup (see text for details). (b) Probability distribution after 28 steps of a symmetric Hadamard walk with initial circular polarization. Stacked bars: Adapted theory split into the two coin states $|V\rangle$ (blue, bottom) and $|H\rangle$ (red, top). Gray dots show experimental data for vertical polarization, black dots show the sum of both polarizations. Error bars correspond to statistical errors.

realized with a half-wave plate (HWP), and a subsequent phase shift implemented by a fast switching electro-optic modulator (EOM), as described in Eq. (2). The properties of the EOM impose that $\phi_V(x)/\phi_H(x) \approx 3.5$. The step operation is realized in the time domain via two polarizing beam splitters (PBS) and a fiber delay line, in which horizontally polarized light follows a longer path [Fig. 1(a)]. The resulting temporal difference of 5.9 ns between both polarization components corresponds to a step in the spatial domain of $x \pm 1$. After a full evolution the photon wave packet is distributed over several discrete spatial positions or, equivalently, over respective time windows. For detection the photon gets coupled out of the loop by a beam splitter with a probability of 12% per step. We employ two avalanche photodiodes (APD) to measure the photon's time and polarization properties, which gives information about the number of steps, the specific position of the photon, as well as its coin state. The probability that a photon undergoes a full round-trip without getting lost or detected is given by $\eta_{\text{setup}} = 0.55$ (0.22) without (with) the EOM, and the detection efficiency is $\eta_{\text{det}} = 0.06$ per step.

To determine the statistical distribution of one specific step we detected more than 10^4 events in an overall measurement time of maximally 1 h, limited by the setup stability. This guaranteed an absolute statistical error of the assessed probability at each position of less than 0.01. An average photon number per pulse at the detected step of less than $\langle n \rangle < 0.003$ ensured a negligible probability of multiphoton events $P(n > 1)/P(n = 1) < 0.02$.

(i) *Homogeneous lattice.*—In the first of our four quantum walk scenarios we investigate a homogeneous environment, thus testing the intrinsic coherence properties of the setup. The spatial distribution after 28 steps can be seen in Fig. 1(b). We used the initial state $|\psi_0\rangle = |0\rangle \otimes \frac{1}{\sqrt{2}} \times (|H\rangle + i|V\rangle)$ and the Hadamard coin ($\theta = \pi/8$) at each position. The final state clearly shows the characteristic shape of a fully coherent quantum walk: the two

pronounced side peaks and the low probability around the initial position. Moreover, the polarization analysis confirms the expected dependence of the particle's final position on its coin state. An adapted theory including only small imperfections of the coin parameter θ , the initial coin state, and differential losses between the two polarizations fully explains the final spatial and polarization distribution. The quality of the result can be quantified by the distance $d(P_m, P_{\text{theor}}) = \frac{1}{2} \sum_x |P_m(x) - P_{\text{theor}}(x)|$ between the measured P_m and the theoretical P_{theor} probability distributions. It ranges between 0 for identical distributions and 1 for a complete mismatch. The distance of the measured walk to the adapted quantum theory is $d(P_m, P_{\text{qw}}) = 0.052 \pm 0.015$. For comparison we calculated the distance to the fully decoherent (classical) scenario, obtaining $d(P_m, P_{\text{cl}}) = 0.661 \pm 0.015$. Hence, our result confirms an almost decoherence free evolution after 28 steps.

(ii) *Static disorder.*—We implemented the evolution of a particle in an environment with static disorder using a quantum walk with variable coin operation. To create a static disorder a coin operation is required, which is position and not step dependent. In our system this is realized by a controlled phase shift $\phi_{H/V}(x)$, such that the photon acquires the same phase any instance it appears at position x . To generate a random static phase pattern we applied a periodic noise signal to the EOM. The periodicity of the signal was carefully adjusted to ensure that the applied phase shift operation is strictly position dependent. Using different phase patterns at subsequent runs allows us to average over various disorders, as considered in the model of Anderson. The strength of disorder is determined by the maximal applied phase shift Φ_{max} , which defines the uniform interval $\phi_V(x) \in [-\Phi_{\text{max}}, \Phi_{\text{max}}]$, from which the phases are chosen. The probability distribution after 11 steps is shown in Fig. 2(a). We used the initial state $|\psi_0\rangle = |0\rangle \otimes |H\rangle$, $\theta = \pi/8$ and a high disorder strength [$\Phi_{\text{max}} = (1.14 \pm 0.05)\pi$]. In contrast to the decoherence free quantum walk [$\Phi_{\text{max}} = 0$, inset of Fig. 2(c)], in the disordered scenario the expansion of the wave packet is highly suppressed. We observe a strictly enhanced arrival probability around the initial position, which also displays the predicted exponential decay. This striking signature of Anderson localization is emphasized by linear fits in the semilog scaled plot [inset of Fig. 2(a)]. Our results are in agreement with a theoretical model determined by a Monte Carlo simulation of 10^4 different phase patterns compatible with our experiment. Compared to (i), the number of steps is reduced due to the additional losses introduced by the EOM.

(iii) *Fast fluctuations.*—To generate a system with dynamic disorder we detuned the temporal length of the noise signal, thus eliminating position dependent phase correlations. Decoherence appears as a consequence of the dynamically varying phase suffered by the quantum particle during the evolution. As a result, the photon undergoes a

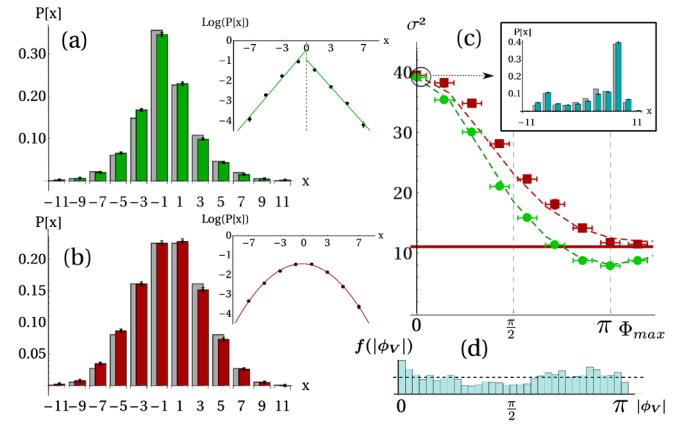


FIG. 2 (color online). Measured probability distribution (front) and respective theory (back, gray bars) of 11 steps of a quantum walk ($\theta = \pi/8$) with static disorder (a), dynamic disorder (b), and in a decoherence free environment [inset (c)]. The insets in (a) and (b) show the measured distribution in semilog scale with linear (a) and parabolic fit (b). (c) Transition of the variance from ballistic quantum walk to diffusive or localized evolution due to dynamic (red squares) and static (green dots) disorder with increasing disorder strength Φ_{max} ; dashed lines: theory with adaption for experimental imperfections. The red solid line marks the variance of a classical random walk. (Vertical error is smaller than the dot size). (d) Relative frequency $f(|\phi_V|)$ of the applied phases ϕ_V for the signal with interval $\Phi_{\text{max}} = (1.02 \pm 0.05)\pi$. The dashed line indicates the uniform distribution.

classical random walk, revealing a binomial probability distribution [Fig. 2(b)]. In contrast to the previous case, the spatial profile of the wave packet does not reflect the asymmetry of the initial state and, furthermore, shows a parabolic shape in the semilog scale [inset, Fig. 2(b)].

A stepwise increase of the disorder strength Φ_{max} nicely demonstrates the controlled transition of the system from the ballistic evolution (decoherence free quantum walk) towards the diffusive evolution (localization) in a scenario with dynamic (static) disorder [Fig. 2(c)]. For this purpose we characterize the resulting expansion profile by its variance σ^2 . Without decoherence ($\Phi_{\text{max}} = 0$) the ballistically spreading wave packet shows a large expansion induced by quantum interference after 11 steps. In a system with dynamic disorder, decoherence reduces the expansion of the wave packet to the level of a diffusive classical particle. In contrast, static disorder leads to a stagnation of the spread and hence an even smaller variance. Our results clearly demonstrate how the amount and kind of disorder influence the expansion of the particle's wave packet.

The agreement between theory and measurement in the completely dephased scenario [Fig. 2(b)] confirms a sufficient randomness of the applied noise signal. Furthermore, an independent interferometric measurement revealed the relative frequency of the used phases $f(|\phi_V|)$, as can be seen in Fig. 2(d) with $\Phi_{\text{max}} = (1.02 \pm 0.05)\pi$. However, imperfections of the EOM lead to a distribution slightly off uniformity. These are included in the theoretical curve in Fig. 2(c).

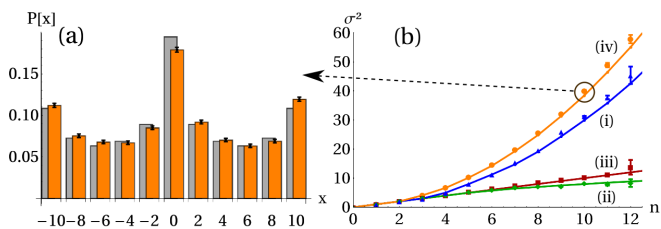


FIG. 3 (color online). (a) Averaged probability distribution in a slow decoherence scenario with different coin angles $\theta \in [0, \pi/4]$: Measurement (orange, front) and theory (gray, back). (b) Measured trend of the variance up to 12 steps (dots) with respective theoretical simulation (lines). Photons in scenario (i) (blue triangles) and (iv) (orange dots) show a ballistic behavior. In scenario (iii) (red squares) they move diffusively, and in (ii) (green diamonds) they stagnate.

(iv) *Slow fluctuations*.—As the fourth scenario we simulated fluctuations in a homogeneous system, but with parameters that change in a time scale much larger than the full duration of a single quantum walk. Although the individual evolution is not affected under these circumstances, an ensemble measurement of subsequent walks results in an average over coherent evolutions in different types of lattices. For this purpose we changed the parameter $\theta \in [0, \pi/4]$ in steps of $\pi/18$ for a quantum walk with initial state $|\psi_0\rangle = |0\rangle \otimes \frac{1}{\sqrt{2}}(|H\rangle + i|V\rangle)$. An average over the full range $\theta \in [0, \pi/4]$ exhibits a nearly uniform spatial distribution of the wave packet with an enhanced probability to arrive at its initial position $x = 0$ after 10 steps [Fig. 3(a)]. In particular, the high chance to reach the outermost positions $x = \pm 10$ differs significantly from all previous scenarios. This increases the variance of the distribution ($\sigma_{(iv)}^2 = 40.00 \pm 0.42$) to a level, which is even higher than in the decoherence free quantum walk with the Hadamard coin ($\sigma_{(i)}^2 = 31.27 \pm 0.19$). The result demonstrates that special kinds of decoherences can even speed up the expansion of wave packets in homogeneous lattices.

Finally, the geometry of the setup allows us to easily observe the wave packet's evolution step by step in all four scenarios [Fig. 3(b)]. For cases (i) and (iv) we observe a ballistic spread, with an even faster expansion in a system with slow fluctuations. The evolution with fast dynamic disorder (iii) is clearly diffusive. Lastly, under the condition of static disorder (ii) the variance saturates after few steps and the dynamics is dominated by the effect of Anderson localization. The parameters used in simulation and experiment are equivalent to the experimental settings used for Figs. 1(b), 2(a), 2(b), and 3(a).

In conclusion, we presented how disorder and fluctuations in a periodic lattice can influence the evolution of a traversing particle and showed the controlled transition between the different regimes. The high flexibility and control allows not only the study of further decoherence phenomena in quantum walks but also to simulate specific

physical scenarios of interest for the solid state and biophysics community. Moreover, the possibility to manipulate quantum walks with time-dependent coin operations is a crucial step towards the realization of quantum-walk-based protocols.

We thank P.P. Rohde for helpful discussions. We acknowledge financial support from the German Israel Foundation (Project No. 970/2007). K.N.C. and I.J. acknowledge support from the AvH Foundation; V.P., A.G., and I.J. from MSMT LC06002 and MSM 6840770039; V.P. from SGS10/294/OHK4/3T/14; and A.G. from OTKA T83858.

*Andreas.Schreiber@mpl.mpg.de

†Also at: Research Institute for Solid State Physics and Optics, Hungarian Academy of Sciences, H-1525 Budapest, P.O. Box 49, Hungary.

- [1] Y. Aharonov, L. Davidovich, and N. Zagury, *Phys. Rev. A* **48**, 1687 (1993).
- [2] A. M. Childs, *Phys. Rev. Lett.* **102**, 180501 (2009).
- [3] M. Mohseni *et al.*, *J. Chem. Phys.* **129**, 174106 (2008); M. B. Plenio and S. F. Huelga, *New J. Phys.* **10**, 113019 (2008).
- [4] P. Reberstrost *et al.*, *New J. Phys.* **11**, 033003 (2009); F. Caruso *et al.*, *J. Chem. Phys.* **131**, 105106 (2009).
- [5] S. Hoyer, M. Sarovar, and K. B. Whaley, *New J. Phys.* **12**, 065041 (2010).
- [6] M. Karski *et al.*, *Science* **325**, 174 (2009).
- [7] H. Schmitz *et al.*, *Phys. Rev. Lett.* **103**, 090504 (2009).
- [8] F. Zähringer *et al.*, *Phys. Rev. Lett.* **104**, 100503 (2010).
- [9] J. Du *et al.*, *Phys. Rev. A* **67**, 042316 (2003).
- [10] C. A. Ryan *et al.*, *Phys. Rev. A* **72**, 062317 (2005).
- [11] H. B. Perets *et al.*, *Phys. Rev. Lett.* **100**, 170506 (2008).
- [12] M. A. Broome *et al.*, *Phys. Rev. Lett.* **104**, 153602 (2010).
- [13] A. Schreiber *et al.*, *Phys. Rev. Lett.* **104**, 050502 (2010).
- [14] A. Peruzzo *et al.*, *Science* **329**, 1500 (2010).
- [15] N. Shenvi, J. Kempe, and K. Birgitta Whaley, *Phys. Rev. A* **67**, 052307 (2003); A. Ambainis, *SIAM J. Comput.* **37**, 210 (2007).
- [16] P. W. Anderson, *Phys. Rev.* **109**, 1492 (1958).
- [17] D. S. Wiersma *et al.*, *Nature (London)* **390**, 671 (1997).
- [18] Y. Lahini *et al.*, *Phys. Rev. Lett.* **100**, 013906 (2008).
- [19] T. Schwartz *et al.*, *Nature (London)* **446**, 52 (2007).
- [20] G. Roati *et al.*, *Nature (London)* **453**, 895 (2008).
- [21] J. Billy *et al.*, *Nature (London)* **453**, 891 (2008).
- [22] P. Törmä, I. Jex, and W. P. Schleich, *Phys. Rev. A* **65**, 052110 (2002).
- [23] J. P. Keating *et al.*, *Phys. Rev. A* **76**, 012315 (2007).
- [24] Yue Yin, D. E. Katsanos, and S. N. Evangelou, *Phys. Rev. A* **77**, 022302 (2008).
- [25] T. A. Brun, H. A. Carteret, and A. Ambainis, *Phys. Rev. Lett.* **91**, 130602 (2003).
- [26] V. Kendon, *Math. Struct. Comput. Sci.* **17**, 1169 (2007), and references therein.
- [27] P. Ribeiro, P. Milman, and R. Mosseri, *Phys. Rev. Lett.* **93**, 190503 (2004).

Appendix 3

H. Lavička, V. Potoček, T. Kiss, E. Lutz, I. Jex

Quantum walks with jumps

European Physics Journal D **64**, p. 119 (2011)

Quantum walk with jumps

H. Lavička^{1,2,a}, V. Potoček¹, T. Kiss³, E. Lutz⁴, and I. Jex¹

¹ Czech Technical University in Prague, Faculty of Nuclear Sciences and Physical Engineering, Department of Physics, Břehová 7, 115 19 Praha 1, Czech Republic

² Czech Technical University in Prague, Faculty of Nuclear Sciences and Physical Engineering, Doppler Institute for Mathematical Physics and Applied Mathematics, Břehová 7, 115 19 Praha 1, Czech Republic

³ Research Institute for Solid State Physics and Optics, Hungarian Academy of Sciences, 1525 Budapest, P.O. Box 49, Hungary

⁴ Department of Physics, University of Augsburg, 86135 Augsburg, Germany

Received 28 February 2011 / Received in final form 2 May 2011

Published online 27 July 2011 – © EDP Sciences, Società Italiana di Fisica, Springer-Verlag 2011

Abstract. We analyze a special class of 1-D quantum walks (QWs) realized using optical multi-ports. We assume non-perfect multi-ports showing errors in the connectivity, i.e. with a small probability the multi-ports can connect not to their nearest neighbor but to another multi-port at a fixed distance – we call this a jump. We study two cases of QW with jumps where multiple displacements can emerge at one timestep. The first case assumes time-correlated jumps (static disorder). In the second case, we choose the positions of jumps randomly in time (dynamic disorder). The probability distributions of position of the QW walker in both instances differ significantly: dynamic disorder leads to a Gaussian-like distribution, while for static disorder we find two distinct behaviors depending on the parity of jump size. In the case of even-sized jumps, the distribution exhibits a three-peak profile around the position of the initial excitation, whereas the probability distribution in the odd case follows a Laplace-like discrete distribution modulated by additional (exponential) peaks for long times. Finally, our numerical results indicate that by an appropriate mapping a universal functional behavior of the variance of the long-time probability distribution can be revealed with respect to the scaled average of jump size.

1 Introduction

The quantum walk (QW) is a quantum mechanical model, a generalization of a classical random walk. It was introduced in 1993 [1–3] and later found fruitful applications as a tool to design efficient quantum algorithms. The model of a quantum walk was defined in two distinct ways: continuous- and discrete-time. In the former, the particles (walkers) are achiral, the Hilbert space is spanned by the discrete position states corresponding to vertices of a graph. In the discrete-time case, the introduction of chirality is unavoidable. The Hilbert space corresponding to the chirality has its dimension equal to the number of possible directions of a step.

A possible experimental implementation of a classical random walk is the Galton board (also known as Quincunx). Here a large number of balls (walkers) fall through the board, changing their direction randomly on periodically arranged pins and forming so a binomial distribution of their final position. A quantum analogy of the Galton board (and one possible implementation of the QW) is shown in Figure 1 where the walker is a coherent light pulse moving through a medium with periodical boundaries that split the signal; finally, there are detec-

tors at the end which represent the quantum equivalent of the bins in the classical model.

The spectrum of investigation of the QW (and its modifications) is broad. The original idea was presented in [1–3] and since then a few review papers have been published [4–6]. Recently, there have been studies of QW allowing Lévy noise in the model. The latter is introduced via randomly performed measurements with waiting times following a Lévy distribution [7,8]. The most relevant paper for the present work is [9] in which the properties of the one-dimensional continuous-time QW in a medium with static and dynamic disorder are examined. Other studies of the QW have focused on the meeting problem of two particles [10,11]. Recurrence properties of the walker have been investigated in [11–13]. Moreover, localization of the walker has been studied in [14]. Finally, a theoretical investigation of the QW in random environment has been performed in [15,16], where a robust mathematical definition of a random environment is provided.

The simplest analytic task in the study of quantum walks is to determine the functional expression of the probability to find a particle at a certain location at a certain time. General analytic calculations of quantum walks are not known. However, asymptotic solutions of several quantum walk models have been found using path

^a e-mail: hynek.lavicka@fjfi.cvut.cz

integral techniques in [14–22] and in [10,11] using Fourier transform.

Since their introduction, many experimental groups have tried to implement quantum walks. A number of successful realizations of one-dimensional QW have been reported in optical lattices [23], trapped ions [24], and cavity QED [25]. More recently, additional realizations of a quantum walk using atoms in an optical lattice [26], trapped ions [27,28] and photons [29] have been announced.

Recent studies of quantum systems [30,31] with random potentials have shown that localization of the particle can occur as a result of the randomness. Focusing on quantum walks, Ribeiro et al. [32] have used two different coin operators switched according to the Fibonacci series and they have observed localization in the system. Yin et al. [9] have numerically simulated the continuous-time QW on a line and they have observed Anderson localization only in the case of static disorder, while dynamic disorder leads to decoherence and a Gaussian position distribution. In addition, effects of spatial errors have been studied by Leung et al. in [33]. They have examined QWs in 1 and 2 dimensions on networks with percolation where the missing edges or vertices absorb the walker, leading to topological randomness of the graph.

The simplest discrete QW is described by the action of the coin and the step operator. Much attention was paid to the alternation of the coin operator – position or time dependent coin and its implications on the walker dynamics have been extensively discussed. However, little focus was given to changes of the step operator. Our analysis takes a step in this direction. While assuming a constant coin we study changes in the step operator. When assuming a Galton board realization this amounts to a change in the connectivity between the layers of beam splitters forming the walks.

In the present paper, we focus on the QWs where signals can jump to a distant location, which is a generalization motivated by Lévy flights in classical mechanics. The jump may be caused by an inhomogeneity of the material, spatial proximity of non-neighbor channels or scrambling in the topology of the network (for instance relabeling of input-output label of multiports forming the network realising the QW).

We study two basic modifications of the QW. In the first case, which we call dynamic disorder, the jumps are prepared as independent and identically distributed in time, whereas in the second case, called static disorder, the positions of the jumps are perfectly correlated. We investigate the problem using computer simulations employing the Zarja library¹ [34] and its offspring library focused on the QW².

The structure of the article is as follows. In Section 2, we motivate our study from an experimental point of view. Then we define a model with next neighbor interactions only. In Section 3, we show the results of the simulations based on Monte Carlo method. In Section 4, we discuss our results and draw conclusions. Finally, we describe in the

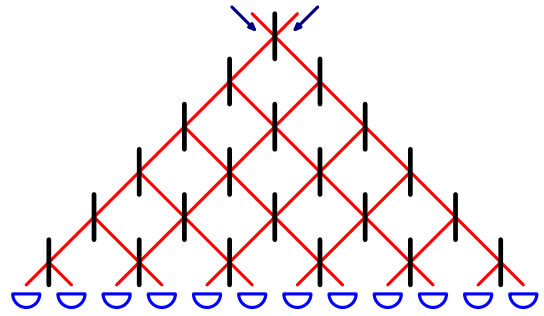


Fig. 1. A schematic of an interferometer simulating material and implementing a random walk. The red lines are the connections of multi-ports along which the signal is transmitted. The light blue half-circles represent detectors. The blue arrows are two selected input channels. Every horizontal layer of the multi-ports is accessed simultaneously.

appendix the set of operators used in the simulations and an algorithm to sample from the appropriate probability distribution.

2 Definition of a quantum walk

We model a sequence of optical layers by an array of multi-ports, or beam splitters (Fig. 2), forming so a large interferometer, see Figure 1 – this is a quantum analog to Galton’s board (Quincunx). Due to the regular structure of the interferometer, it is natural to treat the temporal evolution of the system in discrete steps, discretized by the time needed for an excitation to travel the distance between two consecutive layers at a constant angle. If we let this angle approach the right angle, we obtain so-called static disorder (see Fig. 3d, 3e), where the same set of beam splitters is used repeatedly in every time step. An excitation enters the system of multi-ports at one selected position and spreads due to the coherent interaction with the beam splitters. A number of detectors is placed in the interferometer so that the signal hits one detector in every possible path after a given number of interactions with the medium. The resulting scheme is an implementation of the QW.

In the following, we introduce two ways to describe the system. First we introduce the standard notation for a discrete-time QW. We define the basis states of the system as states localized at the beam splitters just before or after the interaction takes place. Therefore, every basis state is described by a position within the beam splitter layer (an integer number) and a chirality, which can take values L or R for left and right, respectively. Formally, we define the state space \mathcal{H} of the system as

$$\mathcal{H} = \mathcal{H}_S \otimes \mathcal{H}_C \quad (1)$$

where a “position” space \mathcal{H}_S and a “coin” space \mathcal{H}_C (the name stemming from the idea of a random walker tossing a coin to decide the direction of his next step) are defined as

$$\mathcal{H}_S = \text{Span}\{|n\rangle \mid n \in \mathbb{Z}\} \quad (2)$$

¹ <http://sourceforge.net/projects/zarja/>

² <http://sourceforge.net/projects/quantumwalk/>

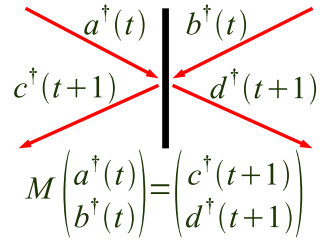


Fig. 2. Action of a beam splitter on the input states $a^\dagger(t)$ and $b^\dagger(t)$ which are transformed to the output states $c^\dagger(t+1)$ and $d^\dagger(t+1)$ using the matrix M .

and

$$\mathcal{H}_C = \text{Span}\{|L\rangle, |R\rangle\}. \quad (3)$$

We define all the numbered states $|n\rangle$, as well as the states $|L\rangle$ and $|R\rangle$, to be normalized and mutually orthogonal. Therefore, \mathcal{H}_S is isomorphic to the space ℓ^2 of quadratically integrable complex sequences and \mathcal{H}_C to \mathbb{C}^2 . The basis states are then constructed as tensor product basis states $|n, R\rangle$ and $|n, L\rangle$, where $n \in \mathbb{Z}$.

Following Konno [16], we define that the state of the system at time t in a random environment ω is described by the positive semi-definite density matrix $\hat{\rho}_\omega(t)$ on \mathcal{H} having $\text{Tr} \hat{\rho}_\omega(t) = 1$. Thus the density matrix of the system $\hat{\rho}(t)$ at time t is

$$\hat{\rho}(t) = \int_{\omega \in \Omega} \hat{\rho}_\omega(t) \mathbb{P}(d\omega), \quad (4)$$

where symbols Ω and \mathbb{P} will be specified later in Section 2.2.

The evolution of the system by one timestep from t to $t+1$ for one particular setup of environment ω is described by a unitary operator $U_\omega(t \rightarrow t+1)$ which acts as follows:

$$\hat{\rho}_\omega(t+1) = U_\omega(t \rightarrow t+1) \hat{\rho}_\omega(t) U_\omega^\dagger(t \rightarrow t+1) \quad (5)$$

just the same way as typical propagator on density matrix in quantum mechanics in, e.g., [35].

2.1 Quantum walk

The QW described, e.g., in [4] assumes that the conditions of the environment are stable and thus it holds $\hat{\rho}(t) = \hat{\rho}_\omega(t)$ for all $\omega \in \Omega$. If we set up the initial density matrix $\hat{\rho}(0)$ as a pure state $|\psi_0\rangle \in \mathcal{H}$ using $\hat{\rho}(0) = |\psi_0\rangle\langle\psi_0|$, then the system is in a pure state $|\psi_T\rangle = \prod_{t=0}^{T-1} U^{QW}(t \rightarrow t+1)|\psi_0\rangle$ (the product expanded in the proper time ordering) at every timestep T and the appropriate density matrix is $\hat{\rho}(T) = |\psi_T\rangle\langle\psi_T|$. Moreover, the original QW was defined with fixed unitary operator $U^{QW}(t \rightarrow t+1)$ in the form of a composition of two unitary operations as follows:

$$U^{QW}(t \rightarrow t+1) = SC. \quad (6)$$

Thus, the evolution of the walker at time T is $|\psi_T\rangle = (U^{QW})^T |\psi_0\rangle$. The operator C is called a *coin operator* and describes the transformation induced by a beam splitter.

Here the position of a localized state stays unchanged and the operation acts only on the coin state as $C = I \otimes M$, where M is a unitary operation transforming the probability amplitudes due to a partial reflection on the beam splitter. We assume for simplicity that all the beam splitters have the same physical properties and perform a Hadamard transform on the input states,

$$M = \frac{1}{\sqrt{2}} \begin{pmatrix} 1 & 1 \\ 1 & -1 \end{pmatrix}. \quad (7)$$

The operator S represents the propagation of an excitation in the free space between the beam splitters. Hence, the chirality of a basis state does not change but the position is shifted by ± 1 , depending on the coin state. We can express S as

$$S = \sum_{n \in \mathbb{Z}} (|n+1, R\rangle\langle n, L| + |n-1, L\rangle\langle n, R|). \quad (8)$$

It is easy to show that the sum converges and defines a unitary operator defined on all the state space \mathcal{H} .

If the initial state of the walker is one of the basis states, for example $|0, R\rangle$, it evolves under the operation U so that in terms of a complete measurement in the position space, the probability spreads to both sides from the starting position. However, it is bounded between the positions $-t$ and t as it can't change by more than 1 in either direction in any step. Moreover, due to the fact that a transition by 1 has to be done in every time step, the walk is restricted at each time t to a subspace spanned by the basis states for which the position shares the same parity with t .

Alternatively, we can describe the path of the walk in terms of the edges of the underlying graph instead of its vertices, following the physical trajectories of the excitation and eliminating the need to describe the propagation between beam-splitters. In the following, we will call these edges “channels”. Due to the fact that every channel lies in between two consecutive positions of the beam splitters, as well as to avoid confusion in the notation, we will denote the channels by half-integer numbers. A notation based on the channel formalism can be introduced and mapped to the previously defined state space in more ways. One such possibility is to identify the channel as a given time t with the state in which the excitation is at the *end* of the propagation, just before hitting another beam splitter (or a detector). This time-dependent mapping is given by the formulas

$$\left|n + \frac{1}{2}; t\right\rangle = \begin{cases} |n, L\rangle & \text{if } t \text{ is even,} \\ |n+1, R\rangle & \text{if } t \text{ is odd} \end{cases} \quad (9)$$

for even n and

$$\left|n + \frac{1}{2}; t\right\rangle = \begin{cases} |n+1, R\rangle & \text{if } t \text{ is even,} \\ |n, L\rangle & \text{if } t \text{ is odd} \end{cases} \quad (10)$$

for odd n . One can verify that such a mapping respects the parity rule and covers all the subspace of \mathcal{H} that is

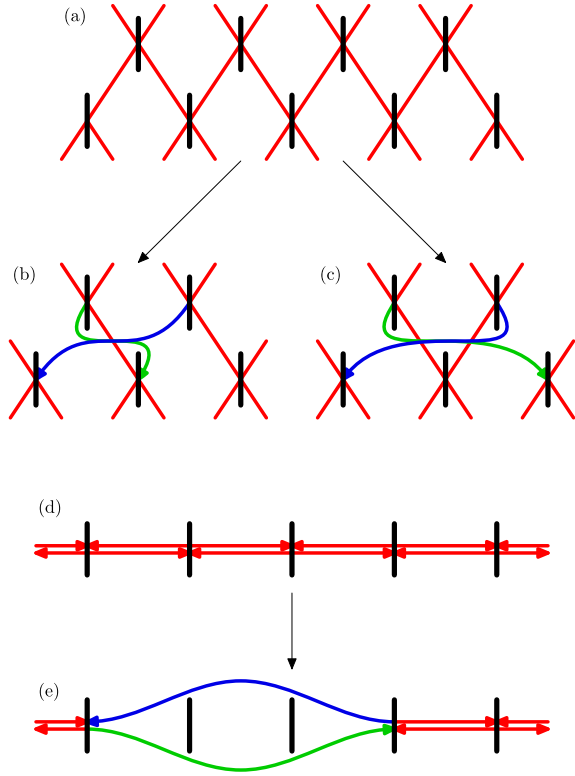


Fig. 3. Schematic picture of different jumps of the signal. Scheme (a) shows a part of interferometer without jumps. Two schemes in the middle, namely (b) and (c), show dynamic disorder pattern where (b) and (c) shows even ($j = 2$) and odd ($j = 3$) size of jump, respectively, which can emerge independently at every level. Scheme (d) shows an interferometer without jumps for static disorder and a jump of size $j = 2$ is illustrated in scheme (e).

actually used by the quantum walk if we assume that the initial state was $|0, R\rangle$ or $|0, L\rangle$. In particular, these two initial states are denoted $|-\frac{1}{2}; 0\rangle$ and $|\frac{1}{2}; 0\rangle$ in the channel notation, respectively; cf. Figure 1 for a visualization. Since the instantaneous chirality of an excitation is uniquely given by the position of the channel and the time, we do not need to specify the coin degree of freedom explicitly in this approach. The “coin toss” and “step” are merged into one unitary operation which mixes neighboring channels in pairs.

The above discussion gives two equivalent ways to describe QW on a line. Throughout this work, we will use the latter approach as it makes it much simpler to describe the jumps in the network.

2.2 Quantum walk with jumps

We will assume that the quantum walk is disturbed by random topological errors, see Figure 3, which are modeled by random changes of connectivities between the multi-ports forming the network in Figure 1. We focus our analysis on two distinct situations. First we will assume that we deal with the repetition of random but station-

ary errors. Stationary errors mean that in each layer the same jumps appear. One could also realize static disorder with a single set of beam splitters, if the incident beam is parallel to the layer of beam splitters and repeatedly sent through them (see Figs. 3d, 3e). The other situation refers to the case when in each layer jumps are generated independently. We refer to the latter situation as dynamic disorder (see Fig. 3a–3c).

In the QW with jumps we assume that the unitary operators $U_\omega(t \rightarrow t+1) = U_\omega^{jump}(t \rightarrow t+1)$ in equation (5) are random (the set of such operators forming a probability space of random unitary operators) and that $U_\omega^{jump}(t \rightarrow t+1)$ can be written in form of a joint action of two unitary operations,

$$U_\omega^{jump}(t \rightarrow t+1) = S_\omega^{jump}(t)U_\omega^{QW}(t \rightarrow t+1), \quad (11)$$

where $U_\omega^{QW}(t \rightarrow t+1)$ is the evolution operator of the 1D QW in a clean media without errors, defined by equation (6).

We define that the set of all unitary operators $S_\omega^{jump}(t)$ forms the probability space $S(\Omega, \mathcal{F}, \mathbb{P})$. For the sake of simplicity of the following discussion and the numerical simulations, we make the set Ω finite by replacing the infinite walking space by a cycle of size N with a periodic boundary condition. If N is chosen sufficiently large, this imposes no restriction on the validity of the results. The sample space Ω is then the set of all the possible combinations of jump operators \mathbf{P}_{j_i} exchanging signals in channels j_i and $j_i + j$, having the matrix form

$$\mathbf{P}_{j_i} = \begin{pmatrix} 1 & 0 & \dots & 0 & \dots & 0 & \dots & 0 & 0 \\ 0 & 1 & \dots & 0 & \dots & 0 & \dots & 0 & 0 \\ \vdots & \vdots & \ddots & \vdots & \vdots & \vdots & \vdots & \vdots & \vdots \\ 0 & 0 & \dots & 0 & \dots & 1 & \dots & 0 & 0 \\ \vdots & \vdots & \vdots & \vdots & \ddots & \vdots & \vdots & \vdots & \vdots \\ 0 & 0 & \dots & 1 & \dots & 0 & \dots & 0 & 0 \\ \vdots & \vdots & \vdots & \vdots & \vdots & \vdots & \ddots & \vdots & \vdots \\ 0 & 0 & \dots & 0 & \dots & 0 & \dots & 1 & 0 \\ 0 & 0 & \dots & 0 & \dots & 0 & \dots & 0 & 1 \end{pmatrix}, \quad (12)$$

i.e., that of a transposition operator. $\mathcal{F} = 2^\Omega$ is the σ -field defined on

$$\Omega = \{\mathbf{E}, \mathbf{P}_{j_1}, \mathbf{P}_{j_1}\mathbf{P}_{j_2}, \dots\} \quad (13)$$

and $\mathbb{P} : \mathcal{F} \rightarrow [0, 1]$ is the probability measure, specified by the probability of elementary events, defined as

$$\mathbb{P}(\pi) = \frac{1}{Z} p^{\text{tr}(\pi)} (1-p)^{N-2\text{tr}(\pi)}. \quad (14)$$

We define $\text{tr}(\pi)$ as the number of transpositions of indexes forming permutation π , N is equal to the size of the system and consequently to the dimension of jump operators \mathbf{P}_{j_i} , p is probability that one pair of errors with distance j occurs and finally $Z = \left(1 + (-p)^{\frac{N}{g}}\right)^g$ is normalization where $g = \text{gcd}(N, j)$ (gcd stands for greatest common denominator).

3 Simulation of the model

The disorder of the system is expressed by the set of unitary operators displacing the signal to a distant location. In general, the system can undergo either static

or dynamic disorder. The system with static disorder is propagated by random unitary operators fixed during the realization, i.e., the operators are correlated in time. On the other hand, the evolution of the system undergoing dynamic disorder is governed by the operators that are independently and identically distributed in time.

3.1 Static disorder

The random unitary operators propagating the system with typical structure of jumps according to equation (12) can have due to mapping 9 and 10 one of two fundamental distinguished forms, according to the parity of the length of the jumps induces by the errors in the media. Jumps of even lengths j do not change chiral state of the walker in Hilbert state \mathcal{H} in contrast to jumps of odd lengths j which swap chirality of the walker from state L to R and vice versa.

3.1.1 Odd jumps

The only tunable parameter that affects the evolution of the walker is the probability p that one error (jump with distance j) occurs. The value of the parameter p close to 0 should produce typical chiral 1D QW pattern, which is clearly visible on the top of Figure 4. Here the QW was initiated in a localized state $|0 + \frac{1}{2}; 0\rangle$ of the walker, causing an asymmetrically distributed walk. Higher values of p produce totally different pattern where high-frequency oscillations of probability distribution of positions of the walker are suppressed. In the middle and at the bottom of Figure 4 the probability distribution of the positions of the walker shows Laplace distribution modulated by Laplace distributed peaks with distance j between neighboring peaks (clearly observable as the small triangular peaks modulated on a bigger structure in Fig. 4).

Previous observations of the fundamental change induced by the variation of p is supported by Figure 5 showing evolution of the probability distribution. The top part shows the typical structure of evolution of the probability distribution of the walker – the quantum carpet [36] – with additional quantum carpets on the border of the main one which were formed at initial stages of evolution. For small values of p , the interference is not strong enough to change the pattern of distribution. In contrast, in the second case displayed at the bottom of Figure 5, where $p = 0.5$, we observe a typical structure of equidistant peaks separated by valleys of width j . The peaks are formed early during evolution and they do not change their positions later.

To support the idea that the walker froze in the close neighborhood of a few preferred locations we analyzed the evolution of entropy and variance of the probability distribution of the position of the walker. The evolution of the variance, shown in Figure 6, visualizes the observation from the previous paragraph. For a probability p close to 0 (unperturbed QW), we see a clear ballistic diffusion of the walker ($\sigma^2 \sim t^2$) – in contrast to this we stress that for a classical random walker $\sigma^2 \sim t$. Increasing p , we observe

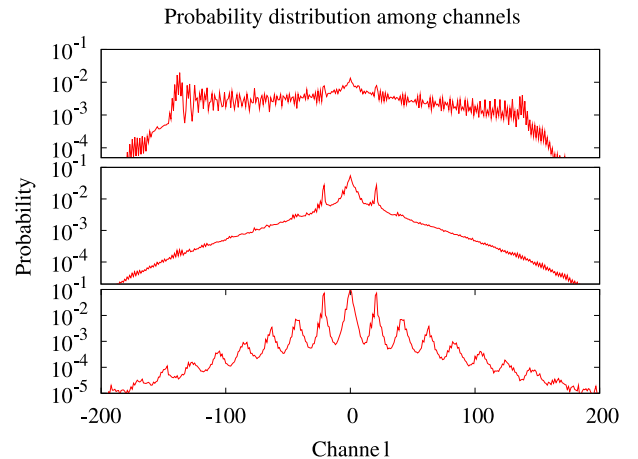


Fig. 4. Typical patterns of probability distribution of position of the walker among channels after $T = 200$ steps for $j = 21$, from the top to the bottom $p = 0.01$, $p = 0.05$ and $p = 0.2$. On the top, the typical structure of the QW without jumps that is perturbed by formation of an extra central peak. In the middle, we see formation of Laplace-like tail and 3 peaks with distance j . Central peak is located at the position of the initial excitation of the system at $T = 0$. On the bottom, the whole distribution follows an overall exponential decay which is modulated by exponential peaks with a distance $j = 21$ between maxima. The graphs were obtained using Monte Carlo method after $R = 20\,000$ runs of the randomized evolution.

sub-ballistic diffusion and finally, in the range close to $1/2$, the variance tends to finite constant.

Next, we turn our attention to the evolution of the classical (Shannon) entropy of the probability distribution of the positions of the walker, which is shown in Figure 7. The evolution of the classical entropy follows an analogous behaviour as described in the case of variance in the previous paragraph. Thus, we can observe for the probability p close to unperturbed QW an increase of classical entropy proportional to $\ln(t)$. However, rising probability p causes slower and slower increase in entropy in time and for the case $p = 0.4$ we observe a saturation of entropy.

The conclusion of the above paragraphs on odd-sized jumps in the QW is that we clearly observe localization of quantum walker in static disorder media described by the probability space of random unitary operators $S(\Omega, \mathcal{F}, P)$ parametrized by probability p . Moreover, the numerical results suggest that taking separately odd and even timesteps the probability distribution of the position of the walker converges to a stationary distribution:

$$\left\langle n + \frac{1}{2}; 2t \left| \hat{\rho}(2t) \right| n + \frac{1}{2}; 2t \right\rangle \xrightarrow{t \rightarrow +\infty} \mathbb{P}_{p,j}^{even} \left(n + \frac{1}{2} \right) \quad (15)$$

$$\left\langle n + \frac{1}{2}; 2t + 1 \left| \hat{\rho}(2t + 1) \right| n + \frac{1}{2}; 2t + 1 \right\rangle \xrightarrow{t \rightarrow +\infty} \mathbb{P}_{p,j}^{odd} \left(n + \frac{1}{2} \right). \quad (16)$$

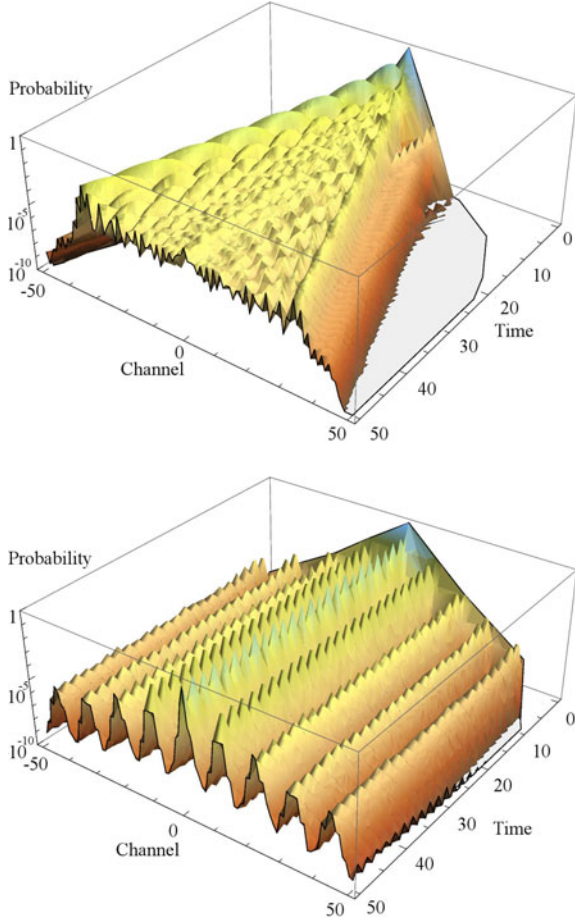


Fig. 5. Probability distribution among channels for $T = 200$, $R = 20\,000$ and $j = 11$; from the top to the bottom $p = 0.01$ and $p = 0.5$. On the top, the maxima of probability move outward similarly to the standard case of the QW. On the bottom, the maxima are formed and they stay at the point of original formation.

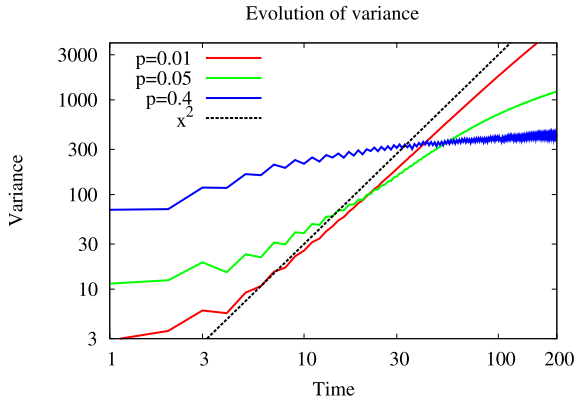


Fig. 6. Evolution of variance of the system for $T = 200$, $R = 20\,000$ and $j = 11$. Transition from the case of ballistic diffusion of the signal for probabilities p close to 0 to the case of sub-ballistic diffusion, demonstrated for $p = 0.05$ can be observed, and finally we observe for $p = 0.4$ that variance tends to a constant, i.e., diffusion coefficient approaches 0 and the walker ceases to “spread” – a characteristic property of localization [37].

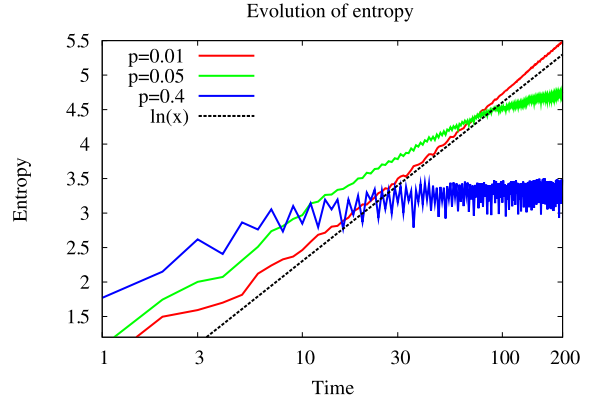


Fig. 7. Evolution of classical (Shannon) entropy of probability distribution of positions of walker for $T = 200$, $R = 20\,000$ and $j = 11$. Classical entropy is a rising function of time t for $p = 0.01$ where the functional form is proportional to $\ln t$. On the other hand, increasing probability p causes “freezing” of the evolution, as can be observed for $p = 0.4$.

$\mathbb{P}_{p,j}^{even}(n + \frac{1}{2})$ and $\mathbb{P}_{p,j}^{odd}(n + \frac{1}{2})$ are universal distributions for odd and even timesteps for probabilities p in range close to $\frac{1}{2}$ and the size of the region of convergence is also dependent on j .

Let us consider the fundamental properties of the asymptotic probability distribution $\mathbb{P}_{p,j}^{even}(n + \frac{1}{2})$; variables of the probability distribution $\mathbb{P}_{p,j}^{odd}(n + \frac{1}{2})$ for odd timesteps are different but general properties are shared. We concluded from Figure 4 that we observe a formation of an overall Laplace distribution modulated by Laplace distribution of peaks, both in the form

$$\mathbb{P}(x) = C \exp\left(-\frac{|x - \mu|}{a}\right), \quad (17)$$

where μ is the mean value of the distribution and a is related to variance via $\text{Var } \mathbb{P}(x) = 2a^2$. Our aim is to estimate the inverse parameter $\frac{1}{a}$ of Laplace distribution in two cases for

- the whole distribution (with mean at the point of injection),
- the modulated peaks (with mean at the center of the peak).

We focus on the shape of the whole probability distribution. The plots in Figure 8 suggest a U -shape function of the fitted inverse parameter $1/a$ of the Laplace distribution for all parameter values. We vary the probability p and we connect points for the same jump sizes j . Defining the x -axis as $x = pj$ we put all minima at a fixed position. Thus, for the minima $pj = x_{min}$ holds where an approximation of the constant is $x_{min} = 2$. The values of minima of the fitted inverse parameter $1/a$, reached for $p = x_{min}/j$, form an increasing function of jump size j . The size of the central peak is j , $j/2$ on the left and on the right from the maximum at 0. Estimation of the inverse parameter $1/a$ of the central peak is shown in Figure 9. The shape of the central peak is an increasing linear function of probability of jump p independent of

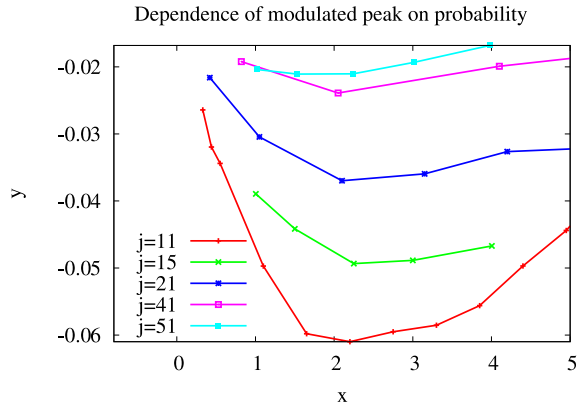


Fig. 8. Fit of the inverse parameter $\frac{1}{a}$ of the probability distribution of position of the walker for $T = 200$ and $R = 15\,000$ with various odd sizes of jump j taking x -axis as $x = pj$ and $y = 1/a$. We observe the formation of a U -shape function for constant sizes of jump j and changing $x = pj$ with a minimum at $x_{min} = 2$.

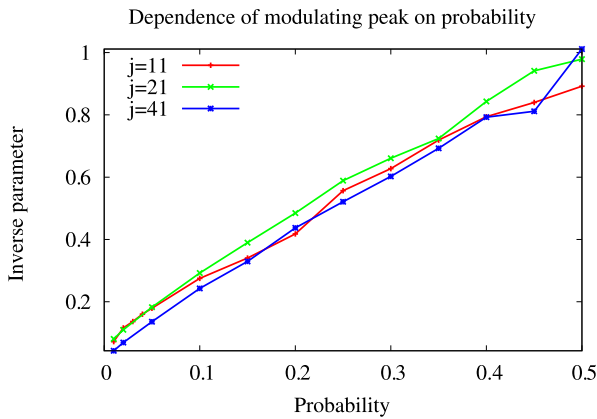


Fig. 9. Fit of the inverse parameter $\frac{1}{a}$ of the central peak of the probability distribution of the position of the walker for $T = 200$ and $R = 15\,000$ with various odd sizes of jump j . Increasing probability causes linear increase of the inverse parameter $\frac{1}{a}$ with p when j is fixed. Moreover we observe a universal dependence on p , independent of the length of jump j .

the size of jump j . Thus the central peak becomes steeper and steeper with increasing p – localization of the walker becomes more evident. This is true not only for the central peak but it holds true for the other peaks as well, see Figure 4.

Let us look at the dependence of entropy of probability distribution $\mathbb{P}_{j,p}(n + \frac{1}{2})$ to find a walker at position $n + \frac{1}{2}$. We plot it in Figure 10 where the entropy was measured by both extensive and non-extensive measures. In the first case, the extensive measure is classical (Shannon) entropy. The non-extensive one is the q -entropy introduced by Tsallis, which for a particular $q = 1$ reduces to the classical entropy (for more about q -statistics, see [38–42]). Both entropies are decreasing functions for increasing disorder measured by p . This leads to a counter-intuitive statement that increasing classical disorder organizes quantum system even if measured by a non-extensive entropy

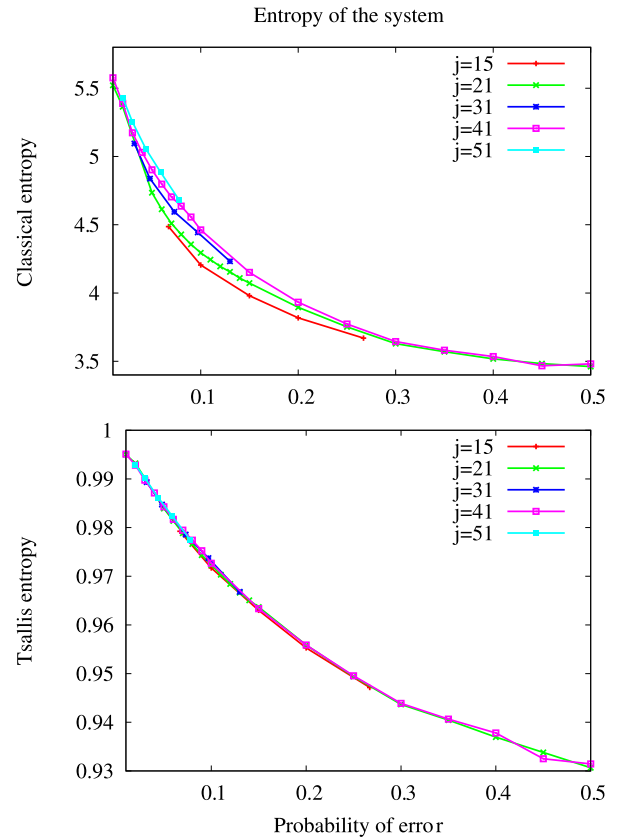


Fig. 10. Classical entropy of the probability distribution is on the top, Tsallis entropy for $q = 2$ on the bottom for parameters set to $T = 200$ and $R = 15\,000$. Classical entropy, on the top, decreases for increasing p but the shape of the dependence is different for different values of j . The shape of the decrease becomes the same for Tsallis entropy with parameter $q = 2$ as seen on the bottom.

(in classical random walk longer jump causes increasing variance and increasing entropy as well). Moreover, the q -entropy of the probability distribution of position of the walker for the parameter value $q = 2$ brings all curves corresponding to different sizes of jump j on one single curve. This means that if we take into account non-additivity of the system quantified by the parameter $|1 - q|$ (taken from the theory of the nonadditive q -entropy), we can map the QWs between each other for different sizes of error j holding probability of occurrence of pair of error positions p constant for $q = 2$.

Finally, the last studied variable for the QW with static disorder was the variance of position displacements $\text{Var } \mathbb{P}_{p,j}$, plotted in Figure 11 on the left and with rescaled axes on right-hand side. The variance forms a U -shaped function of p with moving minima for different but fixed j . Rescaling the axis $x = pj^\alpha$ where $\alpha = 1.04$ and axis $y = j^{-\beta} \text{Var } \mathbb{P}_{p,j}$ where $\beta = 1.67$, we clearly see from Figure 11, right inset, that there is a universal U -shape function $f_{\text{odd}}^*(x)$ fulfilling

$$f_{\text{odd}}^*(x) = j^{-\beta} \text{Var } \mathbb{P}_{x,j}. \quad (18)$$

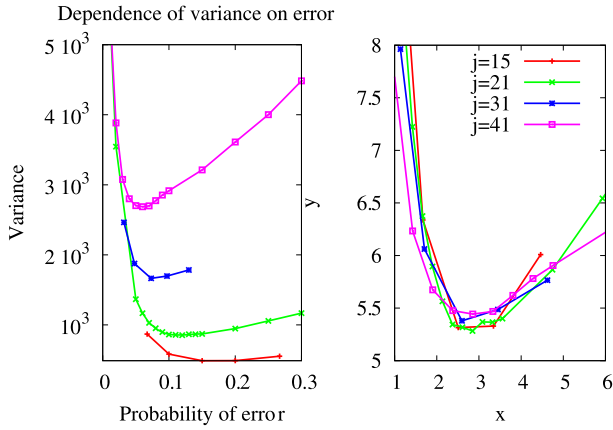


Fig. 11. Dependence of variance of the probability distribution for odd j on p for $T = 200$ and $R = 15\,000$ is shown. The typical U -shape function can be observed with shifted position of the minimum. On the right, there are the same data with rescaled x -axis where $x = pj^\alpha$ where $\alpha = 1.04$ and y -axis where $y = j^{-\beta}\text{Var}(i)$ where $\beta = 1.67$. The data fit on the same U -shape function reaching their minimum at the same place.

Due to relation $\alpha \simeq 1$ and the U -shape of function $f_{\text{odd}}^*(x)$ we can conclude that the overall variance of probability distribution of the walker's position is strongly correlated with the fit of the inverse parameter $1/a$ (of the Laplace distribution) of whole probability distribution.

3.1.2 Even jumps

Let us now assume that the ensemble of the random unitary matrices is still parametrized by the probability p that the pair of erroneous positions occur, but the distance of a pair of errors j is an even number and due to the mappings 9 and 10 the chirality of walker does not change. The typical formation of Laplace-like distribution as in the case of odd jumps is not present, but instead we observe a 3-peaked structure, as seen in Figure 12 (left-right asymmetric due to the initial condition) modulated by a periodic function that has its period equal to the length of jump j . To emphasize the difference between odd and even j , we conclude that both cases form a located peak at the initial position of the walker. However, odd sized jumps j cause Laplace-like overall distribution while the case of even j can form a 3-peaked distribution where the central (localized) peak is sharp but the two others are broad and peaks with distance j are modulated on the overall structure.

3.2 Dynamic disorder

The static disorder analyzed in the preceding sections assumes random, but time-correlated emergence of pairs of errors that are expressed in the set of random unitary operators $S(\Omega, \mathcal{F}, \mathbb{P})$. In contrast, dynamic disorder assumes

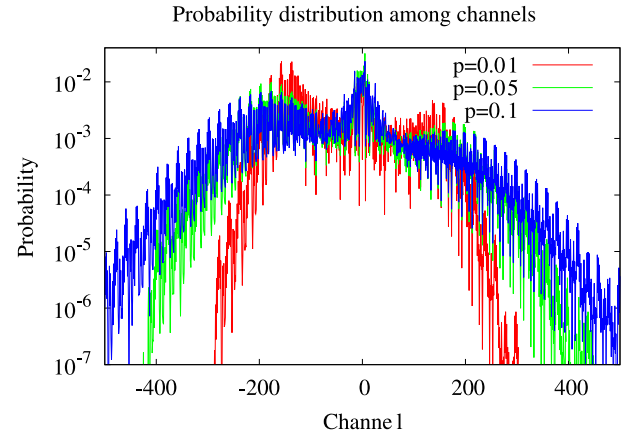


Fig. 12. Probability distribution among channels for $T = 200$ and $R = 15\,000$ in the case of even sized jumps ($j = 20$). The probability distribution forms a 3-peak structure that is modulated by additional periodical small peaks which are separated by j .

independent and identically distributed random unitary operators from the same probability space $S(\Omega, \mathcal{F}, \mathbb{P})$.

Let us consider on the probability distribution of the position of the walker, plotted in Figure 13 on the top. We observe decoherence of the quantum walker forming a distribution reminiscent of a Gaussian distribution modulated by 1D QW patterns for small probabilities of jump p . On the other hand, large p causes a modulation by valleys with distance j between peaks. The functional dependence of the standard deviation of the probability distribution of position of the walker on probability of jump p in Figure 13 on the bottom shows a linear behavior.

4 Discussion and conclusions

We have defined a modification of the QW in 1D where the environment causes long but fixed-size jumps that emerge with a constant probability – the model is no longer deterministic but stochastic, depending on a random variable. In one step, first a unitary QW coin and shift operator act on the state, then a stochastic displacement operator generates jumps. We have studied two classes of QW with disordered connections between beam-splitters. First, dynamic disorder model shows decoherence that leads to Gaussian distribution modulated by residual patterns of QW (for small probabilities of jump p) or by valleys (for large probabilities of jump p). The standard deviation of the position of the walker is a linear function of p . In the second case, the QW is perturbed by static disorder. The behaviour of the model depends on the size of jump and we have investigated odd and even jump sizes separately. Even jump sizes cause localization of the walker at the initial position and two other broad peaks modulated by oscillations with a period of the size of jump j . The focus of the paper, however, was mainly given to jumps with odd size. In this case, the evolution of the variance

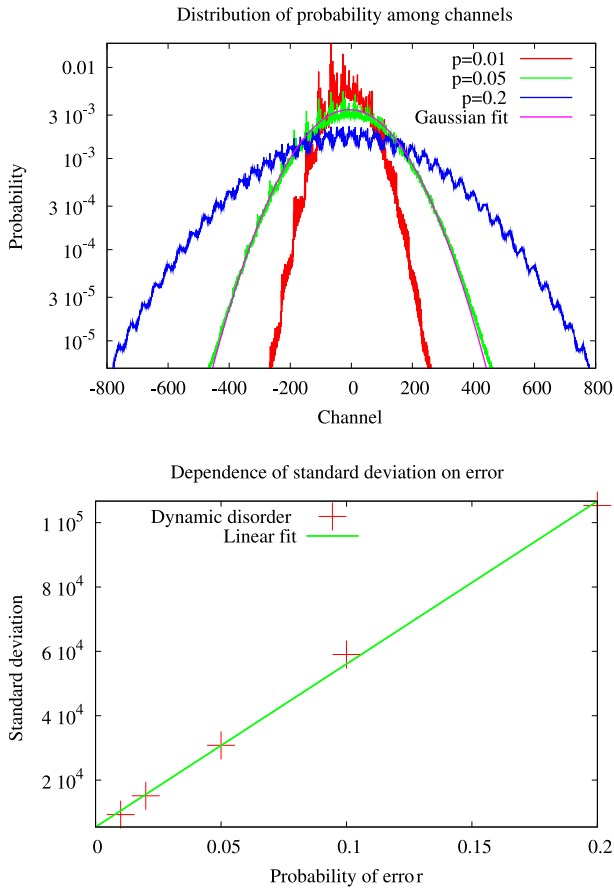


Fig. 13. On top, probability distribution among the channels for dynamic disorder for $T = 100$, $R = 5000$ and $j = 40$. Probability distribution can be fitted to a normal distribution where residual patterns of the QW are present for $p = 0.01$; for $p = 0.2$, formation of periodical valleys modulated on overall distribution (similar to static disorder with an odd size of jump) can be observed. On the bottom, functional dependence of standard deviation of the probability distribution of the position of the walker on probability of error p and its linear fit.

shows a transition from the ballistic diffusion to a no-diffusion regime with increasing p and this observation is supported by numerical calculation of classical entropy which changes from logarithmically increasing regime to a no-growth regime.

In addition, the probability distribution of positions of the walker changes from a pattern typical to the QW to Laplace distribution modulated by Laplace distributed peaks separated by the size of jump j . The formation of Laplace distribution depends on the probability p that a pair of errors occurs. Moreover, the model exhibits the unusual property that classical disorder in quantum system can decrease, i.e., we observe a decrease of both the classical (Shannon) and q -entropy (with $q = 2$) of measurements. Finally, our numerical calculation shows that using non-additive q -entropy with $q = 2$ there is an universal functional dependence of q -entropy on p for arbitrary j . The next part of our investigation was turned to the variance of the probability distribution. Our numerical

results indicate that there is an universal functional form of variance of the probability distribution of the position of the walker – variance multiplied by $j^{-\beta}$ is an universal U -shaped function of one variable pj^α where $\alpha = 1.04$ and $\beta = 1.67$. The functional dependence of the universal function shows a minimum which separates two regimes – one with decreasing variance and the second with increasing variance. To put this result in the broader context of complex systems and game theory, we note that similar behavior of variance of attendance has been observed in Minority Game, exhibiting dynamical phase transition, see, e.g., [34,43].

The financial support by MSM 6840770039, MŠMT LC 06002, GAČR 202/08/H072, the Czech-Hungarian cooperation project (KONTAKT CZ-11/2009), Hungarian Scientific Research Fund (OTKA) under contract No. K83858, the Emmy Noether Program of the DFG (contract No. LU1382/1-1) and the cluster of excellence Nanosystems Initiative Munich (NIM) is gratefully acknowledged.

Appendix: Properties of the set of operators

Let the unperturbed walking space be represented by a cycle graph with N vertices where every vertex represents a channel in the main text. The errors in the network are represented by swapping the walker's probability amplitudes between vertices labelled i and $i + j \bmod N$ for a fixed j , which happens with a relative probability p . With a relative probability $1 - p$, a vertex is left intact. Finally, a vertex already exchanged with another one cannot be used for another transposition in the same permutation.

These conditions give the probability of a permutation π in the form

$$\mathbb{P}(\pi) = \frac{1}{Z^{(N)}} p^{\text{tr}(\pi)} (1 - p)^{N - 2\text{tr}(\pi)}, \quad (\text{A.1})$$

where $\text{tr}(\pi)$ denotes the unique number of independent transpositions forming the permutation π . A factor of 2 in the exponent of $1 - p$ is present due to the fact that every transposition reduces the number of unused vertices by 2. Finally, the factor $Z^{(N)}$ is the normalization constant.

The constant $Z^{(N)}$ is computed as

$$Z^{(N)} = \sum_{k=0}^{\lfloor \frac{N}{2} \rfloor} N_k p^k (1 - p)^{N - 2k}, \quad (\text{A.2})$$

where N_k is the count of all possible permutations formed by exactly k non-incident transpositions of size j .

Lemma 1 *Let $N > 2$, let j and N are relatively prime. Then*

$$Z^{(N)} = 1 + (-p)^N. \quad (\text{A.3})$$

Proof. Due to the relative primality of j and N , we can relabel the vertices by indices 0 through N such that vertices with successive indices have a distance of j in the original

numbering. This way, we can reduce the problem of finding N_k to a combinatorial problem of finding the number of k -element subsets $A \subseteq \{0, 1, \dots, N-1\}$ satisfying the following conditions:

- (a) for all $0 \leq i < N-1$, $\{i, i+1\} \not\subseteq A$,
- (b) $\{0, N-1\} \not\subseteq A$.

In order to find N_k , we discuss two disjoint cases:

- (i) Let us count the subsets which do not contain $N-1$ as an element. For each such set $A = \{a_1, a_2, a_3, \dots, a_k\}$, $a_1 < a_2 < \dots < a_k$, we denote $\tilde{A} = \{a_1, a_2-1, a_3-2, \dots, a_k-k+1\}$. This is a one-to-one mapping, reducing the problem to finding k -element subsets of $N-k$ elements without any additional restriction. This gives $\binom{N-k}{k}$ possible subsets.
- (ii) Let now $N-1 \in A$. Then the other $k-1$ elements of A must lie in $\{1, 2, \dots, N-2\}$, with no two of them successive and $N-2$ excluded. This is a variant of the subproblem (i), giving $\binom{N-k-1}{k-1}$ possibilities for A .

Adding these results, we find that

$$N_k = \binom{N-k}{k} + \binom{N-k-1}{k-1}. \quad (\text{A.4})$$

In order to calculate $Z^{(N)}$, we find the generating function

$$\begin{aligned} F(x) &= \sum_{N=0}^{+\infty} Z^{(N)} x^N \\ &= \sum_{N=2}^{+\infty} \sum_{k=0}^{\lfloor \frac{N}{2} \rfloor} N_k \times p^k (1-p)^{N-2k} x^N. \end{aligned} \quad (\text{A.5})$$

Here, for simplicity, we generalize A.4 also for $N \leq 2$ and we define by convention $\binom{-1}{-1} = 0$. Using standard methods, we obtain for the sum

$$F(x) = \frac{1 + px^2}{1 - x + xp - px^2}. \quad (\text{A.6})$$

This result can be decomposed into partial fractions as

$$F(x) = \frac{1}{1-x} + \frac{1}{1+px} - 1, \quad (\text{A.7})$$

from which the power series can be derived quickly as

$$\begin{aligned} F(x) &= \sum_{N=0}^{+\infty} x^N + \sum_{N=0}^{+\infty} (-px)^N - 1 \\ &= -1 + \sum_{N=0}^{+\infty} \underbrace{(1 + (-p)^N)}_{Z^{(N)}} x^N. \end{aligned} \quad (\text{A.8})$$

QED.

If $N = 2$, the formula A.3 cannot be used. Indeed, computing $Z^{(2)}$ manually gives

$$Z^{(2)} = p + (1-p)^2 = 1 - p + p^2. \quad (\text{A.9})$$

This is because A.4 gives an incorrect result for $k = 1$ in this case. In practical situations, however, $N \gg 2$.

Lemma 2 *Let N and j be positive integers such that $j < N$, $g = \gcd(N, j)$ and $\frac{N}{g} > 2$. Then*

$$Z^{(N)} = \left(1 + (-p)^{\frac{N}{g}}\right)^g. \quad (\text{A.10})$$

Proof. If $g = 1$, then j and N are relatively prime and we can use Lemma 1 to obtain the result. In the case $g > 1$, we first split the set $\{0, 1, 2, \dots, N-1\}$ into g modular classes (mod g). According to the definition, the selection of the errors can be done independently on each of these subsets. Therefore, as $\frac{N}{g}$ is relatively prime to j , we can use Lemma 1 for each of these classes and multiply the partial results to obtain the total partition function in the form stated by the lemma.

References

1. L. Davidovich, N. Zagury, Y. Aharonov, Phys. Rev. A **48**, 1687 (1993)
2. S. Gudder, *Quantum probability* (Academic Press Inc., CA, USA, 1988)
3. G. Grossing, A. Zeilinger, *Complex systems* (1988), pp. 197–208
4. J. Kempe, Cont. Phys. **44**, 307 (2003)
5. D. Meyer, J. Statist. Phys. **85**, 551 (1996)
6. S.E. Vanegas-Andraca, *Quantum Walks for Computer Scientists* (Morgan and Claypool, 2008)
7. A. Romanelli, R. Siri, V. Micenmacher, Phys. Rev. E **76**, 037202 (2007)
8. A. Romanelli, Phys. Rev. A **76**, 054306 (2007)
9. Y. Yin, D.E. Katsanos, S.N. Evangelou, Phys. Rev. A **77**, 022302 (2008)
10. M. Štefaňák, T. Kiss, I. Jex, B. Mohring, J. Phys. A **39**, 14965 (2006)
11. T. Kiss, I. Jex, M. Štefaňák, New J. Phys. **11**, 043027 (2009)
12. M. Štefaňák, I. Jex, T. Kiss, Phys. Rev. Lett. **100**, 020501 (2008)
13. T. Kiss, M. Štefaňák, I. Jex, Phys. Rev. A **78**, 032306 (2008)
14. N. Konno, Quantum Inf. Process. **9**, 405 (2010)
15. N. Konno, Math. Struct. Comp. Sci. **20**, 1091 (2010)
16. N. Konno, Quantum Inf. Process. **8**, 387 (2009)
17. N. Konno, Quantum Inf. Comput. **2**, 578 (2002)
18. N. Konno, in *Cellular Automata, Proceedings*, Lecture Notes In Computer Science, edited by H. Umeo, S. Morishita, K. Nishinari, T. Komatsuzaki, S. Bandini (2008), Vol. 5191, pp. 12–21
19. N. Konno, in *Quantum Potential Theory*, Lecture Notes In Mathematics, edited by M. Schurmann, U. Franz (2008), Vol. 1954, p. 309
20. N. Konno, Stoch. Models **25**, 28 (2009)
21. N. Konno, Phys. Rev. E **72** (2005)
22. N. Konno, Fluc. Noise Lett. **4**, L529 (2005)
23. W. Dür, R. Raussendorf, V.M. Kendon, H.J. Briegel, Phys. Rev. A **66** (2002)

24. B.C. Travaglione, G.J. Milburn, *Phys. Rev. A* **65** (2002)
25. B.C. Sanders, S.D. Bartlett, B. Tregenna, P.L. Knight, *Phys. Rev. A* **67** (2003)
26. M. Karski, L. Foerster, J.-M. Choi, A. Steffen, W. Alt, D. Meschede, A. Widera, *Science* **325**, 174 (2009)
27. H. Schmitz, R. Matjeschk, Ch. Schneider, J. Glueckert, M. Enderlein, T. Huber, T. Schaetz, *Phys. Rev. Lett.* **103** (2009)
28. F. Zaehring, G. Kirchmair, R. Gerritsma, E. Solano, R. Blatt, C.F. Roos, *Phys. Rev. Lett.* **104** (2010)
29. A. Schreiber, K.N. Cassemiro, V. Potoček, A. Gábris, P. J. Mosley, E. Andersson, I. Jex, Ch. Silberhorn, *Phys. Rev. Lett.* **104** (2010)
30. M. El Ghafar, P. Törmä, V. Savichev, E. Mayr, A. Zeiler, W.P. Schleich, *Phys. Rev. Lett.* **78**, 4181 (1997)
31. S.W. Kim, H.-W. Lee, *Phys. Rev. E* **61**, 5124 (2000)
32. P. Ribeiro, P. Milman, R. Mosser, *Phys. Rev. Lett.* **93** (2004)
33. G. Leung, P. Knott, J. Bailey, V. Kendon, *New J. Phys.* **12**, 123018 (2010)
34. H. Lavička, *Simulations of Agents on Social Networks* (LAP Lambert Academic Publishing, 2010)
35. J. Blank, P. Exner, M. Havlíček, *Linear Operators in Quantum Physics (in Czech)* (Carolinum Prague, 1993)
36. M. Berry, I. Marzoli, W.P. Schleich, *Phys. World* **14**, 39 (2001)
37. P.W. Anderson, *Phys. Rev.* **109**, 1492 (1958)
38. C. Tsallis, *J. Statist. Phys.* **52**, 479 (1988)
39. C. Tsallis, E. Brigatti, *Contin. Mech. Thermodyn.* **16**, 223 (2004)
40. C. Tsallis, *Eur. Phys. J. A* **40**, 257 (2009)
41. C. Tsallis, *J. Comput. Appl. Math.* **227**, 51 (2009)
42. C. Tsallis, in *Interdisciplinary Aspects of Turbulence*, edited by W. Hillebrandt, F. Kupka (2009), Vol. 756, pp. 21–48
43. D. Challet, Y.-C. Zhang, *Physica A* **246**, 407 (1997)

Appendix 4

A. Schreiber, K. N. Cassemiro, V. Potoček, A. Gábris, I. Jex, Ch. Silberhorn

Photonic quantum walks in a fiber based recursion loop

AIP Conference Proceedings **1363**, p. 155 (2011)

Photonic quantum walks in a fiber based recursion loop.

A. Schreiber^{*}, K. N. Cassemiro^{*}, V. Potoček[†], A. Gábris^{†,**}, I. Jex[†] and Ch. Silberhorn^{*,‡}

^{*}Max Planck Institute for the Science of Light, Günther-Scharowsky-str. 1 / Bau 24, 91058 Erlangen, Germany.

[†]Department of Physics, FNSPE, Czech Technical University in Prague, Břehová 7, 115 19 Praha, Czech Republic.

^{**}Research Institute for Solid State Physics and Optics, Hungarian Academy of Sciences, H-1525 Budapest, P. O. Box 49, Hungary.

[‡]University of Paderborn, Applied Physics, Warburger Str. 100, 33098 Paderborn, Germany.

Abstract. We present a flexible and robust system for implementing one-dimensional coined quantum walks. A recursion loop in the optical network together with a translation of the spatial into the time domain ensures the possible increment of the step number without need of additional optical elements. An intrinsic phase stability assures a high degree of coherence and hence guarantees a good scalability of the system. We performed a quantum walk over 27 steps and analyzed the 54 output modes. Furthermore, we estimated that up to 100 steps can be realized with only minor changes in the used components.

Keywords: Quantum walk, Quantum simulations

PACS: 03.65.-w, 03.67.-a, 42.50.-p

INTRODUCTION

Quantum walks describe the coherent evolution of quantum particles in a discretized environment. In the case of coined quantum walks the spreading of the particle's wavefunction is determined by an internal quantum state (*coin state*). Superpositions in the coin state induce quantum interference, which leads to a quadratically faster spread compared to the evolution of a classical particle. Quantum walks constitute not only the basis for modelings of natural phenomena like the energy transfer in photosynthesis, but are an important resource for performing quantum algorithms. This emphasizes the need of an experimental implementation, that is not only flexible enough to simulate different physical scenarios but also scalable concerning the number of applicable modes and operations for computational applications. The first implementations of the quantum walk were realized in completely diverse ways: they were based on the manipulation of atoms [1] and ions [2] in traps, energy levels in nuclear magnetic resonance schemes [3] and photons in both, beam splitter arrays [4] and waveguide structures [5]. The major problem with photonic implementations is the lack of scalability or control over the underlying system. Hence our goal is to circumvent this disadvantages and present a photonic implementation with a high flexibility and scalability.

Quantum Communication, Measurement and Computing (QCMC)
AIP Conf. Proc. 1363, 155-158 (2011); doi: 10.1063/1.3630170
© 2011 American Institute of Physics 978-0-7354-0921-7/\$30.00

QUANTUM WALK IN AN OPTICAL NETWORK

In this work we present the implementation of a photonic quantum walk with an integrated feedback loop [6] and investigate its scalability. To manipulate the path of the photons in the experiment we use their linear horizontal $|H\rangle$ or a vertical polarization $|V\rangle$ as the coin state. Each step of the walk consists of a coin operation \hat{C} acting on the polarization state and a subsequent step operation \hat{S} conditionally moving the photon's wavepacket to a new position $x \rightarrow x \pm 1$. A typical coin operation is the Hadamard gate, transforming the coin state in an equal superposition of basis states. The wavefunction of the photon after n steps of the walk is given by $|\psi_n\rangle = (SC)^n |\psi_0\rangle$ with the initial state $|\psi_0\rangle$. At each step the probability of finding the photon at position x with a coin state c is determined by $P(x, c)_n = |\langle x, c | \psi_n \rangle|^2$.

Functional principle: Experimental setup

Our setup is depicted in Fig.1 (left). An attenuated laser pulse ($\lambda = 805$ nm, pulse width = 88 ps) is initialized in an arbitrary polarization state via a half- (HWP) and a quarter-wave plate before getting coupled into the setup with a 3/97 beam splitter (BS_i). For simplicity the initial position is defined as $x = 0$. The polarization of the photon is rotated via another HWP, which constitutes the coin operation \hat{C} . By changing the orientation of the HWP's axes we are able to implement quantum walks with completely different coin operations. A separation and recombination of the polarization components via polarizing beam splitters (PBS) leads to a temporal shift determined by an unequal travelled path length. The spread in time is analogous to a spatial step of length ± 1 , thus realizing the step operator \hat{S} . To implement further steps of the walk without additional optical elements we simply use a loop structure, ensuring that the photon is sent back to the same elements used before. We extract the timing (i.e. position) and polarization information of the photon with two avalanche photo diodes (APDs), by reflecting it out of the setup with a probability of 12% (BS_o) per step. The experiment is repeated with a rate of 110 kHz, allowing to obtain the statistics $P(x, c)_n$ up to a high number of steps.

Scalability: Experimental results

We measured the distribution $P(x, c)_{27}$ after 27 steps of a quantum walk with a symmetric initial state $|H\rangle + i|V\rangle$ and the Hadamard coin. A time and polarization analysis reveals the spread of the photon's wavepacket over the resulting 54 output modes (Fig. 1, right). While the probability to end up near the initial position gets suppressed by quantum interference, the outer positions are strictly enhanced. Furthermore, the asymmetric distribution in both coin states is in marked contrast to the symmetric binomial distribution of a classical random walk. This emphasizes the high degree of coherence in the setup. After 27 steps even small inaccuracies of the used optical components have an impact on the fidelity of the final state, compared to the ideal quantum walk. Such

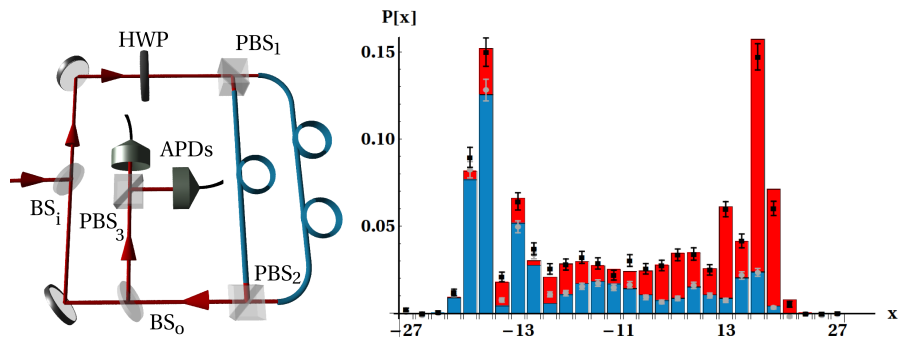


FIGURE 1. Left: Scheme of the setup. The photons get coupled in and out of the setup probabilistically by the beam splitters $BS_{i/o}$. The coin operation is applied via a half-wave plate (HWP). A separation in time induced by two polarizing BS ($PBS_{1,2}$) and polarization maintaining fibers of unequal length implements the step operation. A time and polarization resolving detection is done with two avalanche photodiodes APDs; Right: Arrival distribution $P(x, c)_{27}$ after 27 steps of the symmetric Hadamard walk: Adapted theory for vertical (blue bars) and horizontal polarization (red bars) and measured probabilities (vertical: Gray dots; Vertical + horizontal: Black squares).

imperfections are taken into account in the theory presented in Fig.1 (right). The current limitation of steps is mainly induced by the losses at the optical components: The efficiency per step is equal to 0.55, i.e. a photon will get either lost or detected with a probability of 45% in one round trip. The resulting low arrival rate at the higher step numbers increases the contribution of dark counts detected with the APDs, and hence falsifies the final distribution.

In the following we want to examine in detail the three mentioned limiting factors and give an estimation of their impact on the scalability of the system.

Losses: The losses can be divided into two parts: The intrinsic losses due to in-/ and outcoupling with the beam splitters $BS_{i/o}$ and the common losses at optical components and fiber couplings. To guarantee as many roundtrips as possible, the reflectivity of BS_o can be minimized further, which reduces the probability of a detection at earlier steps. A more efficient way is to replace the passive coupling method by an active switch. In this scheme the photons would be injected in the unused input port of PBS_1 . A polarization modulator in each output arm would induce a 90 degree rotation to guide the injected photons to the correct output port of PBS_2 . A further active rotation after the desired number of steps would eject the photon at the unused output of PBS_2 for detection.

Since the losses at the optical components are inevitable, a valid method to increase the arrival probability for higher step numbers is to increase the average photon number per initial pulse. We want to emphasize at this point that the quantum interference effect underlying the quantum walk can be simulated with the interference of a coherent light pulse as long as the initial state is localized at one position [7]. A replacement of the laser source with a 1 W Laser and the switch to an active coupling system would give us the possibility to implement 100 steps of the quantum walk.

Accuracy: Based on manufacturing and alignment imperfections the performance of the individual components can influence the quality of the quantum walk. To quantify the overall effect we estimated the degree of accuracy for each component and did a Monte Carlo simulation combining the individual errors. The fidelity of the final state

between the ideal walk and the simulation is above 90% for the first 32 steps and drops to 50% for 100 steps, considering a walk with a Hadamard coin and an initial polarization $|H\rangle$.

Decoherence: So far we've realized 27 steps of a quantum walk without a sign of decoherence. One reason to be mentioned here is the intrinsic insensitivity of the setup to static, polarization dependent phase shifts. These are automatically compensated by the geometry of the setup and therefore irrelevant for the coherence of the walk. Nevertheless, dynamic phase fluctuations due to mechanical vibrations still influence the experiment to some extent. Typically, unavoidable vibrations of the optical components occur at a frequency below 500 Hz, corresponding to a time scale of 2 ms. Since the limit of steps is defined by the losses in the setup it is enough to restrict the analysis to 100 steps. The time duration for realizing 100 steps in the current setup would be approximately 50 μ s and hence a factor of 20 smaller than the typical vibrations. This means that the impact of decoherence due to vibrations of the optical components is negligible in the first 100 steps.

CONCLUSION

We presented a robust and flexible implementation of a one dimensional coined quantum walk. We demonstrated a low degree of decoherence in the setup by analyzing all 54 output modes after 27 steps of the quantum walk and showed the potential to perform up to 100 steps. The good scalability and control make the setup a perfect test bed for quantum walk based simulations. Furthermore, an addition of another spatial dimension opens up the possibility to implement efficient quantum algorithms, relying on the quantum walk principle.

ACKNOWLEDGMENTS

We acknowledge financial support from the German Israel Foundation (Project 970/2007). K.N.C. and I.J. acknowledge financial support from the Alexander von Humboldt Foundation; V.P., A.G. and I.J. from MSMT LC06002, MSM 6840770039 and CZ-10/2007.

REFERENCES

1. M. Karski *et al.*, *Science* **325**, 174 (2009).
2. H. Schmitz *et al.*, *Phys. Rev. Lett.* **103**, 090504 (2009). F. Zähringer *et al.*, *Phys. Rev. Lett.* **104**, 100503 (2010).
3. J. Du *et al.*, *Phys. Rev. A* **67**, 042316 (2003). C.A. Ryan *et al.*, *Phys. Rev. A* **72**, 062317 (2005).
4. M. A. Broome *et al.*, *Phys. Rev. Lett.* **104**, 153602 (2010).
5. Y. Lahini *et al.*, *Phys. Rev. Lett.* **100**, 170506 (2008). A. Peruzzo *et al.*, *Science* **329**, 1500 (2010).
6. A. Schreiber *et al.*, *Phys. Rev. Lett.* **104**, 050502 (2010)
7. P. P. Rohde *et al.*, arXiv:1006.5556v1 [quant-ph] (2010)

Appendix 5

A. Schreiber, A. Gábris, P.P. Rohde, K. Laiho, M. Štefaňák,
V. Potoček, C. Hamilton, I. Jex, Ch. Silberhorn

A 2D Quantum Walk Simulation of Two-Particle Dynamics

Science **336**, p. 55, (2012)

28. L. Pitaevskii *et al.*, in *Superconductivity: Volume 1: Conventional and Unconventional Superconductors*, K. H. Bennemann, J. B. Ketterson, Eds. (Springer Verlag, Berlin, 2008), chapter 2.
29. G. B. Arnold, *Phys. Rev. B* **18**, 1076 (1978).
30. X. L. Qi, T. Hughes, S. C. Zhang, *Phys. Rev. B* **82**, 184516 (2010).

Acknowledgments: This work is supported by National Basic Research Program of China (grants 2011CBA00103, 2011CB921902, 2012CB927401, and 2012CB927403), National Natural Science Foundation of China (grants 91021002, 10928408, 10874116, 10904090, 11174199, and 11134008), Shanghai Committee of Science and

Technology, China (grants 09JC1407500, 10QA1403300, 10JC1407100, and 10PJ1405700), the Project “Knowledge Innovation Program” of Chinese Academy of Sciences (grant KJCX2.YW.W10), and the Program for New Century Excellent Talents in University. D.Q. acknowledges support from the “Shu Guang” project supported by Shanghai Municipal Education Commission and Shanghai Education Development Foundation and the Program for Professor of Special Appointment (Eastern Scholar) at Shanghai Institutions of Higher Learning. Y.L. acknowledges support from the U.S. NSF under grant DMR 0908700. The Advanced Light Source is supported by the Director, Office of Science, Office of Basic Energy

Sciences, of the U.S. Department of Energy under contract DE-AC02-05CH11231.

Supporting Online Material

www.sciencemag.org/cgi/content/full/science.1216466/DC1
Materials and Methods
Supplementary Text
Figs. S1 to S4
References (31–34)

10 November 2011; accepted 2 March 2012
Published online 15 March 2012;
10.1126/science.1216466

A 2D Quantum Walk Simulation of Two-Particle Dynamics

Andreas Schreiber,^{1,2*} Aurél Gábris,^{3,4} Peter P. Rohde,^{1,5} Kaisa Laiho,^{1,2} Martin Štefaňák,³ Václav Potoček,³ Craig Hamilton,³ Igor Jex,³ Christine Silberhorn^{1,2}

Multidimensional quantum walks can exhibit highly nontrivial topological structure, providing a powerful tool for simulating quantum information and transport systems. We present a flexible implementation of a two-dimensional (2D) optical quantum walk on a lattice, demonstrating a scalable quantum walk on a nontrivial graph structure. We realized a coherent quantum walk over 12 steps and 169 positions by using an optical fiber network. With our broad spectrum of quantum coins, we were able to simulate the creation of entanglement in bipartite systems with conditioned interactions. Introducing dynamic control allowed for the investigation of effects such as strong nonlinearities or two-particle scattering. Our results illustrate the potential of quantum walks as a route for simulating and understanding complex quantum systems.

Quantum simulation constitutes a paradigm for developing our understanding of quantum mechanical systems. A current challenge is to find schemes that can be readily implemented in the laboratory to provide insights into complex quantum phenomena. Quantum walks (1, 2) serve as an ideal test bed for studying the dynamics of such systems. Examples include understanding the role of entanglement and interactions between quantum particles, the occurrence of localization effects (3), topological phases (4), energy transport in photosynthesis (5, 6), and the mimicking of the formation of molecule states (7). Although theoretical investigations already take advantage of complex graph structures in higher dimensions, experimental implementations are still limited by the required physical resources.

All demonstrated quantum walks have so far been restricted to evolution in one dimension. They have been realized in a variety of architectures, including photonic (8–11) and atomic

(12–14) systems. Achieving increased dimensionality in a quantum walk (15) is of practical interest because many physical phenomena cannot be simulated with a single walker in a one-dimensional (1D) quantum walk, such as multiparticle entanglement and nonlinear interactions. Furthermore, in quantum computation based on quantum walks (16, 17), search algorithms exhibit a speed-up only in higher dimensional graphs (18–20). The first optical approaches to increasing the complexity of a linear quantum walk (21, 22) showed that the dimensionality of the system is effectively expanded by using two walkers, keeping the graph one-dimensional. Although adding additional walkers to the system is promising, introducing conditioned interactions and, in particular, controlled nonlinear interactions at the single-photon level is technologically very challenging. Interactions between walkers typically result in the appearance of entanglement and have been shown to improve certain applications, such as the graph isomorphism problem (23). In the absence of such interactions, the two walkers remain effectively independent, which severely limits observable quantum features.

We present a highly scalable implementation of an optical quantum walk on two spatial dimensions for quantum simulation, using frugal physical resources. One major advance of a 2D system is the possibility to simulate a discrete evolution of two particles, including controlled interactions. In particular, one walker, in our case a coherent light pulse, on a 2D lattice is topolog-

ically equivalent to two walkers acting on a 1D graph. Thus, despite using an entirely classical light source, our experiment is able to demonstrate several archetypal two-particle quantum features. For our simulations, we exploited the similarity between coherent processes in quantum mechanics and classical optics (24, 25), as it was used, for example, to demonstrate Grover’s quantum search algorithm (26).

A quantum walk consists of a walker, such as a photon or an atom, which coherently propagates between discrete vertices on a graph. A walker is defined as a bipartite system consisting of a position (x) and a quantum coin (c). The position value indicates at which vertex in the graph the walker resides, whereas the coin is an ancillary quantum state determining the direction of the walker at the next step. In a 2D quantum walk, the basis states of a walker are of the form $|x_1, x_2, c_1, c_2\rangle$ describing its position $x_{1,2}$ in spatial dimensions one and two and the corresponding two-sided coin parameters with $c_{1,2} = \pm 1$. The evolution takes place in discrete steps, each of which has two stages, defined by coin (\hat{C}) and step (\hat{S}) operators. The coin operator coherently manipulates the coin parameter, leaving the position unchanged, whereas the step operator updates the position according to the new coin value. Explicitly, with a so-called Hadamard (H) coin $\hat{C}_H = \hat{H}_1 \otimes \hat{H}_2$, a single step in the evolution is defined by the operators,

$$\hat{H}_i|x_i, \pm 1\rangle \rightarrow (|x_i, 1\rangle \pm |x_i, -1\rangle)/\sqrt{2}, \forall i = 1, 2$$

$$\hat{S}|x_1, x_2, c_1, c_2\rangle \rightarrow |x_1 + c_1, x_2 + c_2, c_1, c_2\rangle \quad (1)$$

The evolution of the system proceeds by repeatedly applying coin and step operators on the initial state $|\psi_{\text{in}}\rangle$, resulting in $|\psi_n\rangle = (\hat{S}\hat{C})^n|\psi_{\text{in}}\rangle$ after n steps. The step operator \hat{S} hereby translates superpositions and entanglement between the coin parameters directly to the spatial domain, imprinting signatures of quantum effects in the final probability distribution.

We performed 2D quantum walks with photons obtained from attenuated laser pulses. The two internal coin states are represented by two polarization modes (horizontal and vertical) in two different spatial modes (27), similar to the proposal in (28). Incident photons follow, depending on their polarization, four different paths in a fiber network (Fig. 1A). The four paths correspond to the four different directions a walker

¹Applied Physics, University of Paderborn, Warburger Straße 100, 33098 Paderborn, Germany. ²Max Planck Institute for the Science of Light, Günther-Scharowsky-Straße 1/Bau 24, 91058 Erlangen, Germany. ³Department of Physics, Faculty of Nuclear Sciences and Physical Engineering, Czech Technical University in Prague, Břehová 7, 115 19 Praha, Czech Republic. ⁴Wigner Research Centre for Physics, Hungarian Academy of Sciences, H-1525 Budapest, Post Office Box 49, Hungary. ⁵Centre for Engineered Quantum Systems, Department of Physics and Astronomy, Macquarie University, Sydney NSW 2113, Australia.

*To whom correspondence should be addressed. E-mail: andreas.schreiber@uni-paderborn.de

can take in one step on a 2D lattice. Different path lengths in the circuit generate a temporally encoded state, where different position states are represented by discrete time bins (Fig. 1B). Each round trip in the setup implements a single-step operation, whereas the quantum coin operation is performed with linear optical elements (half-wave plates, HWP) (27). In order to adjust the coin operator independently at each position, we used a fast-switching electrooptic modulator (EOM). A measurement with time-resolving single-photon counting modules allowed for the reconstruction of the output photostatistics (27).

We have implemented two different kinds of quantum coins in our 2D quantum walks. First, we investigated quantum walks driven only by separable coin operations, $\hat{C} = \hat{C}_1 \otimes \hat{C}_2$. Here, the separability can directly be observed in the spatial spread over the lattice, when initializing the walker in a separable state. As an example, we measured a Hadamard walk with photons initially localized at position $|x_1, x_2\rangle = |0, 0\rangle$. The probability distribution showing at which position the photons were detected after 10 steps (Fig. 2, A

and B) can be factorized into two independent distributions of 1D quantum walks (15), stating no conceptual advantage of a 2D quantum walk. However, 2D quantum walks allow for much greater complexity using controlled operations. These operations condition the transformation of one coin state on the actual state of the other. Because of the induced quantum correlations, one obtains a nontrivial evolution resulting in an inseparable final state. The probability (P) distribution for a Hadamard walk with an additional controlling operation can be seen in Fig. 2, C and D. We compare the ideal theoretical distribution with the measured photostatistics via the similarity,

$$S = \left[\sum_{x_1, x_2} \sqrt{P_{\text{th}}(x_1, x_2) P_{\text{exp}}(x_1, x_2)} \right]^2$$

the equality of two classical probability distributions ($S = 0$ for completely orthogonal distributions and $S = 1$ for identical distributions). For the Hadamard walk (Fig. 2, A and B), we observe $S = 0.957 \pm 0.003$, and for the quantum walk with controlling gates (Fig. 2, C and D) $S = 0.903 \pm 0.018$ (after 10 steps, across 121 positions).

Increasing the number of walkers in a quantum walk effectively increases its dimensionality (21). Specifically, for a given 1D quantum walk with N positions and two walkers, there exists an isomorphic square lattice walk of size N^2 with one walker. By this topological analogy, a measured spatial distribution from a 2D lattice with positions (x_1, x_2) can be interpreted as a coincidence measurement for two walkers at positions x_1 and x_2 propagating on the same linear graph. Hereby each combined coin operation of both particles, including controlled operations, has an equivalent coin operation in a 2D quantum walk. This allows us to interpret the 2D walk in Fig. 2, C and D, as a quantum walk with controlled two-particle operations, a system typically creating two-particle entanglement. The inseparability of the final probability distribution is then a direct signature of the simulated entanglement.

In Fig. 2E, we show a lower bound for the simulated entanglement between the two particles during the stepwise evolution with four different coin operations. We quantified the simulated

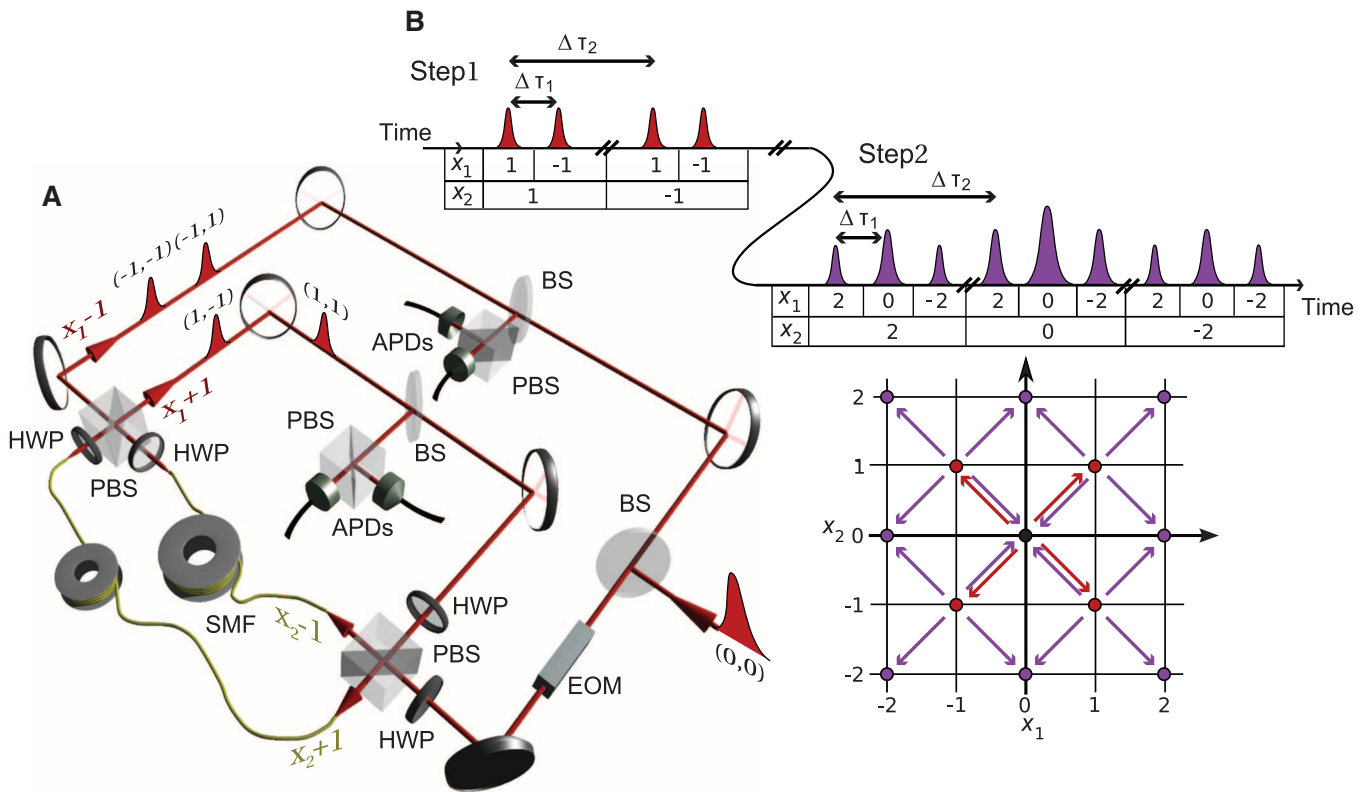


Fig. 1. (A) Experimental setup. Our photon source is a pulsed diode laser with a pulse width of 88 ps, a wavelength of 805 nm, and a repetition rate of 110 kHz. The photons are initialized at position $|x_1, x_2\rangle = |0, 0\rangle$ in horizontal polarization (corresponding to coin state $|c_1, c_2\rangle = |-1, -1\rangle$). Once coupled into the setup through a low-reflectivity beam splitter (BS, reflectivity 3%), their polarization state is manipulated with an EOM and a HWP. The photonic wave packets are split by a polarizing beam splitter (PBS) and routed through single-mode fibers (SMF) of length 135 or 145 m, implementing a temporal step in the x_2 direction. Additional HWPs and a second PBS perform a step in the x_1 direction based on the same principle. The split wave packet

after the first step with equal splitting is indicated in the picture. At each step, the photons have a probability of 12% in loops $x_1 - 1$ (or 4% in loops $x_1 + 1$) of being coupled out to a polarization and hence coin state resolving detection of the arrival time via four avalanche photodiodes (APDs). Including losses and detection efficiency, the probability of a photon continuing the walk after one step is 52% without the EOM and 12% with the EOM. (B) Projection of the spatial lattice onto a 1D temporally encoded pulse chain for step one and two. Each step consists of a shift in both x_1 direction, corresponding to a time difference of $\Delta t_1 = 3.11$ ns, and x_2 direction with $\Delta t_2 = 46.42$ ns.

entanglement via the von Neumann entropy, E , assuming pure final states after the quantum walk (27). For this calculation, the relative phases between the positions and coins were reconstructed from the obtained interference patterns, whereas phases between the four coin states were chosen to minimize the entanglement value. Without conditioned operations, the two particles evolve independently ($E = 0$), whereas an evolution including controlled operations reveals a probability distribution characterized by bipartite entanglement. We found that the interactions presented

in Fig. 2, C and D, exhibit an entropy of at least $E = 2.63 \pm 0.01$ after 12 steps, which is 56% of the maximal entropy (given by a maximally entangled state). The nonzero entropies obtained in the higher steps of the separable Hadamard walk are attributed to the high sensitivity of the entropy measure to small errors in the distribution for $E \approx 0$.

The investigated interactions can be interpreted as long-distance interactions with the interaction strength being independent of the spatial distance of the particles. This is a unique effect and highly

nontrivial to demonstrate in actual two-particle quantum systems.

Contrary to the position-independent interactions is the evolution of two-particle quantum walks with short-range interactions, that is, interactions occurring only when both particles occupy the same position. These interactions can be interpreted as two-particle scattering or nonlinear interactions. When using a 2D quantum walk to simulate two walkers, all vertices on the diagonal of the 2D lattice correspond to both walkers occupying the same position. Hence, we can introduce nonlinear

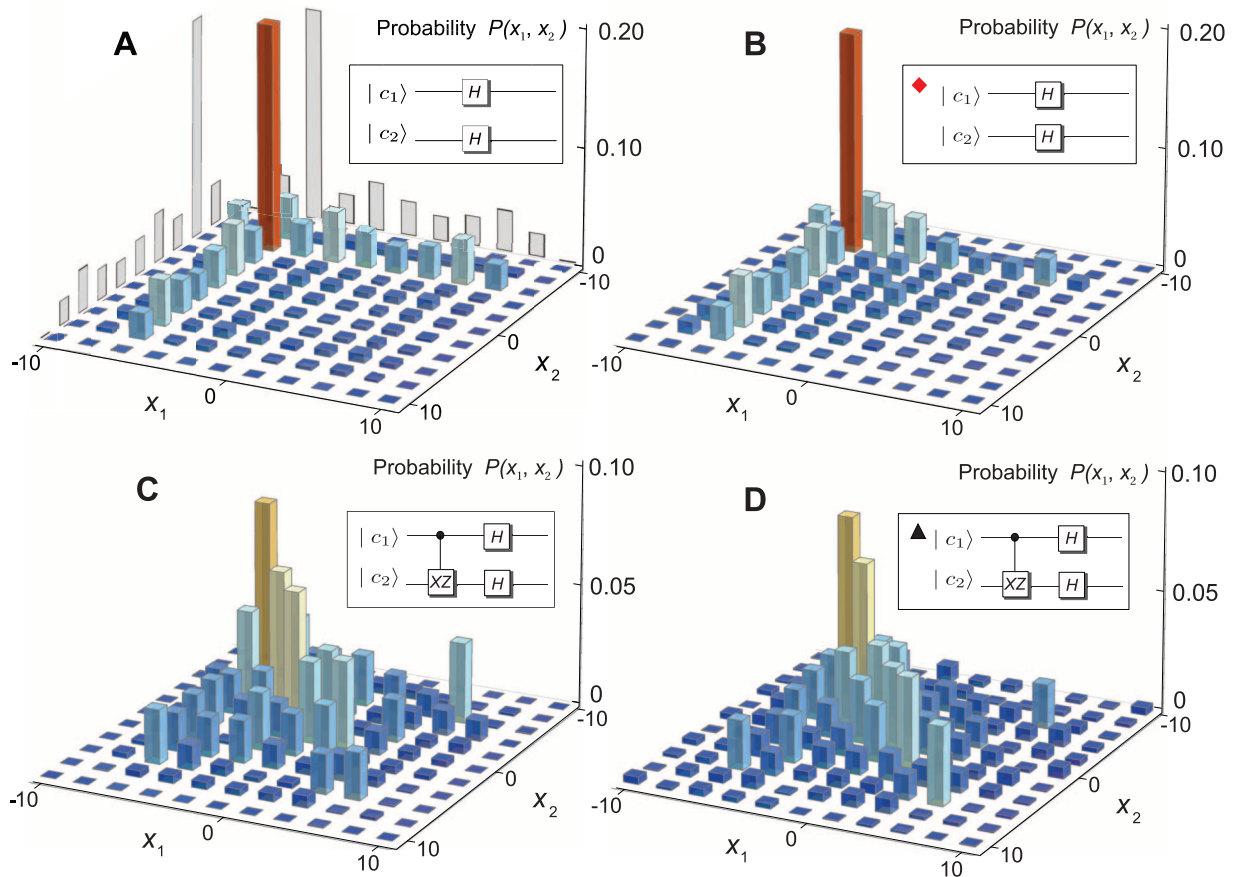


Fig. 2. Measured and simulated probability distribution $P(x_1, x_2)$ (traced over the coin space) after 10 steps of a 2D quantum walk with initial state $|0, 0, -1, -1\rangle$. Theoretical (A) and measured (B) probability distribution of a 2D Hadamard walk using the operation \hat{C}_H (Eq. 1). Because only separable coin operations were performed (inset), the distribution is separable, given by a product of two 1D distributions (gray). Theoretical (C) and measured (D) probability distribution of a 2D walk with controlled-not X and controlled-phase operation Z , resulting in an unfactorizable distribution. Here, c_2 is only transformed by $XZ|\pm 1\rangle \rightarrow \pm|\mp 1\rangle$ if $c_1 = -1$. The results in (B) and (D) are obtained by detecting over 7×10^3 events and calibrated by the detection efficiencies of all four coin basis states. (E) Dynamic evolution of the von Neumann entropy E generated by quantum walks (B) and (D) and quantum walks using controlled Hadamard coin operations (inset). The exper-

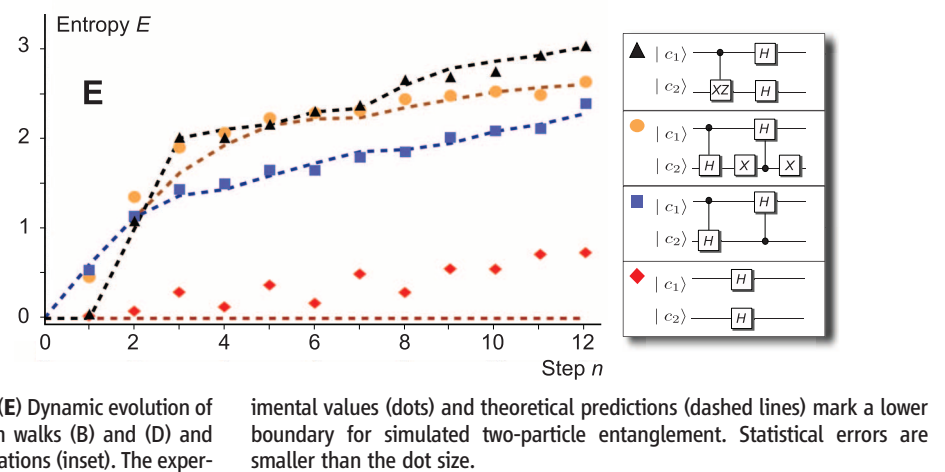
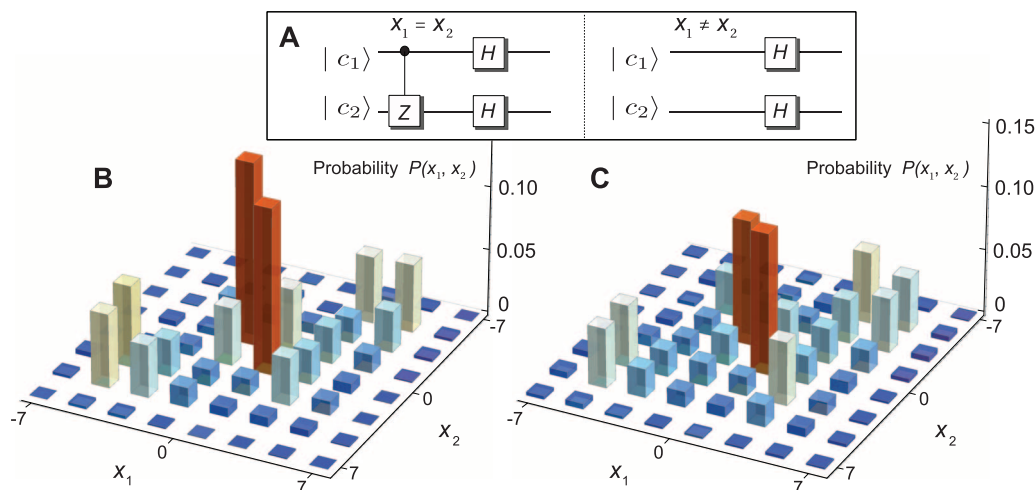


Fig. 3. (A) Circuit representation of coin operations simulating nonlinear interactions via 2D quantum walk. Only when the two virtual particles meet ($x_1 = x_2$) is a controlled operation applied. Theoretical (B) and measured (C) coincidence distributions $P(x_1, x_2)$ (traced over the coin space) after seven steps of a simulated two-particle quantum walk with initial state $|0, 0, -1, -1\rangle$. The high probability that both particles are at the same position (diagonal) is a notable signature of bound states. The measured distribution is reconstructed by detecting over 8×10^3 events and has a similarity of $S = 0.957 \pm 0.013$. Adding the EOM to the setup for dynamical control limits the step number to $n = 7$ because of the higher losses per step. Small imperfections of the EOM are included in the theoretical plot.



interactions by modifying the coin operator on the diagonal positions while keeping all other positions unaffected. As an example of a two-particle quantum walk with nonlinear interactions (Fig. 3), the coin operator on the diagonal is in the form $C_{nl} = (H_1 \otimes H_2)C_Z$, where C_Z is a controlled phase operation implemented by a fast switching EOM. The chosen operation simulates a quantum scenario of particular interest: the creation of bound molecule states, predicted as a consequence of two-particle scattering (7). Evidently, the quantum walk is to a large extent confined to the main diagonal $[\sum_x P(x, x) = 0.317 \pm 0.006$ as opposed to the Hadamard walk $\sum_x P(x, x) = 0.242 \pm 0.001]$, a signature of the presence of a bound molecule state. In general, using a coin invariant under particle exchange, bosonic, or fermionic behavior can be simulated, depending on whether the initial states are chosen to be symmetric or antisymmetric with respect to particle permutations. With our initial state being invariant under particle exchange, we simulated an effective Bose-Hubbard type nonlinearity for two bosons (29).

We have demonstrated an efficient implementation of a 2D quantum walk and proved the experimental feasibility to simulate a diversity of interesting multiparticle quantum effects. Our experiment overcomes the technical challenges of two-particle experiments while exhibiting very high similarity and scalability. Combined with the flexibility in the choice of input state, controlling the coin at each position independently allows for simulations of a broad spectrum of dynamic quantum systems under different physical conditions.

Our experimental architecture can be generalized to more than two dimensions, with the addition of extra loops and orbital angular momentum modes as coin states (30). This opens a largely unexplored field of research, facilitating quantum simulation applications with multiple

walkers, including bosonic and fermionic behavior, and nonlinear interactions. It may be possible to study the effects of higher dimensional localization or graph percolations or to use the network topology in conjunction with single- or two-photon states. Additionally, a foreseeable future application for our system is the implementation of a quantum search algorithm. We demonstrated that, with a physical resource overhead, a classical experiment can simulate many genuine quantum features. Although our experiment is important for simulation applications, it is equally interesting for understanding fundamental physics at the border between classical and quantum coherence theory.

References and Notes

1. Y. Aharonov, L. Davidovich, N. Zagury, *Phys. Rev. A* **48**, 1687 (1993).
2. D. Aharonov, A. Ambainis, J. Kempe, U. Vazirani, in *Proceedings of the Thirty-Third Annual ACM Symposium on Theory of Computing*, STOC '01, Heronissos, Greece, 6 to 8 July 2001 [Association for Computing Machinery (ACM), New York, 2001], pp. 50–59.
3. N. Inui, Y. Konishi, N. Konno, *Phys. Rev. A* **69**, 052323 (2004).
4. T. Kitagawa, M. S. Rudner, E. Berg, E. Demler, *Phys. Rev. A* **82**, 033429 (2010).
5. M. Mohseni, P. Rebentrost, S. Lloyd, A. Aspuru-Guzik, *J. Chem. Phys.* **129**, 174106 (2008).
6. M. B. Plenio, S. F. Huelga, *New J. Phys.* **10**, 113019 (2008).
7. A. Ahlbrecht *et al.*, <http://arxiv.org/abs/1105.1051> (2011).
8. D. Bouwmeester, I. Marzoli, G. P. Karman, W. Schleich, J. P. Woerdman, *Phys. Rev. A* **61**, 013410 (1999).
9. A. Schreiber *et al.*, *Phys. Rev. Lett.* **104**, 050502 (2010).
10. M. A. Broome *et al.*, *Phys. Rev. Lett.* **104**, 153602 (2010).
11. A. Schreiber *et al.*, *Phys. Rev. Lett.* **106**, 180403 (2011).
12. H. Schmitz *et al.*, *Phys. Rev. Lett.* **103**, 090504 (2009).
13. M. Karski *et al.*, *Science* **325**, 174 (2009).
14. F. Zähringer *et al.*, *Phys. Rev. Lett.* **104**, 100503 (2010).
15. T. D. Mackay, S. D. Bartlett, L. T. Stephenson, B. C. Sanders, *J. Phys. A* **35**, 2745 (2002).
16. A. M. Childs, *Phys. Rev. Lett.* **102**, 180501 (2009).
17. N. B. Lovett, S. Cooper, M. Everitt, M. Trevers, V. Kendon, *Phys. Rev. A* **81**, 042330 (2010).
18. N. Shenvi, J. Kempe, K. B. Whaley, *Phys. Rev. A* **67**, 052307 (2003).
19. A. Ambainis, J. Kempe, A. Rivosh, in *Proceedings of the Sixteenth ACM-SIAM Symposium on Discrete Algorithms*, SODA '05, Vancouver, Canada, 23 to 25 January 2005 (Society for Industrial and Applied Mathematics, Philadelphia, 2005), pp. 1099–1108.
20. M. Hillery, D. Reitzner, V. Buzek, *Phys. Rev. A* **81**, 062324 (2010).
21. A. Peruzzo *et al.*, *Science* **329**, 1500 (2010).
22. L. Sansoni *et al.*, *Phys. Rev. Lett.* **108**, 010502 (2012).
23. S. D. Berry, J. B. Wang, *Phys. Rev. A* **83**, 042317 (2011).
24. R. J. C. Spreeuw, *Found. Phys.* **28**, 361 (1998).
25. N. J. Cerf, C. Adami, P. G. Kwiat, *Phys. Rev. A* **57**, R1477 (1998).
26. N. Bhattacharya, H. B. van Linden van den Heuvell, R. J. C. Spreeuw, *Phys. Rev. Lett.* **88**, 137901 (2002).
27. Materials and methods are available as supporting material on Science Online.
28. E. Roldán, J. C. Soriano, *J. Mod. Opt.* **52**, 2649 (2005).
29. Y. Lahini *et al.*, <http://arxiv.org/abs/1105.2273> (2011).
30. C. S. Hamilton, A. Gábris, I. Jex, S. M. Barnett, *New J. Phys.* **13**, 013015 (2011).

Acknowledgments: We acknowledge financial support from the German Israel Foundation (project no. 970/2007). A.G., M.S., V.P., C.H., and I.J. acknowledge grant support from MSM6840770039 and MSMT LC06002, SGS10/294/OHK4/3T/14, GA CR 202/08/H078, and OTKA T83858. P.P.R. acknowledges support from the Australian Research Council Centre of Excellence for Engineered Quantum Systems (project no. CE110001013).

Supporting Online Material

www.sciencemag.org/cgi/content/full/science.1218448/DC1
Materials and Methods
Fig. S1
References (31–33)

27 December 2011; accepted 22 February 2012
Published online 8 March 2012;
10.1126/science.1218448

Appendix 6

V. Potoček

Symmetries in discrete time quantum walks on Cayley graphs

pre-print manuscript, arXiv:1211.0172v1 [quant-ph]

Symmetries in discrete time quantum walks on Cayley graphs

V. Potoček^{1,*}

¹*Department of Physics, FNSPE, Czech Technical University in Prague, Břehová 7, 115 19 Praha, Czech Republic.*

We address the question of symmetries of an important type of quantum walks. We introduce all the necessary definitions and provide a rigorous formulation of the problem. Using a thorough analysis, we reach the complete answer by presenting a constructive method of finding all solutions of the problem with minimal additional assumptions. We apply the results on an example of a quantum walk on a line to demonstrate the practical significance of the theory.

PACS numbers: 03.65.Fd, 03.67.Ac, 05.40.Fb

I. INTRODUCTION

The search for symmetries is an important problem in all fields of physics. In both classical and quantum mechanics, the knowledge of symmetries of a given system can help significantly in finding a solution of its equations of motion, in reducing the number of parameters, or identifying the integrals of motion.

In this paper, we aim to find the symmetries of the time evolution equation of a broad class of discrete time quantum walks. We note that this important question has been addressed partly by other authors. Symmetries of particular quantum walk scenarios have been classified, e.g., in [1]. A special class of symmetries of discrete time quantum walks on Cayley graphs has been studied in [2] in relation to global analytic properties of the quantum walks. Symmetries have played an essential role in an approximate analytic solution of time evolution in the Shenvi-Kempe-Whaley algorithm [3] for quantum database searching. Another use of symmetries has been presented in a recent experimental realization of a quantum walk on a line [4] when a reduced set of parameters have been shown to cover all possible configurations of the model. However, no general study focused on the symmetries themselves has been presented so far.

The article is structured as follows. In Section II, we define the class of discrete time quantum walk to be studied in more detail. In Section III, we use a general method to find all symmetries of the time evolution equation which preserve measurement probabilities. In Section IV, we extend the result by generalizing the notion of symmetries of the system to allow automorphisms of the underlying graph. In Section V, we conclude and discuss our results.

II. QUANTUM WALKS ON CAYLEY GRAPHS

In the scope of this paper, we will restrict our study to discrete time quantum walks on Cayley graphs, with the quantum coin reflecting the graph structure. This class of

graphs, however, covers all the most important cases used in algorithmic applications of quantum walks—lattices both with and without periodic boundary conditions [5], hypercube graphs [3], among many others.

In general, Cayley graphs are defined as follows:

Definition 1. Let G be a discrete group finitely generated by a set S . The (uncolored) *Cayley graph* $\Gamma = \Gamma(G, S)$ is a directed graph (G, E) , where the set of vertices is identified with the set of elements of G and the set of edges is

$$E = \{(g, gs) \mid g \in G, s \in S\}.$$

A discrete quantum walk on a given Cayley graph is defined as the time evolution of a particle confined to the vertices of the graph, and allowed to move along its edges, one per a discrete time step. Thus, the Hilbert space corresponding to the spatial degree of freedom of the particle is the space of ℓ^2 functions defined on G , or equivalently, the space spanned by orthonormal basis states corresponding to the elements of G :

$$\mathcal{H}_S = \ell^2(G) = \text{Span}_{\mathbb{C}}\{|x\rangle \mid x \in G\}. \quad (1a)$$

Besides the spatial degree of freedom, we will require the particle undergoing the walk (the walker) to have an internal degree of freedom whose dimension equals the cardinality of S .

$$\mathcal{H}_C = \ell^2(S) = \text{Span}_{\mathbb{C}}\{|c\rangle \mid c \in S\}. \quad (1b)$$

This is in a direct analogy to [6] where quantum walks on general regular graphs have been introduced. The need for the presence of an internal degree of freedom has been shown to be crucial for quantum walks on Euclidean lattices [7] in order to reach nontrivial unitary time evolutions. A generalization of this “No-Go Lemma” to all Cayley graphs has been negated in [8]. In the scope of this article, however, we will keep the assumption about the internal degree of freedom as stated above.

Definition 2. The Hilbert spaces defined in Eqs. (1a) and (1b) are called *position* and *coin Hilbert spaces*, respectively. The full state space of the system is then

$$\mathcal{H} = \mathcal{H}_S \otimes \mathcal{H}_C = \text{Span}_{\mathbb{C}}\{|x, c\rangle \mid x \in G, c \in S\},$$

*Electronic address: vaclav.potocek@fjfi.cvut.cz

where $|x, c\rangle = |x\rangle_S \otimes |c\rangle_C$. We will refer to the systems $\{|x\rangle \mid x \in G\}$, $\{|c\rangle \mid c \in S\}$, and $\{|x, c\rangle \mid x \in G, c \in S\}$, as to *geometrical bases* of \mathcal{H}_S , \mathcal{H}_C and \mathcal{H} , respectively.

In the following, the symbols G , S , Γ , \mathcal{H}_S , \mathcal{H}_C and \mathcal{H} will always denote the objects introduced in Definitions 1 and 2. Moreover, a tensor product of two vectors or operators will be always understood to follow the factorization of \mathcal{H} into \mathcal{H}_S and \mathcal{H}_C .

This factorization of the state space plays a key role in the idea of a quantum walk. The general assumption is that operations which keep the position of the walker intact are generally available, whereas the position register can only be affected via controlled transitions of the walker on the underlying graph Γ . We will formalize the former in the following definition:

Definition 3. Let $A \in GL(\mathcal{H})$. We will call A a *local operation* if and only if there is a map $\omega_A : G \rightarrow GL(\mathcal{H}_C)$ such that A allows the following decomposition:

$$A = \sum_{x \in G} |x\rangle\langle x| \otimes \omega_A(x). \quad (2)$$

It trivially follows that for each local operation A , the decomposition by Eq. (2) is unique. Moreover, if $A \in U(\mathcal{H})$, then all the components $\omega_A(x)$ are elements of $U(\mathcal{H}_C)$, and *vice versa*. For a local operation A , we will use notation $A_x = \omega_A(x)$ for the components in this decomposition.

We note that the set of local operations depends not only on the separation of \mathcal{H} to a tensor product of \mathcal{H}_S and \mathcal{H}_C but also on the choice of the basis in \mathcal{H}_S . In any case, however, the local operations form a subgroup of $GL(\mathcal{H})$.

It is important to distinguish local operations on \mathcal{H} from operations acting only on \mathcal{H}_C , that is, operators of the form $B = Id \otimes B'$. The latter form a subgroup of the group of local operations: indeed, any such B is local with $B_x = B'$ for all $x \in G$.

Out of the other class of operations, altering the position of the walker, one representative is sufficient:

Definition 4. The *step operator* T is a controlled shift operator on \mathcal{H}_S conditioned by the coin register, as prescribed by its action on the basis states $|x, c\rangle$,

$$T|x, c\rangle = |xc, c\rangle. \quad (3)$$

Clearly, T is defined by Eq. (3) on the whole of \mathcal{H} via linearity and is a bounded operator. As the tensor product basis states, specified by Definition 2, are solely permuted under T , it is obvious that T is a unitary operator on \mathcal{H} and can thus form a time evolution operator in a discrete time quantum system.[10]

Before defining a quantum walk, we need one last supporting definition:

Definition 5. Let $\mathcal{C} = (C_n)_{n=0}^{+\infty}$ is an infinite sequence of local unitary operations on \mathcal{H} . We call \mathcal{C} a *quantum coin*.

If the sequence is constant, we call the quantum coin \mathcal{C} *time-homogeneous*. If every term C_n of the sequence is a tensor product $Id \otimes C'_n$, we call the quantum coin \mathcal{C} *space-homogeneous*. In general, however, a quantum coin may be both time- and position-dependent.

We call a generic \mathcal{C} a time- and position-dependent coin since, in accordance with Definition 3, we can find unitary operators $C_{n,x} \in U(\mathcal{H}_C)$ for each time $n \in \mathbb{N}_0$ and position $x \in G$ which alter the coin register in dependence on both the current time and the state of the position register, provided that the latter is well-defined.

The set of all quantum coins forms a group under element-wise composition.

The coin and step operators lead us to the definition of a discrete time quantum walk on a Cayley graph Γ .

Definition 6. Let Γ is a Cayley graph, let $\mathcal{C} = (C_n)_{n=0}^{+\infty}$ is a quantum coin on its corresponding Hilbert space \mathcal{H} . A *discrete-time quantum walk* on Γ with the coin \mathcal{C} is a quantum protocol described by the following: an initial state $|\psi_0\rangle \in \mathcal{H}$ and the evolution operator

$$W_{\mathcal{C}} : \mathbb{N}_0 \rightarrow U(\mathcal{H}) : W_{\mathcal{C}}(n) = TC_{n-1}TC_{n-2} \dots TC_0. \quad (4a)$$

For $n \in \mathbb{N}_0$, we say that the state of the walker after n steps is

$$|\psi_n\rangle = W_{\mathcal{C}}(n)|\psi_0\rangle. \quad (4b)$$

III. SYMMETRIES PRESERVING MEASUREMENT PROBABILITIES

Symmetry of a system is an invariance of the system under some kind of transformation acting on its parameters and/or the initial state. Invariance does not necessarily mean that the time evolution is exactly the same, some variations may take place in the internal state as long as they do not influence the observable properties of the system, that is, the measurement probabilities of the spatial degree of freedom. Of all such transformations, we will be interested only in those which respect the unitary nature of quantum mechanics. Formally, we can state the requirement as follows:

Definition 7. Let \mathcal{T} be an endomorphism on the Cartesian product of the set of quantum coins and initial states of a quantum walk on Γ . We call \mathcal{T} a *unitary quantum walk symmetry* on Γ if there is a sequence of local unitary operators $(U_n)_{n=0}^{+\infty}$ such that for each quantum coin $\mathcal{C} = (C_n)_{n=0}^{+\infty}$ and for each initial state $|\psi_0\rangle$,

$$\forall n \in \mathbb{N}_0 : W_{\tilde{\mathcal{C}}}(n)|\tilde{\psi}_0\rangle = U_n W_{\mathcal{C}}(n)|\psi_0\rangle, \quad (5)$$

where $\tilde{\mathcal{C}} = (\tilde{C}_n)_{n=0}^{+\infty}$ and $|\tilde{\psi}_0\rangle$ denote the image of \mathcal{C} and $|\psi_0\rangle$ under \mathcal{T} .

The above definition is motivated by the fact that local unitary operations preserve measurement probabilities in

the geometrical basis of \mathcal{H}_S ,

$$\sum_{c \in S} |\langle x, c | \phi \rangle|^2 =: \|\langle x | \psi \rangle\|^2 = \|\langle x | U_{\text{local}} | \psi \rangle\|^2.$$

Lemma 1. *Let, in the notation of Definition 7, $(\tilde{\mathcal{C}}, |\tilde{\psi}_0\rangle) = \mathcal{T}(\mathcal{C}, |\psi_0\rangle)$. Then the condition of Eq. (5) is satisfied if and only if*

$$|\tilde{\psi}_0\rangle = U_0 |\psi_0\rangle, \quad (6a)$$

$$\forall n \in \mathbb{N}_0 : \quad T\tilde{C}_n = U_{n+1}TC_nU_n^\dagger, \quad (6b)$$

Proof. The first part is readily obtained by studying the special case of Eq. (5) where $n = 0$. Inserting Eq. (6a) back into Eq. (5), we get

$$\forall n \in \mathbb{N}_0 : \quad W_{\tilde{\mathcal{C}}}(n)U_0|\psi_0\rangle = U_nW_{\mathcal{C}}(n)|\psi_0\rangle \quad (7)$$

The generality of Eq. (7) with respect to $|\psi_0\rangle$ implies an equivalence of the operators,

$$W_{\tilde{\mathcal{C}}}(n)U_0 = U_nW_{\mathcal{C}}(n).$$

Substituting $n + 1$ for n , we get another identity,

$$W_{\tilde{\mathcal{C}}}(n+1)U_0 = U_{n+1}W_{\mathcal{C}}(n+1).$$

Comparing with

$$\begin{aligned} W_{\tilde{\mathcal{C}}}(n+1) &= T\tilde{C}_nW_{\tilde{\mathcal{C}}}(n), \\ W_{\mathcal{C}}(n+1) &= TC_nW_{\mathcal{C}}(n), \end{aligned}$$

we obtain the relation

$$T\tilde{C}_nU_nW_{\mathcal{C}}(n) = U_{n+1}TC_nW_{\mathcal{C}}(n).$$

Due to the unitarity of the time evolution operators and U_n , this is equivalent to Eq. (6b). \square

Lemma 2. *Let \mathcal{T} be a unitary quantum walk symmetry imposing a local unitary transform $(U_n)_{n=0}^{+\infty}$ on the instantaneous state of a quantum walk, as given by Definition 7. Then $U_{n,x}$ is diagonal in the geometrical basis of \mathcal{H}_C for each $n \in \mathbb{N}$ (i.e. $n \geq 1$) and all $x \in G$, that is, there are complex units $u_{n,x,c}$ for each $n \in \mathbb{N}$, $x \in G$, and $c \in S$ such that*

$$U_n = \sum_{x \in G} \sum_{c \in S} u_{n,x,c} |x, c\rangle \langle x, c| \quad (8)$$

Proof. Starting from Eq. (6b), we can rearrange the terms so that U_{n+1} is isolated:

$$U_{n+1} = T\tilde{C}_nU_nC_n^\dagger T^\dagger.$$

Let $x \in G$ and $c, d \in S$. We can compare the corresponding matrix elements on both sides:

$$\langle x, c | U_{n+1} | x, d \rangle = \langle x, c | T\tilde{C}_nU_nC_n^\dagger T^\dagger | x, d \rangle.$$

From Definition 4 and the subsequent comment, we can derive that

$$T^\dagger |x, d\rangle = |xd^{-1}, d\rangle \quad (9a)$$

and similarly

$$\langle x, c | T = (T^\dagger |x, c\rangle)^\dagger = \langle xc^{-1}, c|. \quad (9b)$$

Noting that all the other operators are local, we can factor out the position register to get

$$\begin{aligned} \langle x | x \rangle \langle c | U_{n+1,x} | d \rangle &= \\ &= \langle xc^{-1} | xd^{-1} \rangle \langle c | \tilde{C}_{n,xd^{-1}} U_{n,xd^{-1}} C_{n,xd^{-1}}^\dagger | d \rangle \end{aligned}$$

If $c \neq d$, the right hand side is zero due to its leftmost term. Since $\langle x | x \rangle = 1$, we obtain the implication

$$c \neq d \Rightarrow \langle c | U_{n+1,x} | d \rangle = 0,$$

meaning that $U_{n+1,x}$ is diagonal in the geometrical basis of \mathcal{H}_C for all $n \in \mathbb{N}_0$.

The second part of the Lemma is a trivial application of the corresponding definitions. \square

Theorem 1. *Let \mathcal{T} be a unitary symmetry of a quantum walk on Γ . Then there is a unique local unitary operation U_0 on \mathcal{H} and a unique sequence of local unitary operations $(U_n)_{n=1}^{+\infty}$ diagonal in the geometrical basis of \mathcal{H} such that for each quantum coin \mathcal{C} and each initial state $|\psi_0\rangle$, the transformed values read $|\tilde{\psi}_0\rangle = U_0|\psi_0\rangle$ and*

$$\forall n \in \mathbb{N}_0 : \quad \tilde{C}_n = \sum_{x \in G} (|x\rangle \langle x| \otimes (V_{n,x} C_{n,x} U_{n,x}^\dagger)), \quad (10a)$$

where $V_{n,x} \in U(\mathcal{H}_C)$ is related to U_{n+1} by

$$V_{n,x} = \sum_{c \in S} u_{n+1,xc,c} |c\rangle \langle c|, \quad (10b)$$

using the notation of Eq. (8). Conversely, given any U_0 and $(U_n)_{n=1}^{+\infty}$ satisfying the aforementioned conditions, there is a unique symmetry \mathcal{T} yielding these values. Therefore, the symmetry group of Eq. (4) is $U(\mathcal{H}_C)^G \times U(1)^{G \times \mathbb{N} \times S}$.

Proof. The proof follows from Eq. (6b) and its equivalent form,

$$\tilde{C}_n = T^\dagger U_{n+1} T C_n U_n^\dagger.$$

Comparing the matrix elements, we obtain

$$\langle x, c | \tilde{C}_n | x, d \rangle = \langle x, c | T^\dagger U_{n+1} T C_n U_n^\dagger | x, d \rangle$$

Using Eq. (3) and the locality of the U and C operations, we find that

$$\langle c | \tilde{C}_n | d \rangle = \langle xc, c | U_{n+1} T (|x\rangle \otimes C_{n,x} U_{n,x}^\dagger | d) \rangle.$$

Using Lemma 2 and Eq. (9a),

$$\begin{aligned} \langle xc, c|U_{n+1}T = (T^\dagger U_{n+1}^\dagger |xc, c) \rangle^\dagger &= \\ &= (u_{n+1,xc,c} T^\dagger |xc, c) \rangle^\dagger = u_{n+1,xc,c}^* \langle x, c|, \end{aligned}$$

whence it follows that

$$\begin{aligned} \langle c|\tilde{C}_n|d \rangle &= u_{n+1,xc,c}^* \langle x|x \rangle \langle c|C_{n,x}U_{n,x}^\dagger|d \rangle = \\ &= \langle c|V_{n,x}C_{n,x}U_{n,x}^\dagger|d \rangle, \end{aligned}$$

as stated by the theorem.

Conversely, given the unitary operations U_0 and $(U_n)_{n=1}^{+\infty}$, Eq. (6b) describes a way to construct a symmetry operation \mathcal{T} . \square

According to Theorem 1, the sequence $(U_n)_{n=0}^{+\infty}$ provides a full classification of all the unitary quantum walk symmetries. If there is no restriction on the homogeneity of the quantum coins \mathcal{C} and $\tilde{\mathcal{C}}$ or the initial state, the choice of U_n is free, up to the restriction of Lemma 2. More interesting cases arise when the coin has some global property that is required to be preserved under the symmetry.

Before stating the main theorem regarding homogeneous quantum coins, we introduce a means of classifying various walking spaces.

Definition 8. Let G is a discrete group generated by a subset S , let S^{-1} denote the set of inverses of all elements of S . The causal subgroup of G with respect to S is defined as

$$S^{(0)} = \left\langle \bigcup_{n \in \mathbb{Z}} S^n S^{-n} \right\rangle. \quad (11a)$$

The future causal subgroup of G with respect to S is defined as

$$S_+^{(0)} = \left\langle \bigcup_{n=1}^{+\infty} S^n S^{-n} \right\rangle. \quad (11b)$$

A Cayley graph $\Gamma = \Gamma(G, S)$ is called nonseparating if $S_+^{(0)} = S^{(0)}$.

In other words, the causal subgroup $S^{(0)}$ contains all the elements of G which can be written as a product of generators and their inverses in such a way that the exponents add up to zero. The causal subgroup has several important properties, as shown in the following Theorem.

Theorem 2. *The causal group $S^{(0)}$ is a normal subgroup of G . Moreover, $G/S^{(0)}$ is a cyclic group generated by the coset of any element in S .*

Proof. Let $c \in S$, let $s \in S^n S^{-n}$ for some $n \in \mathbb{Z}$. Then it is simple to show that both csc^{-1} and $c^{-1}sc$ are elements of $S^{(0)}$. Indeed, let $n > 0$. Then $csc^{-1} \in SS^n S^{-n} S^{-1} = S^{n+1} S^{-(n+1)} \subset S^{(0)}$. Similarly, $c^{-1}sc \in S^{-1} S^n S^{-n} S = (S^{-1} S^1)(S^{n-1} S^{-(n-1)})(S^1 S^{-1}) \subset S^{(0)}$. The case $n < 0$ is analogous, $n = 0$ is trivial.

Using elementary algebra, this result can be generalized to any $c \in G$ and $s \in S^{(0)}$, which is one of the conditions equivalent to $S^{(0)}$ being normal in G .

For the second part, let c_0 be an arbitrary fixed element of S . We first show that the coset cS equals c_0S for any $c \in S$. Indeed,

$$cS = (c_0 c_0^{-1})cS = c_0 \underbrace{(c_0^{-1}c)}_{\in S} S = c_0 S.$$

Analogously, $c^{-1}S = c_0^{-1}S$.

Let now g be an arbitrary element of G . We can decompose g into

$$g = c_1^{\epsilon_1} c_2^{\epsilon_2} \dots c_k^{\epsilon_k},$$

where $c_i \in S$ and $\epsilon_i \in \mathbb{Z}$ for all $1 \leq i \leq k$. Using the above result, the coset gS is equal to

$$gS = c_0^{\epsilon_1} c_0^{\epsilon_2} \dots c_0^{\epsilon_k} S = c_0^{\epsilon_1 + \epsilon_2 + \dots + \epsilon_k} S = (c_0 S)^{\epsilon_1 + \epsilon_2 + \dots + \epsilon_k}.$$

This completes the proof. \square

Remark. The future causal subgroup $S_+^{(0)}$ generally does not share these properties. As they are extremely helpful for the theorems to follow, we will restrict the analysis below to quantum walks on nonseparating Cayley graphs, where there is no difference between $S_+^{(0)}$ and $S^{(0)}$.

We note without proof that a sufficient condition for the equality $S_+^{(0)} = S^{(0)}$ is that for each $c, d \in S$, $c^{-1}d$ is an element of $S_+^{(0)}$. This is satisfied automatically in, but not restricted to, all abelian groups. On the other hand, an example that this property is not universal is provided by the free group on 2 or more generators. In such cases, the quantum walk splits the initial excitation into a potentially unlimited number of mutually independent branches which never can interfere again.

In the following, we denote $[G : S^{(0)}] = \chi(G, S)$. This characteristic plays its role in an important corollary of Theorem 2:

Corollary 1. *Let c_0 be a fixed element of S . For each $x \in G$, there is $\tilde{x} \in S^{(0)}$ and $k \in \mathbb{Z}$ such that $x = \tilde{x}c_0^k$. This decomposition is unique if and only if $[G : S^{(0)}]$ is infinite, otherwise k is determined up to an integer multiple of $\chi(G, S)$.*

Let \mathcal{T} be a unitary quantum walk symmetry, as defined in Definition 7. From Theorem 3, we know that the quantum coin and the initial state are transformed independently. The following theorem studies two important cases where the transformation of the coin is restricted.

Let \mathcal{C} denote a quantum coin and $\tilde{\mathcal{C}}$ its image under \mathcal{T} . We say that \mathcal{T} preserves time or space homogeneity of the quantum coin if the respective property of \mathcal{C} implies that the same property is held for $\tilde{\mathcal{C}}$.

Theorem 3. Let \mathcal{T} be a unitary symmetry of a quantum walk on a nonseparating Cayley graph, let $(U_n)_{n=0}^{+\infty}$ be the transformation induced in the instantaneous state of the quantum walk.

- \mathcal{T} preserves space homogeneity of the quantum coin if and only if the unitary operators $U_{n,x}$, forming the decomposition of U_n , are of the form

$$U_{n,\tilde{x}c_0^k} = \eta_{n-k}\rho(\tilde{x})U'_n, \quad \forall n \in \mathbb{N}_0, \quad (12a)$$

where $(\eta_m)_{m \in \mathbb{Z}}$ is an arbitrary doubly infinite sequence of complex units, periodic with the period $\chi(G, S)$ if the latter is finite, $\rho(s)$ is a one-dimensional unitary representation of $S^{(0)}$ and the operators U'_n act on \mathcal{H}_C only. The group of symmetries preserving space homogeneity is $(U(1)^{\chi(G,S)}/U(1)) \times \text{Rep}(S^{(0)}) \times U(1)^{\mathbb{N} \times S} \times U(\mathcal{H}_C)$, where $\text{Rep}(S^{(0)})$ is the group of one-dimensional unitary representations of $S^{(0)}$ with pointwise multiplication.

- \mathcal{T} preserves time homogeneity of the quantum coin if and only if the unitary operations $U_{n,x}$ are restricted by

$$U_{n,x} = \eta_{n-k}\epsilon^n U_x, \quad \forall n \in \mathbb{N}_0, \quad (12b)$$

where η_m is defined the same way as above, ϵ is an arbitrary complex unit and U_x are the components of a unitary operation $U \in U(\mathcal{H})$ diagonal in the geometrical basis of \mathcal{H} . If $\chi(G, S)$ is infinite, we can take ϵ fixed at 1. The group of symmetries preserving time homogeneity is $(U(1)^{\chi(G,S)}/U(1)) \times U(1) \times U(1)^{G \times S}$ if $\chi(G, S) < +\infty$ and $(U(1)^{\chi(G,S)}/U(1)) \times U(1)^{G \times S}$ otherwise.

Proof. In both cases, we start from Eq. (10). Let $x \in G$ and $c, d \in S$. Comparing matrix elements on both sides, we obtain

$$\langle x, c|\tilde{C}_n|x, d\rangle = \langle c|\tilde{C}_{n,x}|d\rangle = \langle c|V_{n,x}C_{n,x}U_{n,x}^\dagger|d\rangle.$$

Using the result of Lemma 2, the right hand side can be simplified substantially:

$$\langle c|\tilde{C}_{n,x}|d\rangle = \frac{u_{n,x,c,c}}{u_{n,x,d}} \langle c|C_{n,x}|d\rangle. \quad (13)$$

Let e be another element of S . We compare the last equation with another matrix element equation,

$$\langle c|\tilde{C}_{n,x}|e\rangle = \frac{u_{n,x,c,c}}{u_{n,x,e}} \langle c|C_{n,x}|e\rangle.$$

As these formulas hold for any quantum coin \mathcal{C} , we select one for which all the matrix elements of $C_{n,x}$ are nonzero for all $n \in \mathbb{N}$ and $x \in G$. We can then divide the above two equations to get

$$\frac{u_{n,x,e}}{u_{n,x,d}} = \frac{\langle e|C_{n,x}|c\rangle \langle d|\tilde{C}_{n,x}|c\rangle}{\langle e|\tilde{C}_{n,x}|c\rangle \langle d|C_{n,x}|c\rangle}. \quad (14)$$

Part A. In the case of a space-homogeneous coin, the right hand side of Eq. (14) is constant in x . This allows us to factorize $u_{n,x,c}$ into

$$u_{n,x,c} = v_{n,x}\delta_{n,c}.$$

Without loss of generality, we will require both the factors to have a modulus of 1. Similarly, we find from Eq. (13) that the ratio $v_{n+1,x,c}/v_{n,x}$ does not depend on x , that is, for each $y \in G$,

$$\frac{v_{n+1,y,c}}{v_{n,y}} = \frac{v_{n+1,x,c}}{v_{n,x}}, \quad \frac{v_{n+1,y,c}}{v_{n+1,x,c}} = \frac{v_{n,y}}{v_{n,x}}. \quad (15)$$

Let $k \in \mathbb{N}$, let $c_1, \dots, c_k, d_1, \dots, d_k \in S$. By repeated use of Eq. (15), we find that

$$\begin{aligned} \frac{v_{n,y}}{v_{n,x}} &= \frac{v_{n+1,y,c_1}}{v_{n+1,x,c_1}} = \dots = \frac{v_{n+k,y,c_1 c_2 \dots c_k}}{v_{n+k,x,c_1 c_2 \dots c_k}} = \\ &= \frac{v_{n+k-1,y,c_1 c_2 \dots c_k d_1^{-1}}}{v_{n+k-1,x,c_1 c_2 \dots c_k d_1^{-1}}} = \dots = \\ &= \frac{v_{n,y,c_1 c_2 \dots c_k d_1^{-1} \dots d_k^{-1}}}{v_{n,x,c_1 c_2 \dots c_k d_1^{-1} \dots d_k^{-1}}} \end{aligned}$$

Hence for all $n \in \mathbb{N}$, $x, y \in G$ and $s \in S_+^{(0)} = S^{(0)}$,

$$\frac{v_{n,y,s}}{v_{n,y}} = \frac{v_{n,x,s}}{v_{n,x}}. \quad (16)$$

Let $s, s' \in S^{(0)}$. By putting $x = e$ —the identity element of G —and $y = s'$, we obtain from Eq. (16)

$$\frac{v_{n,s's}}{v_{n,s'}} = \frac{v_{n,e}}{v_{n,e}} = \frac{v_{n,s}}{v_{n,e}}.$$

The last equation implies that $v_{n,s}/v_{n,e}$ for fixed $n \in \mathbb{N}$ is a homomorphism from $S^{(0)}$ to $U(1)$ and thus a one-dimensional unitary representation of $S^{(0)}$. Let us call this representation ρ_n .

Let now x be a general element of G . By Corollary 1, taking any fixed $c_0 \in S$, we can find $k \in \mathbb{Z}$ and $\tilde{x} \in S^{(0)}$ such that $x = \tilde{x}c_0^k$. We then find $v_{n,x}$ to equal

$$v_{n,x} = v_{n,\tilde{x}c_0^k} = \alpha_{n,k}\rho_n(\tilde{x}).$$

Inserting this form into Eq. (15), we find that the expression

$$\frac{v_{n+1,x,c}}{v_{n,x}} = \frac{v_{n+1,\tilde{x}c_0^k c}}{v_{n,\tilde{x}c_0^k}} = \frac{\alpha_{n+1,k+1}\rho_{n+1}(\tilde{x} \overbrace{c_0^k c c_0^{-(k+1)}}^{\in S^{(0)}})}{\alpha_{n,k}\rho_n(\tilde{x})}$$

is independent of x , that is, of both \tilde{x} and k . This implies that ρ_n is constant in n , so that we can call it ρ . Moreover,

$$\frac{\alpha_{n+1,k+1}\rho(c_0^k c c_0^{-(k+1)})}{\alpha_{n,k}}$$

must be constant in k .

By choosing $c = c_0$, the last equation becomes $\alpha_{n+1,k+1}/\alpha_{n,k} = \beta_n$, whence we obtain

$$\alpha_{n,k} = \beta_0 \beta_1 \dots \beta_{n-1} \alpha_{0,n-k} = \gamma_n \tilde{\alpha}_{n-k}.$$

If $\chi(G, S)$ is a finite number, the decomposition of Corollary 1 is not unique. The value of $\chi(G, S)$ is then equal to the least positive power l for which $c_0^l \in S^{(0)}$. Let $\tilde{x}_0 = c_0^{\chi(G, S)}$. The equality

$$\tilde{x}c_0^k = \tilde{x}\tilde{x}_0c_0^{k-\chi(G, S)}$$

then imposes a condition on the choice of $\alpha_{n,k}$ and subsequently $\tilde{\alpha}_m$:

$$\begin{aligned} \alpha_{n,k}\rho(\tilde{x}) &= \alpha_{n,k-\chi(G, S)}\rho(\tilde{x})\rho(\tilde{x}_0) \\ \Rightarrow \alpha_{n,k+\chi(G, S)} &= \alpha_{n,k}\rho(\tilde{x}_0) \\ \Rightarrow \tilde{\alpha}_{m-\chi(G, S)} &= \tilde{\alpha}_m\rho(\tilde{x}_0). \end{aligned}$$

In this case, the freedom in choosing $\tilde{\alpha}$ is restricted to $\chi(G, S)$ independent complex units. If $\chi(G, S)$ is infinite, all elements of the doubly infinite sequence can be chosen freely.

Putting together all the above elements, we find that the complete solution of Eq. (14) with the right hand side independent of x can be written as

$$u_{n,x,c} = \gamma_n \tilde{\alpha}_{n-k} \rho(\tilde{x}) \delta_{n,c} \quad (17)$$

for $x = \tilde{x}c_0^k$, where

- γ_n and $\delta_{n,c}$ are any complex units for all $n \in \mathbb{N}$ and $c \in S$,
- $\tilde{\alpha}_m$ is a sequence of $\chi(G, S)$ independent complex units,
- ρ is a one-dimensional unitary representation of $S^{(0)}$.

Clearly, the sequence γ_n can be absorbed into $\delta_{n,c}$. Besides that, only one degree of freedom is counted twice—a global phase factor, which can come from both $\tilde{\alpha}$ and δ .

At this point, we emphasize that the parameter n so far has been greater than or equal to 1; Lemma 2 puts no restriction on the form of U_0 except that it is local. Thus the case $n = 0$ must be studied separately. According to Lemma 1, the transformation of the quantum coin element C_0 reads

$$\tilde{C}_0 = T^\dagger U_1 T C_0 U_0^\dagger.$$

Expressing U_0 , we obtain

$$U_0 = \tilde{C}_0^\dagger T^\dagger U_1 T C_0. \quad (18)$$

Comparing the corresponding matrix elements on both sides and expanding the matrix product on the right hand side while using the locality property of the C and U matrices gives

$$\langle c|U_{0,x}|d\rangle = \sum_{a \in S} \langle c|\tilde{C}_0^\dagger|a\rangle u_{1,x,a} \langle a|C_0|d\rangle.$$

This relates the components of U_0 to those of U_1 , which are described by Eq. (17). Inserting the final form, we can see that

$$\begin{aligned} \langle c|U_{0,x}|d\rangle &= \sum_{a \in S} \langle c|\tilde{C}_0^\dagger|a\rangle \tilde{\alpha}_{1-k} \rho(\tilde{x}) \delta_{1,a} \langle a|C_0|d\rangle = \\ &= \alpha_{1-k} \rho(\tilde{x}) f(c, d), \end{aligned}$$

where $x = \tilde{x}c_0^k$ and f represents the matrix elements of some unitary matrix (any matrix can be reached with a suitable choice of \tilde{C}_0). Therefore, the components of U_0 are complex unit multiples of one constant unitary operator on \mathcal{H}_C , where the dependence on x follows the same rule as in the case of any other U_n , $n \geq 1$.

We conclude that the symmetry group under the aforementioned conditions is isomorphic to

$$(U(1)^{\chi(G, S)}/U(1)) \times \text{Rep}(S^{(0)}) \times U(1)^{\mathbb{N} \times S} \times U(\mathcal{H}_C),$$

as stated by the theorem.

Part B. If \mathcal{C} and $\tilde{\mathcal{C}}$ are simultaneously time-homogeneous, the right hand side of Eq. (14) is constant in n , which leads to a factorization

$$u_{n,x,c} = w_{n,x} \delta_{x,c},$$

where we again assume both terms to be complex units. Eq. (13) then gives for $w_{n,x}$ that the ratio $w_{n+1,x}/w_{n,x}$ does not depend on n and thus for each $x \in G$ and $m, n \in \mathbb{N}_0$,

$$\frac{w_{m+1,x}}{w_{m,x}} = \frac{w_{n+1,x}}{w_{n,x}}, \quad \frac{w_{m+1,x}}{w_{n+1,x}} = \frac{w_{m,x}}{w_{n,x}}. \quad (19a)$$

In a complete analogy to the above, we obtain for each $x \in G$, $n \in \mathbb{N}_0$, and $s \in S_+$,

$$\frac{w_{m,xs}}{w_{m,x}} = \frac{w_{n,xs}}{w_{n,x}}. \quad (19b)$$

This means that for each m and n in \mathbb{N}_0 and each right coset $xS_+^{(0)}$, the ratio between $w_{m,y}$ and $w_{n,y}$ is a constant complex unit for all $y \in xS_+^{(0)}$, so that we can factorize

$$w_{n,x} = \alpha(n, xS_+^{(0)}) q_x. \quad (20)$$

Once more, we will require both factors to be unitary. If, by assumption, $S_+^{(0)} = S^{(0)}$, the cosets are identified by the power of one generator of S —as $c_0^k S^{(0)}$, where $k \in \mathbb{Z}$, so that we obtain

$$w_{n,x} = w_{n, \tilde{x}c_0^k} = \alpha_{n,k} q_x.$$

We note that if $\chi(G, S)$ is finite, then $\alpha_{n,k+\chi(G, S)}$ must be equal to $\alpha_{n,k}$ to retain consistency. Inserting this form into Eq. (19a), we find that the ratio

$$\frac{\alpha_{n+1,k+1} q_x}{\alpha_{n,k} q_x}$$

should not depend on n . This is equivalent to the condition that $\alpha_{n+1,k+1}/\alpha_{n,k}$ depends on k only. Denoting this ratio β_k , we find that

$$\begin{aligned} \alpha_{n,k} &= \beta_{k-1} \alpha_{n-1,k-1} = \beta_{k-1} \beta_{k-2} \alpha_{n-2,k-2} = \\ &= \dots = \beta_{k-1} \beta_{k-2} \dots \beta_{k-n} \alpha_{0,k-n} \end{aligned}$$

Denoting

$$\gamma_K = \begin{cases} \prod_{k=0}^{K-1} \beta_k & \text{for } K \geq 0, \\ \prod_{k=1}^{-K} \beta_{-k}^{-1} & \text{otherwise,} \end{cases}$$

we can write

$$\alpha_{n,k} = \frac{\gamma_k}{\gamma_{k-n}} \alpha_{0,k-n}.$$

Unlike $\alpha_{0,k}$, γ_k is not constant on the modular class $\text{mod } \chi(G, S)$ for $\chi(G, S) < +\infty$. Instead,

$$\gamma_{m+\chi(G,S)} = \prod_{k=0}^{\chi(G,S)-1} \beta_k \gamma_m =: \epsilon^{\chi(G,S)} \gamma_m.$$

In the case of infinite χ , let $\epsilon = 1$. This allows us to write the solution uniformly as

$$\begin{aligned} \alpha_{n,k} &= \epsilon^n \eta_{n-k} \gamma_k, \\ u_{n,x,c} &= \epsilon^n \eta_{n-k} \gamma_k \delta_{x,c}, \end{aligned} \quad (21)$$

where $x = \tilde{x}c_0^k$ and

- $\delta_{x,c}$ are arbitrary complex units for all $x \in G$, $c \in S$,
- γ_m and η_m are arbitrary sequences of $\chi(G, S)$ complex units,
- ϵ is an arbitrary complex unit in the case of finite $\chi(G, S)$ and 1 otherwise.

Again, as the term of γ_k depends only on x , it can be immersed into $\delta_{x,c}$. Also, a global phase factor can be factored out of η_m and put into $\delta_{x,c}$.

As opposed to the previous case, it's simple to determine the zeroth element U_0 : starting from Eq. (18), we note that for time-homogeneous coins, there is a local unitary C such that $C_n = C$ for all $n \in \mathbb{N}_0$. Similarly, $\tilde{C}_n = \tilde{C}$ for all $n \in \mathbb{N}_0$. Thus,

$$U_0 = \tilde{C}^\dagger T^\dagger U_1 T C.$$

We can compare this equation with its equivalent for $n = 1$,

$$U_1 = \tilde{C}^\dagger T^\dagger U_2 T C.$$

Noting that by Eq. (21), $U_{2,\tilde{x}c_0^k} = \epsilon \frac{\eta_{2-k}}{\eta_{1-k}} U_{1,\tilde{x}c_0^{k-1}}$, we obtain

$$U_{0,\tilde{x}c_0^k} = \epsilon^{-1} U_{1,\tilde{x}c_0^{k+1}},$$

so that the operator U_0 is also diagonal in the geometrical basis of \mathcal{H} and its matrix elements are given simply by extending the validity of Eq. (21) to the case $n = 0$.

We conclude the proof by establishing the group of time-homogeneity preserving symmetries. Taking into account Eq. (21) and the following notes, each symmetry is determined by specifying $\delta_{x,c}$, η_m (up to a global phase) and possibly ϵ . As all of these parameters are just tuples of complex units, this immediately gives the group in the form stated by the theorem. \square

In the case of a both space- and time-homogeneous coin, we can easily combine the partial results given by Theorem 3 as follows.

Corollary 2. *Let Γ be nonseparating, let \mathcal{T} be a unitary quantum walk symmetry described by a sequence of unitary operators $(U_n)_{n=0}^{+\infty}$. Then \mathcal{T} preserves both time and space homogeneity of the quantum coin if and only if the components of U_n are of the form*

$$U_{n,x} = \eta_{n-k} \epsilon^n \gamma(x) U' \quad (22)$$

for all $n \in \mathbb{N}_0$, where η_m is defined the same way as in Theorem 3, ϵ is a complex unit, fixed at 1 in the case where $\chi(\Gamma)$ is infinite, γ is a one-dimensional unitary representation of G , and $U' \in U(\mathcal{H}_C)$ is a unitary operation diagonal in the geometrical basis of \mathcal{H}_C . The group of symmetries with this restriction is

$$(U(1)^{\chi(G,S)}/U(1)) \times U(1) \times \text{Rep}(S^{(0)}) \times U(1)^S$$

if $\chi(\Gamma) < +\infty$ and

$$(U(1)^{\chi(G,S)}/U(1)) \times \text{Rep}(S^{(0)}) \times U(1)^S$$

otherwise.

Example. In this example, we apply the above theory to a quantum walk on a line, where G is the additive group of integers, \mathbb{Z} , generated by $S = \{-1, 1\}$, with a homogeneous coin. Even in this simplest case the above theory produces useful results. Let Γ denote the Cayley graph $\Gamma(\mathbb{Z}, S)$.

A general quantum coin with this property is given by $\mathcal{C} = (\text{Id} \otimes C)_{n=0}^{+\infty}$, where C , expressed in the geometrical basis of \mathcal{H}_C , is a general unitary matrix of rank 2,

$$C = \omega \begin{pmatrix} \mu & 0 \\ 0 & \mu^* \end{pmatrix} \begin{pmatrix} \cos \psi & \sin \psi \\ -\sin \psi & \cos \psi \end{pmatrix} \begin{pmatrix} \nu & 0 \\ 0 & \nu^* \end{pmatrix}. \quad (23)$$

Here $\omega, \mu, \nu \in \mathbb{C}$, $\psi \in \mathbb{R}$, $|\omega| = |\mu| = |\nu| = 1$.

The causal subgroup is equal to $2\mathbb{Z}$, because any product of an odd number of generators is an even number, and 2 can be written as $c + (-d) \in S + (-S) \subset S^{(0)}$ if $c = 1$, $d = -1$. The condition of Γ being nonseparating is a trivial property of any abelian walking space. We note that $\chi(G, S) = 2$ and the elements of $G : S^{(0)}$ correspond to the subsets of even and odd integers. Indeed, walks started in either of these subsets never interfere.

A general form of a unitary representation of $2\mathbb{Z}$ on \mathbb{C} is

$$\gamma(x) = e^{i\phi x}, \quad \phi \in \mathbb{R}.$$

According to Corollary 2, the symmetries of the above system are classified by five continuous parameters: $\eta_{\text{odd}}/\eta_{\text{even}}$, ϵ , ϕ , δ_{+1} , δ_{-1} . The transformed coin reads

$$\tilde{C} = \omega \epsilon \begin{pmatrix} e^{i\phi} & 0 \\ 0 & e^{-i\phi} \end{pmatrix} \begin{pmatrix} \delta_{+1} & 0 \\ 0 & \delta_{-1} \end{pmatrix} \begin{pmatrix} \mu & 0 \\ 0 & \mu^* \end{pmatrix} \cdot \begin{pmatrix} \cos \psi & \sin \psi \\ -\sin \psi & \cos \psi \end{pmatrix} \begin{pmatrix} \nu & 0 \\ 0 & \nu^* \end{pmatrix} \begin{pmatrix} \delta_{+1}^* & 0 \\ 0 & \delta_{-1}^* \end{pmatrix} \quad (24a)$$

and the transformed initial state is

$$U_0|\psi_0\rangle = \sum_{x \in \mathbb{Z}} \eta_{(x \bmod 2)} e^{i\phi x} \begin{pmatrix} \delta_{+1} & 0 \\ 0 & \delta_{-1} \end{pmatrix} |x\rangle \langle x|\psi_0\rangle. \quad (24b)$$

Based on these formulas, some of the parameters assume a straightforward mathematical meaning:

- ϵ is related to the invariance of the system with respect to multiplying C by a scalar. This is a phase that the system accumulates per every step of the quantum walk.
- A common prefactor of δ_{\pm} is related to the freedom of global phase of the initial state.

The global phase can be completely moved from δ_{\pm} into η_{ξ} by introducing a constraint $\delta_{-1} = \delta_{+1}^*$ and making η_{even} and η_{odd} two independent parameters.

In general, any continuous symmetry can be used to reduce the number of parameters determining nonequivalent instances of a given physical system. In our example, by choosing appropriate values of ϵ , ϕ , and $\delta_{\pm 1}$, we can find a quantum walk equivalent with W_C in which the coin is simplified to

$$\tilde{C} = \begin{pmatrix} \cos \psi & \sin \psi \\ -\sin \psi & \cos \psi \end{pmatrix} \quad (25)$$

and thus determined by a single parameter. The rest of the information about the particular quantum walk can be encoded into the initial state.

Besides this result, Eq. (25) has one nontrivial consequence: the transformed coin is a real-valued matrix and so is the infinite matrix of the step operator in the geometrical basis of \mathcal{H} . Therefore, an initial state with real coefficients in the geometrical basis will stay real-valued during the whole time evolution and an analogical result holds for a pure imaginary-valued initial vector. As a consequence, the real and imaginary parts of the transformed initial state define two quantum walks which never interfere, although visiting the same set of vertices. The contributions to measurement probabilities can be computed separately in the field of real numbers and classically summed.

Moreover, if the initial state of the walker is localized at a vertex x_0 , i.e., of the form

$$|\psi_0\rangle = |x_0\rangle \otimes |\chi_0\rangle,$$

then this property is kept under the transformation Eq. (24b). If we also neglect the global phase, which can be done using η_{ξ} with no effect on the coin, the initial state is completely determined by two parameters (the spherical angles on the Bloch sphere). Thus any quantum walk on a line with position- and time-independent coin starting from a state localized at a given position is completely determined by a total of three degrees of freedom. This particular result has been exploited in a recent experimental realization [4] where there was only one adjustable parameter of the quantum coin, corresponding

precisely to ψ in this example, and a full control of the initial chirality χ_0 (up to a global phase) using two adjustable optical elements.

IV. SYMMETRIES INVOLVING PERMUTATION OF THE MEASUREMENT PROBABILITIES

In order to extend the applicability of the theory, we generalize the notion of quantum walk symmetries. According to Definition 7, the probability distribution of a complete measurement of the position register was required to stay invariant under a symmetry transformation. We obtain a broader class of solutions if we allow transformations which do affect the probability distribution, but in such a way that the original distribution is easily reconstructible—more precisely, such that the probabilities merely undergo some fixed permutation. In order to respect the underlying group structure of the Cayley graph, we assume that the permutation is given by an automorphism on G and an optional multiplication by a fixed element of G , and define a wider class of symmetries which impose this kind of transformation on the measurement probability.

Definition 9. Let ϕ be an automorphism of G such that $\phi(S) = S$, let $g \in G$. We call the map $g\phi : G \rightarrow G : x \mapsto g \cdot \phi(x)$ a *shifted S -preserving automorphism* on G . We associate three operators with $g\phi$: a *spatial permutation operator* $P_{g\phi}^{(S)}$ on \mathcal{H}_S , defined by its action on geometrical basis states

$$P_{g\phi}^{(S)}|x\rangle = |g\phi(x)\rangle \quad (26a)$$

for all $x \in G$; a *coin permutation operator* $P_{g\phi}^{(C)}$ on \mathcal{H}_C , defined by

$$P_{g\phi}^{(C)}|c\rangle = |\phi(c)\rangle \quad (26b)$$

for all $c \in S$; and a *total permutation operator*

$$P_{g\phi} = P_{g\phi}^{(S)} \otimes P_{g\phi}^{(C)} \quad (26c)$$

on \mathcal{H} .

Note that the automorphism part ϕ of a shifted S -preserving automorphism $g\phi$, needed in the definition of $P_{g\phi}^{(C)}$, can be extracted using

$$\phi(c) = (g\phi(e))^{-1}(g\phi(c)).$$

Definition 10. Let \mathcal{T} be an endomorphism on the Cartesian product of the set of quantum coins and initial states of a quantum walk on Γ . We call \mathcal{T} a *generalized unitary quantum walk symmetry* on Γ if there is a sequence of local unitary operators $(U_n)_{n=0}^{+\infty}$ and a shifted automorphism $g\phi$ such that for each quantum coin $C = (C_n)_{n=0}^{+\infty}$ and for each initial state $|\psi_0\rangle$,

$$\forall n \in \mathbb{N}_0 : W_{\tilde{C}}(n)|\tilde{\psi}_0\rangle = P_{g\phi} U_n W_C(n)|\psi_0\rangle, \quad (27)$$

where $\tilde{\mathcal{C}}$ and $|\tilde{\psi}_0\rangle$ have the same meaning as in Definition 7 and $P_{g\phi}$ denotes the total permutation operator associated with the shifted S -preserving automorphism $g\phi$.

The (unshifted) automorphisms to be considered have to preserve the generating set S in order to preserve the edges of the Cayley graph $\Gamma(G, S)$. We note, however, that the automorphism group of $\Gamma(G, S)$ may be more general.[11] As shown by the following Lemma, the shifted S -preserving automorphisms form a subgroup of the automorphism group of Γ .

Lemma 3. *The set of all automorphisms on G which preserve S forms a subgroup $Aut(G | S)$ of $Aut(G)$. The set of all shifted S -preserving automorphisms on G with the operation of map composition forms a group isomorphic to $G \rtimes Aut(G | S)$.*

Proof. For the first part, it suffices to show that for any pair ϕ_1, ϕ_2 of automorphisms on G preserving S , $\phi_1^{-1} \circ \phi_2$ preserves S . This is simple as both ϕ_1 and ϕ_2 act as permutations when restricted to S .

To show that the shifted S -preserving automorphisms constitute a group, we have to prove that the four group axioms are satisfied.

Closure. Let $\phi_1, \phi_2 \in Aut(G | S)$ and $g_1, g_2 \in G$. The composition of $g_1\phi_1$ and $g_2\phi_2$ is a map $G \rightarrow G$ prescribed by

$$(g_1\phi_1 \circ g_2\phi_2)(x) = g_1\phi_1(g_2\phi_2(x)) = g_1\phi_1(g_2) \cdot (\phi_1 \circ \phi_2)(x). \quad (28a)$$

Noting that $g_1\phi(g_2) \in G$ and that $\phi_1 \circ \phi_2 \in Aut(G | S)$, the composed map is by definition a shifted S -preserving automorphism.

Associativity. Associativity is granted by the operation of composition.

Identity. The identity element is the shifted S -preserving automorphism eId , where e is the identity element in G . Indeed, this is the identity map on G and thus the neutral element with respect to map composition.

Inverse. Let $\phi \in Aut(G | S)$, let $g \in G$. Then the inverse element of the shifted S -preserving automorphism $g\phi$ with respect to composition is a map $G \rightarrow G$ defined by

$$(g\phi)^{-1}(x) = \phi^{-1}(g^{-1}x) = \phi^{-1}(g^{-1}) \cdot \phi^{-1}(x) \quad (28b)$$

This is a shifted S -preserving automorphism as $\phi^{-1}(g^{-1}) \in G$ and $\phi^{-1} \in Aut(G | S)$.

Let us denote this group \mathcal{G} . In order to show that $\mathcal{G} \cong G \rtimes Aut(G | S)$, we first identify G with a subgroup G' of \mathcal{G} using the monomorphism

$$\gamma : G \rightarrow \mathcal{G} : g \mapsto gId$$

and similarly identify $Aut(G | S)$ with a subgroup A' of \mathcal{G} using the monomorphism

$$\alpha : Aut(G | S) \rightarrow \mathcal{G} : \phi \mapsto e\phi.$$

It follows directly from the definition that $\mathcal{G} = G'A'$ and that $G' \cap A' = \{e\}$. In order to show that the product is semidirect, we show that G' is a normal subgroup of \mathcal{G} . Let $hId \in G'$, let $g\phi$ be an arbitrary element of \mathcal{G} . Using Eq. (28a) and Eq. (28b), we simplify the composition

$$\begin{aligned} g\phi \circ hId \circ (g\phi)^{-1} &= g\phi \circ hId \circ \phi^{-1}(g^{-1})\phi^{-1} = \\ &= g\phi \circ (h\phi^{-1}(g^{-1})\phi^{-1}) = \\ &= g\phi(h\phi^{-1}(g^{-1}))(\phi \circ \phi^{-1}) = \\ &= (g\phi(h)g^{-1})Id \in G'. \end{aligned}$$

This proves that $\mathcal{G} = G' \rtimes A' \cong G \rtimes Aut(G | S)$. \square

Lemma 4. *In the notation of Definition 10, the condition of Eq. (27) is satisfied for each \mathcal{C} and each $|\psi_0\rangle$ if and only if*

$$\begin{aligned} |\tilde{\psi}_0\rangle &= P_{g\phi}U_0|\psi_0\rangle, \\ \forall n \in \mathbb{N}_0 : \quad T\tilde{\mathcal{C}}_n &= P_{g\phi}U_{n+1}TC_nU_n^\dagger P_{g\phi}^\dagger. \end{aligned} \quad (29)$$

Here, $\tilde{\mathcal{C}}$ and $|\tilde{\psi}_0\rangle$ denote the image of \mathcal{C} and $|\psi_0\rangle$ under T .

Proof. The proof is done in a straightforward analogy to the proof of Lemma 1. \square

Lemma 5. *Let $\phi \in Aut(G | S)$, let $g \in G$. Then the total permutation operator $P_{g\phi}$ commutes with the step operator T . Furthermore, let U be a local unitary operation. Then $P_{g\phi}^\dagger U P_{g\phi}$ is a local unitary operation. If U is of the form $Id \otimes U'$, then $P_{g\phi}^\dagger U P_{g\phi}$ is of the form $Id \otimes (P_{g\phi}^{(C)\dagger} U' P_{g\phi}^{(C)})$.*

Proof. To show the commutation of T and $P_{g\phi}$, we compare the action of both $TP_{g\phi}$ and $P_{g\phi}T$ on the same basis state $|x, c\rangle$.

$$\begin{aligned} TP_{g\phi}|x, c\rangle &= T|g\phi(x), \phi(c)\rangle = |g\phi(x)\phi(c), \phi(c)\rangle \\ P_{g\phi}T|x, c\rangle &= P_{g\phi}|xc, c\rangle = |g\phi(xc), \phi(c)\rangle \end{aligned}$$

The equality $\phi(x)\phi(c) = \phi(xc)$ follows from the fact that ϕ is a group automorphism.

In order to prove the second part of the Lemma, we first note that all the operators $P_{g\phi}^{(S)}$, $P_{g\phi}^{(C)}$, and $P_{g\phi}$ are unitary. This can be shown promptly from the fact that the operators act as permutations in the corresponding geometrical basis systems. Thus for any unitary operator U , $P_{g\phi}^\dagger U P_{g\phi}$ is also unitary.

If U is local, we can show using Eq. (26c)

$$\begin{aligned} \tilde{U} &:= P_{g\phi}^\dagger \left(\sum_{x \in G} |x\rangle\langle x| \otimes U_x \right) P_{g\phi} = \\ &= \sum_{x \in G} \left(\left(P_{g\phi}^{(S)\dagger} |x\rangle\langle x| P_{g\phi}^{(S)} \right) \otimes \left(P_{g\phi}^{(C)\dagger} U_x P_{g\phi}^{(C)} \right) \right) \end{aligned}$$

If we change the summation variable from x to $y = \phi^{-1}(g^{-1}x)$, such that $g\phi(y) = x$, we obtain

$$\tilde{U} = \sum_{y \in G} \left(P_{g\phi}^{(S)\dagger} |g\phi(y)\rangle\langle g\phi(y)| P_{g\phi}^{(S)} \right) \otimes \left(P_{g\phi}^{(C)\dagger} U_{g\phi(y)} P_{g\phi}^{(C)} \right).$$

We used the fact that the composition of an automorphism and left multiplication is a bijection on G .

Using the unitarity of $P_{g\phi}^{(S)}$, from which it follows that

$$P_{g\phi}^{(S)\dagger}|g\phi(y)\rangle = \left(P_{g\phi}^{(S)}\right)^{-1}|g\phi(y)\rangle = |y\rangle$$

and

$$\langle g\phi(y)|P_{g\phi}^{(S)} = \left(P_{g\phi}^{(S)\dagger}|g\phi(y)\rangle\right)^\dagger = \langle y|,$$

we can simplify \tilde{U} to the form

$$\tilde{U} = \sum_{y \in G} |y\rangle\langle y| \otimes \left(P_{g\phi}^{(C)\dagger} U_{g\phi(y)} P_{g\phi}^{(C)}\right),$$

which proves that \tilde{U} is a local operator.

Similarly, let $U = Id \otimes U'$. Then

$$\begin{aligned} P_{g\phi}^\dagger (Id \otimes U') P_{g\phi} &= \\ &= \left(P_{g\phi}^{(S)\dagger} Id P_{g\phi}^{(S)}\right) \otimes \left(P_{g\phi}^{(C)\dagger} U' = P_{g\phi}^{(C)}\right) = \\ &= Id \otimes \left(P_{g\phi}^{(C)\dagger} U' P_{g\phi}^{(C)}\right). \end{aligned}$$

□

As shown by the following Theorem, the search for generalized unitary quantum walk symmetries can be reduced to the problem already solved in Section III.

Theorem 4. *Let \mathcal{T} be an endomorphism on the Cartesian product of the set of quantum coins and initial states of a quantum walk on Γ , let $\mathcal{T}(\mathcal{C}, |\psi_0\rangle) = (\tilde{\mathcal{C}}, |\tilde{\psi}_0\rangle)$, $\tilde{\mathcal{C}} = (\tilde{C}_n)_{n=0}^{+\infty}$. Then \mathcal{T} is a generalized unitary quantum walk symmetry if and only if there is a ordinary unitary quantum walk symmetry $\mathcal{T}' : (\mathcal{C}, |\psi_0\rangle) \mapsto (\mathcal{C}', |\psi'_0\rangle)$, $\mathcal{C}' = (C'_n)_{n=0}^{+\infty}$, and a shifted S -preserving automorphism $g\phi$ such that*

$$\begin{aligned} |\tilde{\psi}_0\rangle &= P_{g\phi} |\psi'_0\rangle \\ \forall n \in \mathbb{N}_0 : \quad \tilde{C}_n &= P_{g\phi} C'_n P_{g\phi}^\dagger. \end{aligned} \quad (30)$$

Theorem 4 solves in general the problem of symmetries without any assumptions about the coin. The restricted problems with position- and/or time-independent coins can also be addressed. As a direct consequence of Lemma 5, the restriction is transferred from the quantum coin \mathcal{C} to the quantum coin \mathcal{C}' of the original problem, where we can use Theorem 3 or Corollary 2 to find all solutions.

It also trivially follows that the symmetry group is in all cases simply augmented by the group of shifted S -preserving automorphisms.

Proof. Let us define $|\psi'_0\rangle$ and C'_n such that Eq. (30) is held. Then, according to Eq. (29), these objects must satisfy

$$|\psi'_0\rangle = U_0 |\psi_0\rangle \quad (31a)$$

and

$$TP_{g\phi} C'_n P_{g\phi}^\dagger = P_{g\phi} U_{n+1} T C_n U_n^\dagger P_{g\phi}^\dagger. \quad (31b)$$

Using the commutativity of T and $P_{g\phi}$, Eq. (31b) becomes

$$T C'_n = U_{n+1} T C_n U_n^\dagger. \quad (31c)$$

However, Eq. (31a) and Eq. (31c) are exactly the conditions of Lemma 1. Therefore \mathcal{T} is a generalized unitary quantum walk symmetry if and only if the map $(\mathcal{C}, |\psi_0\rangle) \mapsto (\mathcal{C}', |\psi'_0\rangle)$ is an ordinary unitary quantum walk symmetry. □

Example. We show an application of the generalized quantum walk symmetries again on a quantum walk on a line with a homogeneous coin. Given a coin $\mathcal{C} = (Id \otimes C)_{n=0}^{+\infty}$ and an initial state $|\psi_0\rangle$, we can use Theorem 4 to find a new homogeneous quantum coin $\tilde{\mathcal{C}} = (Id \otimes \tilde{C})_{n=0}^{+\infty}$ and an initial state $|\tilde{\psi}_0\rangle$ such that the evolution of the new quantum walk is a mirror image of the original one.

Taking the S -preserving automorphism $P : x \mapsto -x = 0 + (-1)x$, we construct the tuple of permutation operators $P_P^{(i)}$ easily. We note that the matrix of the coin permutation operator is the Pauli X -matrix, or the quantum NOT gate.

In the simplest case, we can choose to only perform the permutation, choosing the identity transform as \mathcal{T}' in Theorem 4. Doing so, not only the measurement probabilities but also the amplitudes are preserved, they only undergo the permutation in both position and coin geometrical bases. In this case, the transformed coin is described by the matrix

$$\tilde{C} = X C X^\dagger = X C X$$

and the transformed initial state satisfies

$$\langle x | \tilde{\psi}_0 \rangle = X \langle -x | \psi_0 \rangle$$

for all $x \in \mathbb{Z}$.

If we use the general form of the coin as described by Eq. (23), after the transformation we obtain

$$\tilde{C} = \omega \begin{pmatrix} \mu^* & 0 \\ 0 & \mu \end{pmatrix} \begin{pmatrix} \cos \psi & -\sin \psi \\ \sin \psi & \cos \psi \end{pmatrix} \begin{pmatrix} \nu^* & 0 \\ 0 & \nu \end{pmatrix}.$$

We note that it is now possible, if desired, to transform the coin back to its original state, using the results of Section III only. This way, the probability distribution stays unchanged, i.e. mirrored with respect to the original quantum walk, thus we obtain a new initial state $|\psi_1\rangle$ for the original coin \mathcal{C} for which the time evolution has flipped sides.

We can do so by the following transform:

$$\begin{aligned} C &= \omega \begin{pmatrix} \mu^* & 0 \\ 0 & \mu \end{pmatrix} \begin{pmatrix} \mu^2 \nu^2 & 0 \\ 0 & (\mu^2 \nu^2)^* \end{pmatrix} \begin{pmatrix} -i\nu^{*2} & 0 \\ 0 & i\nu^2 \end{pmatrix} \times \\ &\quad \begin{pmatrix} \cos \psi & -\sin \psi \\ \sin \psi & \cos \psi \end{pmatrix} \begin{pmatrix} i\nu^2 & 0 \\ 0 & -i\nu^{*2} \end{pmatrix} \begin{pmatrix} \nu^* & 0 \\ 0 & \nu \end{pmatrix}. \end{aligned}$$

This corresponds to choosing $\delta_- = \delta_+^* = i\nu^2$, $e^{i\phi} = \mu^2 \nu^2$, and $\epsilon = 1$ in the notation of the Example in Section III. The choice of η_{even} and η_{odd} is free, so we can let them be 1. The transformed initial state is then given by

$$|\psi_1\rangle = \sum_{x \in \mathbb{Z}} \begin{pmatrix} -i\nu^{*2} & 0 \\ 0 & i\nu^2 \end{pmatrix} X | -x \rangle \langle x | \psi_0 \rangle.$$

If the initial state $|\psi_0\rangle$ is localized at $x = 0$, the transition to $|\psi_1\rangle$ is simply a linear transformation of the initial chirality, described in the geometrical basis by the matrix

$$Q = \begin{pmatrix} -i\nu^{*2} & 0 \\ 0 & i\nu^2 \end{pmatrix} X = \begin{pmatrix} 0 & -i\nu^{*2} \\ i\nu^2 & 0 \end{pmatrix}$$

Having this result enables us to find initial states which produce a symmetric probability distribution at each iteration of the quantum walk. These are simply the eigenstates of the matrix Q , tensor multiplied by $|0\rangle$ in the position register. The eigenvalues of Q are ± 1 and the corresponding normalized eigenvectors are

$$|\chi_0\rangle_{\pm} = \frac{1}{\sqrt{2}} \begin{pmatrix} \nu^* \\ \pm i\nu \end{pmatrix}$$

in the coin space basis. Except for the degenerate cases of $\psi = k\pi$, $k \in \mathbb{Z}$, the parameter ν is defined uniquely up to a sign and therefore there are exactly two localized initial states producing a symmetric probability distribution and these are orthonormal.

V. CONCLUSIONS

We used analytic and algebraic methods to study the symmetries of discrete time quantum walks on Cayley graphs, where the quantum coin was allowed to transform along with the initial state. We constructed a general way of obtaining transformations which preserve the measurement probabilities, and our results grant that we obtained the complete set of such transformations in a

uniform manner. We described the symmetry group of the quantum walk time evolution operator using the results of the analysis.

Some of the symmetries found this way correspond to trivial properties of any discrete time quantum system, but most of the symmetries are specific to quantum walks. Once the symmetry group is found, any continuous symmetry can be used to reduce the problem. We have demonstrated this fact on the quantum walk on a line with a constant coin, where the result was that two out of three physical parameters of the quantum coin could be dropped without loss of generality. Quantum walks on more complicated graphs allow even more significant reduction.

An open question is how the results change if we drop the condition that the Cayley graph is nonseparating. An example where this condition is not held is a quantum walk on any group which contains the free group of order 2 or higher. Counterexamples to the forms provided by Theorem 3 can be found for such graphs, indicating that a more general treatment is necessary to cover all Cayley graphs.

However, the most important open question, which could be addressed in a subsequent work, is how the results change if the definition of a quantum walk is generalized such that the dimension of the coin space is different from the out-degree of the Cayley graph.

Acknowledgments

This work was supported by the Grant Agency of the Czech Technical University in Prague, grant No. SGS10/294/OHK4/3T/14.

-
- [1] C. M. Chandrashekar, R. Srikanth, and S. Banerjee, “Symmetries and noise in quantum walk”, *Phys. Rev. A* **76**, 022316 (2007)
- [2] H. Krovi, “Symmetry in quantum walks”, Ph.D. thesis, University of Southern California (2007)
- [3] N. Shenvi, J. Kempe, and K. B. Whaley, “Quantum random-walk search algorithm”, *Phys. Rev. A* **67**, 052307 (2003)
- [4] A. Schreiber *et al.*, “Photons Walking the Line: A Quantum Walk with Adjustable Coin Operations”, *Phys. Rev. Lett.* **104**, 050502 (2010)
- [5] A. Ambainis, J. Kempe, and A. Rivosh, “Coins make quantum walks faster”, in *Proceedings of the Sixteenth Annual ACM-SIAM Symposium on Discrete Algorithms* (2005), pp. 1099–1108
- [6] D. Aharonov, A. Ambainis, J. Kempe, and U. Vazirani, “Quantum walks on graphs”, in *Proceedings of the Thirty-third ACM Symposium on Theory of Computing* (2001), pp. 50–59
- [7] D. Meyer, “On the absence of homogeneous scalar unitary cellular automata”, *Phys. Lett. A* **223**, pp. 337–340 (1996)
- [8] O. L. Acevedo, J. Roland, and N. J. Cerf, “Exploring scalar quantum walks on Cayley graphs”, *Quant. Inform. Comp.* **8** (2008), pp. 68–81
- [9] O. L. Acevedo and T. Gobron, “Quantum walks on Cayley graphs”, *J. Phys. A: Math. Gen.* **39** (2006) 585–599
- [10] We note that the above definition of a step operation on the Hilbert space \mathcal{H} is not the only possible one; as shown in [9], the concept of quantum coin can be altered so that the basis coin states do not imply the transition over individual edges from the vertex x in a one-to-one manner. Throughout the text, however, we will stay with Definition 4.
- [11] Consider, for example, a free group over three generators, a , b , and c . The elements are uniquely described by words in the alphabet $\mathcal{A} = \{a, b, c, a^{-1}, b^{-1}, c^{-1}\}$. Define a map $\mathcal{A}^* \rightarrow \mathcal{A}^*$ which substitutes b for c and *vice versa* for words beginning with an a and leaves all other words intact. Such a map induces a graph automorphism of the Cayley graph but is not a group automorphism itself.

Prohlášení

Prohlašuji, že jsem svou dizertaci vypracoval samostatně pod vedením prof. Ing. Igora Jexe, DrSc. a použil jsem pouze literaturu uvedenou v seznamu literatury.

Nemám závažný důvod proti užití tohoto školního díla ve smyslu § 60 Zákona č. 121/2000 Sb., o právu autorském, o právech souvisejících s právem autorským a o změně některých zákonů (autorský zákon).

V Praze dne

.....
podpis